COS Prelaunch Calibration Data

Date:	March 13, 2008
Document Number:	COS-01-0008
Revision:	Revision A
Contract No.:	NAS5-98043
CDRL No.:	AV-04

Prepared By:	Dr. Erik Wilkinson	5/14/04
	Dr. E. Wilkinson, COS Project Scientist, CU	Date
Reviewed By:	Dr. Dennis Ebbets	5/14/04
	Dr. D. Ebbets, COS Calibration Scientist, BATC	Date
Reviewed By:	Dr. Ken Brownsberger	5/14/04
	Dr. K. Brownsberger, COS Experiment Manager, CU	Date
Approved By:	Dr. James Green	5/3/04
	Prof. J. C. Green, COS Principal Investigator, CU	Date
Approved By:	Tom LaJeunesse	5/14/04
	Mr. Tom LaJeunesse, COS Program Manager, BATC	Date

Center for Astrophysics & Space Astronomy
University of Colorado
Campus Box 593
Boulder, Colorado 80309

REVISIONS

Letter	ECO No.	Description	Check	Approved	Date
-		Initial Release		EW	5/14/04
A	COS-090	Incorporates results from 2006 thermal vacuum tests.		CSF	

Original Release Name	Date
Drawn: E. Wilkinson	4-12-04
Reviewed:	
Approved:	

THE UNIVERSITY OF COLORADO

At Boulder

The Center for Astrophysics and Space Astronomy

COS Prelaunch Calibration Data

Size	Code Indent No.	Document No.	Rev
A		COS-01-0008	A
Scale: N/A			

TABLE OF CONTENTS

1. INTRODUCTION

This document presents the final results of the ground calibration of the Cosmic Origins Spectrograph (COS). The data were acquired as part of the formal thermal vacuum testing of COS where the testing procedures were documented in Appendices A, B, and C of the thermal vacuum procedure. Data taken as part of Appendix A were largely intended to gather data and experience necessary to facilitate more extensive testing during Appendix B and to identify early on any potential performance issues. Appendix B was a thorough test of all instrument performance characteristics conducted in 2003. In the summer of 2006, the COS electronics boards were removed from the instrument and modified to replace the power converters with more robust components and to correct for minor workmanship issues. Appendix C was a repeat of several key calibration tests, undertaken in late 2006 to verify continued nominal performance of the instrument after the modification and reinstallation of the electronics boards. The exposure list for all the data acquired during Appendices A,B, and C are available as COS-03-0091 (exposurelist_A_master.xls), COS-03-0092 (exposurelist_B_master.xls), and COS03-0093 (exposurelist_C_master.xls) from the controlled documents archive of the COS instrument development team.

This document is organized in the following manner. Section 2 lists relevant documents that provide a complete description of the COS instrument, how it works, how to operate it, and how to reduce the data. Section 3 lists the COS reference files delivered to the Space Telescope Science Institute for use in the COS data reduction pipeline. Section 4 describes the calibration systems used to calibrate COS and Section 5 presents the various calibration results. Section 5 is organized in a similar fashion to the top-level controlling document for COS, the Contract End Item Specification. Finally, Section 6 consists of a variety of appendices that contain calibration planning and exposure logs for Appendix A as well as final results for the target acquisition testing conducted in 2003.

2. CONTROLLING DOCUMENTS

This document is the third publication in a triumvirate that provide a complete top-level description of COS instrument. The other two documents are…

Cosmic Origins Spectrograph (COS) Science Operations Requirements Document
(CDRL OP-01; CU/CASA document COS-01-0001)
COS Calibration Requirements & Procedures
(CDRL AV-03; CU/CASA document COS-01-0003)

Also worth examining is the top-level controlling document for COS:

Hubble Space Telescope Cosmic Origins Spectrograph Contract End Item Specification (GSFC document STE-63).

3. COS REFERENCE FILES

The data acquired during science calibration tests in 2003 and 2006 were used to generate reference files to initially populate the COS data reduction pipeline, the software package provided to general observers by the Space Telescope Science Institute (STScI) for COS data calibration. The reference files, listed in Table 4.1-1, were delivered to STScI in 2007. This document describes the tests undertaken in 2003 and 2006 and the subsequent data analysis and characterization of the instrument properties. A description of the creation of the files is provided in COS-03-0090, "Generating the COS Reference Files.

Table 4.1-1: COS Reference Files

Title	IDT filename	STScI filename	Description
Flat Field	nuv_flat.fits	s5n1735al_flat.fits	The flat field reference file is an image with pixel-to-pixel flat; the large-scale fluctuations in sensitivity are accounted for in the photometric correction table.
Geometric Distortion	FUV02_GEOCORR.fits	nb61015el_geo.fits	The geometric distortion reference file is used to correct for the intrinsic nonlinearity (INL) of the FUV detector.
Detector Deadtime	fuv02_dead.fits nuv_dead.fits	s5n1734pl_dead.fits s5n17358l_dead.fits	The deadtime reference frame table gives the livetime factor for various values of the observed global count rate.
Data Quality	fuv_bpix.fits nuv_bpix.fits	s5n1734sl_bpix.fits s5n17357l_bpix.fits	The data quality initialization table gives the locations of rectangular regions that cover portions of the detector that are known to be less than optimal.
Baseline Reference Frame	ref_brf.fits	nan1523nl_brf.fits	The baseline reference frame table gives the "actual" location of each of the two electronic stims, for each FUV segment. These are necessary to perform the thermal correction.
Pulse Height Thresholds	fuv_pha.fits	s5n17352l_pha.fits	The pulse height parameters reference table gives thresholds for checking FUV data based on pulse height filtering for TIME-TAG data and PHA distribution

			verification for ACCUM data.
1-D Extraction	fuv_1dx_2003.fits fuv_1dx_2006.fits nuv_1dx_2003.fits nuv_1dx_2006.fits	s5n1734ql_1dx.fits s5n1734rl_1dx.fits s5n17355l_1dx.fits s5n17356l_1dx.fits	The 1-D extraction parameters table gives the location of the spectrum to be extracted from a 2-D image.
Calibration Lamp Templates	fuv_lamp.fits nuv_lamp.fits	s5n17351l_lamp.fits s5n1735bl_lamp.fits	The template cal lamp spectra table contains template wavecal spectra, to be compared with observed wavecal spectra.
Photometric Sensitivity	fuv_phot.fits nuv_phot.fits	s5n17353l_phot.fits s5n1735cl_phot.fits	The photometric sensitivity reference table gives the instrumental sensitivity at each element of a 1-D extracted spectrum.
Dispersion Solutions	fuv_disp.fits nuv_disp.fits	s5n17350l_disp.fits s5n17359l_disp.fits	The dispersion relation table gives a set of polynomial coefficients for computing wavelength from pixel number.
Wavelength Calibration Parameters	fuv_wcp.fits nuv_wcp.fits	s5n17354l_wcp.fits s5n1735dl_wcp.fits	The wavecal parameters reference table gives parameters that are relevant to wavecal processing (pixels per FPPOS position, number of pixels per resolution element, etc.).

4. RELEVANT CALIBRATION INFORMATION

4.1 2003 THERMAL VACUUM TEST CONFIGURATION

In 2003 (Appendices A and B), COS Thermal-Vacuum Testing and Science Calibration took place in the large "Rambo" vacuum chamber located in Ball's FT1 environmental test facility. The photograph in Figure 4.1-1 gives an idea of its size, while Figure 4.1-2 shows the high level arrangement of the equipment. COS was inside the vacuum chamber, inside its thermal balance fixture, and sitting on a vibration isolated table. The Reflective Aberration Simulator for CALibration (RASCAL) sent an image to the COS entrance aperture that reproduced the aberration content of a point source (single or multiple) as seen by HST. The Calibration Delivery System (CDS) delivered light with the desired spectral content and intensity to RASCAL. CDS consisted of two sections – an external platform outside the vacuum chamber and a set of relay optics inside the chamber that illuminated the RASCAL input pinholes.

The layout of the external platform is shown in Figure 4.1-3. There were two channels. One included an Acton VM-504 vacuum UV monochromator, which isolated a wavelength region approximately 10 Å in width, centered on any wavelength in the COS range 1150 Å < λ < 3200 Å. The second channel bypassed the monochromator and allowed the entire spectral content of

its lamp to reach COS. This was known as the 'lamp-only channel'. A manually operated flat turning mirror selected the desired channel and fed a collimating mirror. The collimated beam passed through a 10 cm long absorption cell and six filter wheels in series. A manually operated shutter blocked all light when inserted. A MgF_2 window separated CDS from RAMBO, allowing each to respond to its own system of vacuum pumps.

An IST Pt-Ne hollow cathode lamp illuminated the input slit of the monochromator, and was the only source used on this channel. On the lamp-only channel we used a Pt-Ne lamp, a D_2 hollow cathode lamp, and a Vici-Condyne Kr continuum lamp for the various experiments. Swapping lamps took about half an hour. The absorption cell was filled with CO for FUV tests, and O_2 for NUV measurements. The pressure could be set to any value between about a milli-Torr and one atmosphere. The cell was removed when not in use. Each filter wheel contained one open position and two filters. Neutral density filters ranging from ND 0.3 to ND 3.0 could be used individually or in series, providing a large range of discrete steps of attenuation. A CaF long-pass filter blocked the Ly α emission line for certain experiments, and a fused silica long-pass filter blocked all FUV light shortward of about 1650 Å when NUV measurements were under way. Bandpass filters centered at 122, 145, 157, 185, 220 and 280 nm allowed restriction of the spectral content to the wavelength regions of the COS gratings. In general these were only used during setup, and not during the COS exposures.

The movement of the grating turret in the monochromator was controlled by a Labview program running on the RASCAL computer. All other equipment on the CDS external platform, including the monochromator slit widths, was operated manually. The lamps were connected to their power supplies and operated manually. As a matter of safe practice the RASCAL PMT was inserted into the light path during the setup phase for each test. The lamp intensity and selection of filters were made to produce a count rate on the PMT that would ensure adequate but safe levels of illumination for COS. The expected hardware configuration and target event rates were documented in the calibration planning documents and procedures.

The external platform also contained an alignment camera that viewed the RASCAL entrance apertures. It was only used during the pre-test setup to guide the alignment of the relay optics to RASCAL.

The RASCAL entrance aperture accommodates four different pinholes and one fully open position. A 10μm diameter circular pinhole simulated a point source, and a 100μm circular aperture produced a slightly extended image for efficiency measurements. These were used during all phases of the calibration program. A 4μm pinhole was in place during Appendix A, but was not used. A pair of 10μm holes separated by the equivalent of 1 arc second were used to verify spatial resolution. For the Appendix B tests these were replaced by a linear array of 7 pinholes (10μm pinholes equally spaced at 1" in the cross-dispersion direction) and a 2D array of pinholes (10μm pinholes on a 100μm x 338 [disp x cross-dispersion] grid) needed for FUV

geometrical distortion measurements. The aperture selection was made from the menu on the RASCAL computer.

The alignment of the RASCAL powered optics to produce the required aberration content and focus was performed by the cognizant GSFC optical scientists prior to the COS calibration. Adjusting RASCAL image quality was not part of the CU/Ball calibration effort.

The output beam of RASCAL could be steered in tip and tilt via commands from its computer menu. Similarly the CsTe PMT could be inserted into and extracted from the optical beam with this program. The PMT was operated with a separate Labview program running on the same computer. The calibration and use of the PMT are described elsewhere in this report.

Figure 4.1-1: The RAMBO chamber where the COS calibration activity was conducted in 2003.

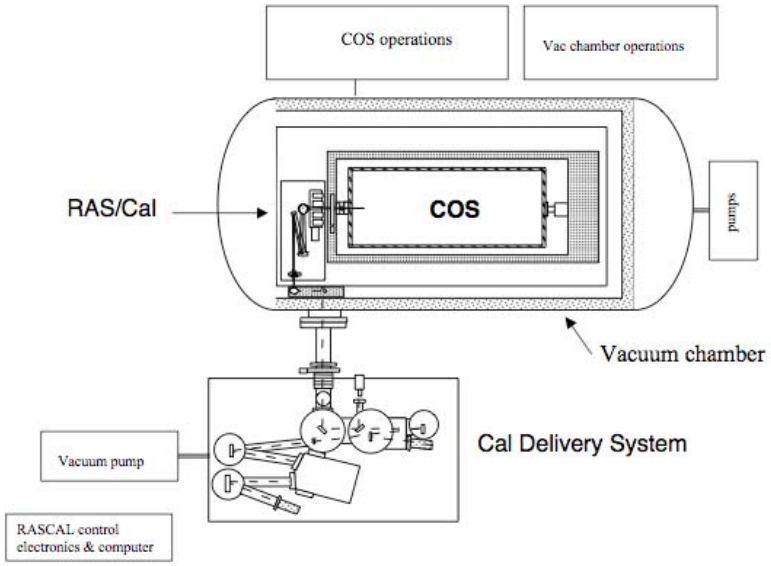

Figure 4.1-2 : Overall layout of the test setup used during the 2003 COS calibration and thermal vacuum test.

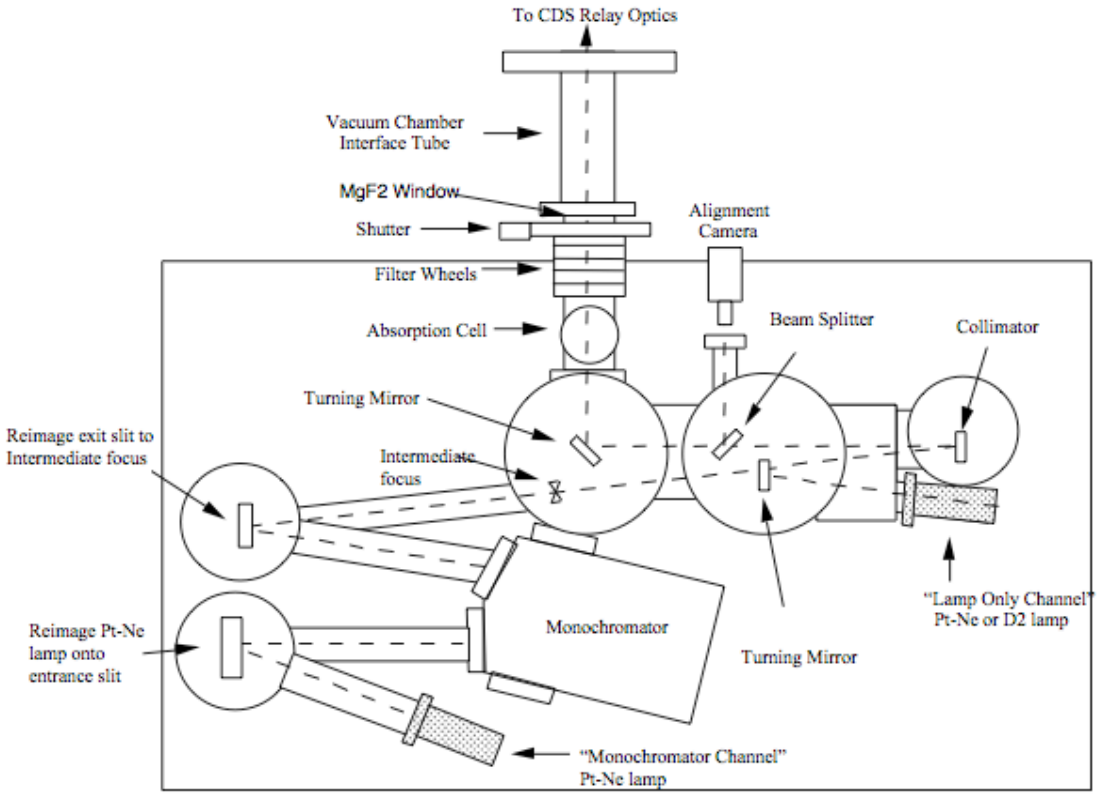

Figure 4.1-3 : The Calibration Delivery Sub-system (CDS) used during COS calibration in 2003 to inject monochromatic or polychromatic light into the RAMBO chamber where the RASCAL instrument formatted the input light into an aberrated beam for use by COS.

4.2 2006 THERMAL VACUUM TEST CONFIGURATION

The 2006 Thermal Vacuum Testing and Science Calibration (Appendix C) took place in the Space Environment Simulator (SES) at the Goddard Space Flight Center. The configuration of the chamber required that COS, RASCAL, and the CDS all reside on the same vibration isolated table in the SES vacuum chamber (see Figure 4.2-1 and Figure 4.2-2). As with the previous setup, the CDS fed light to the RASCAL Relay Optics which in turn fed light through one of 5 selectable pinholes or pinhole arrays and into RASCAL. RASCAL recreates the HST aberrations and feeds light at the appropriate beam speed into the science instrument. RASCAL

is equipped with a NIST traceable photomultiplier tube which is placed in the calibration beam path after the last reflection for photometric calibration.

A new vacuum compatible CDS was developed with all the capabilities of the previous version except for the absorption cell and the Kr lamp. The layout of the calibration setup is shown in Figure 4.2-3 and the CDS is illustrated in Figure 4.2-4. The vacuum CDS consisted of a remotely selectable lamp array feeding a vacuum compatible monochromator system. This was followed by a two bank filter wheel and a fold mirror. The final element before the relay optics was a MgF_2 wedge polarization scrambler with a 25mm clear aperture. The CDS was also fitted with a remotely operated shutter, an alignment camera, a deployable beam splitter for the camera, and a heated cover for stray light suppression and thermal control.

The lamp array consisted of two non-flight IST hollow cathode Pt/Ne lamps and two non-flight IST Deuterium lamps, as well as a Hureas Pt/Cr/Ne hollow cathode lamp (unused) and a LED alignment lamp. Lamps were heat sunk and mounted on a lamp select translation stage. The monochromator system consisted of a McPherson 234/302 scanning monochromator system (a 0.2 meter corrected holographic grating monochromator fed by a model 615B condenser and in turn feeding a 30mm collimator). The filter mechanism consisted of two nine position wheels (the available filters are listed in Table 4.2-1). All CDS controls were concentrated in a single control rack near the RASCAL control station, and the CDS configuration could be automatically logged during science calibration.

RASCAL is described in the previous section, and was used in the same configuration as is described for appendix B testing (three circular pinholes; 1mm ('open'), 100µm, 10µm, and two arrays; a 1x7 (cross dispersion) and a 7x7 array of 10µm pinholes).

Table 4.2-1: Calibration Delivery System Filter Array

Position	Filter Wheel 1	Filter Wheel 2
1	Open	Open
2	F122	CaF2
3	F145	ND 0.3
4	F157	ND 0.5
5	F185 + Fused Silica	ND 1.0
6	F220 + Fused Silica	ND 2.0
7	F280 + Fused Silica	ND 3.0
8	ND 0.5	Fused Silica
9	Open	Open

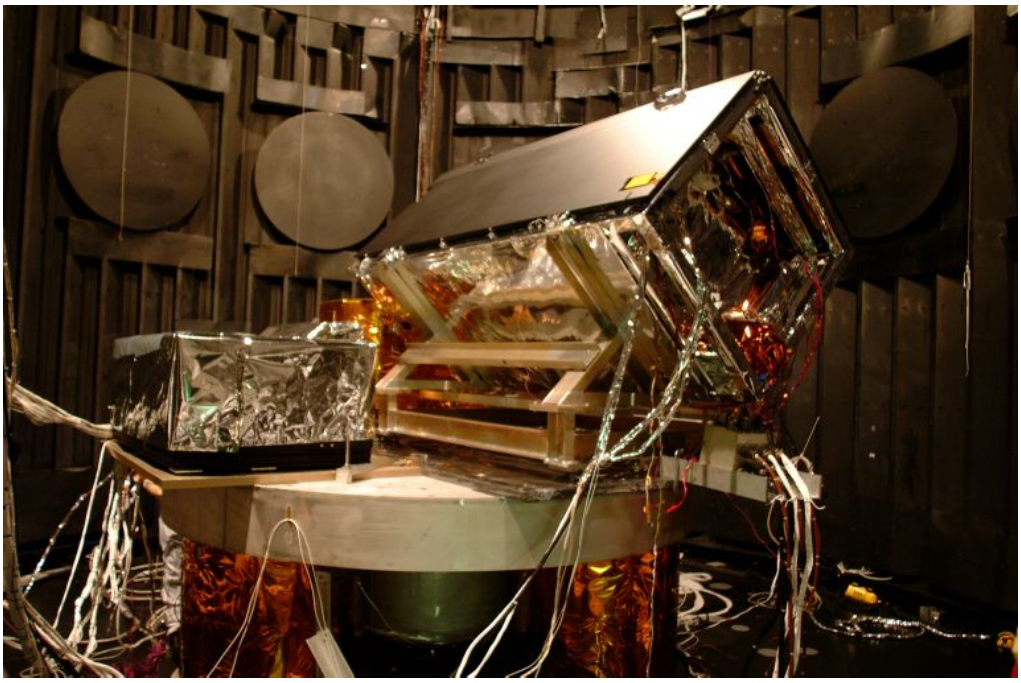

Figure 4.2-1 COS Thermal Vacuum 2006 calibration test configuration – COS and all optical GSE are installed in the Space Environment Simulator (SES) vacuum chamber at Goddard Space Flight Center. COS is supported in the thermal balance fixture (TBF) in the 'diamond' configuration, and the CDS is to the left of COS under the CDS thermal enclosure. All components are mounted on a two piece support plate which is in turn mounted to the circular vibration isolated table.

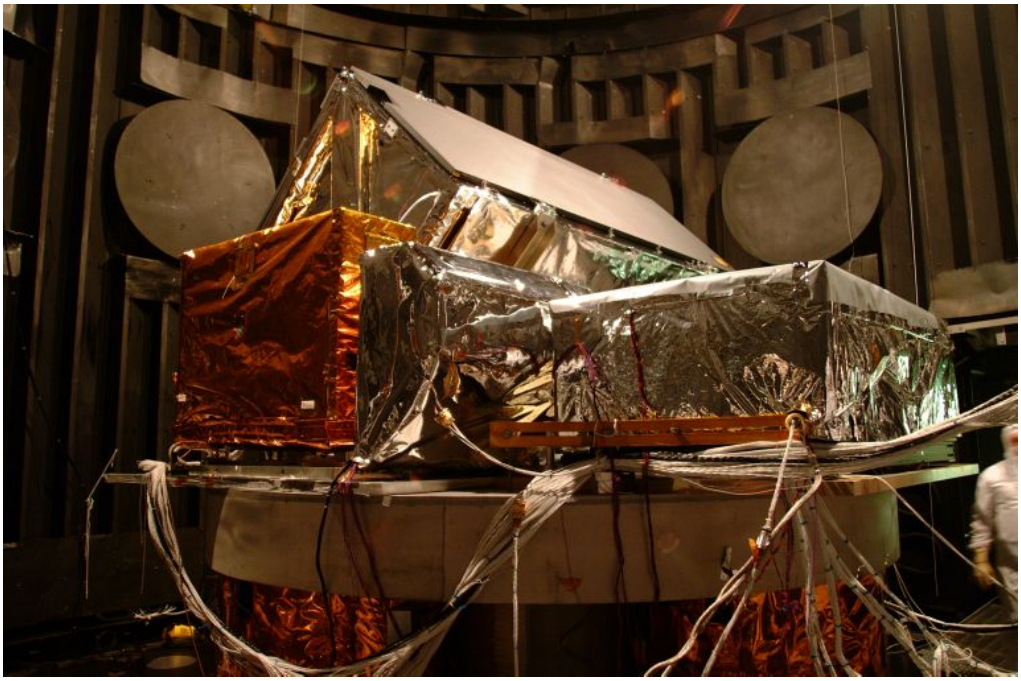

Figure 4.2-2: COS Thermal Vacuum 2006 calibration test configuration showing CDS (far left), the relay optics and RASCAL with COS above and behind.

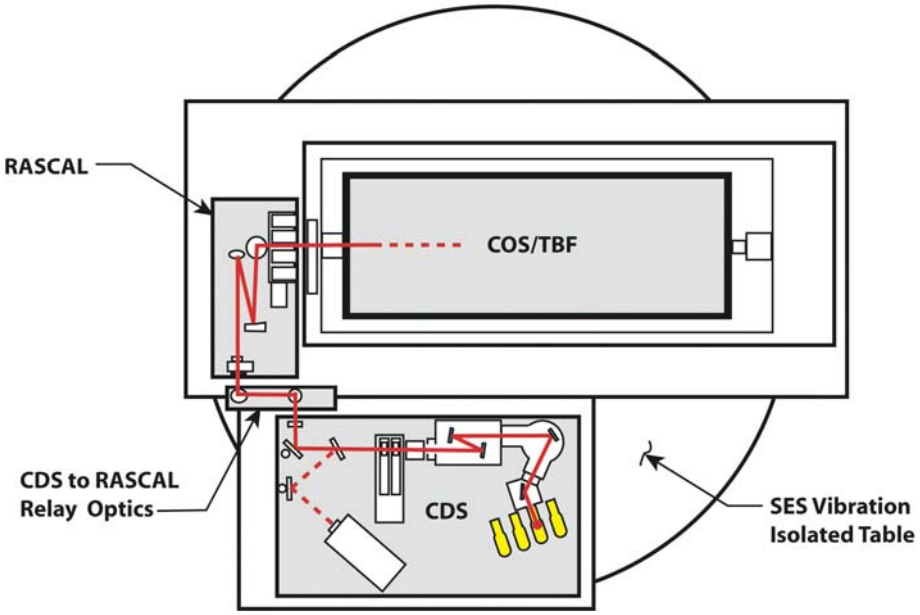

Figure 4.2-3: COS Thermal Vacuum 2006 calibration test configuration. The CDS, relay Optics, RASCAL and COS/TBF were mounted on the vibration isolated table in the GSFC SES chamber. The base plates for CDS and COS/RASCAL were bolted together. The Relay Optics were hard mounted to the COS base plate, while the CDS, RASCAL and COS/TBF were placed on kinematic mounts. The light path from the calibration lamps through the COS entrance aperture is shown. Illustration is not to scale.

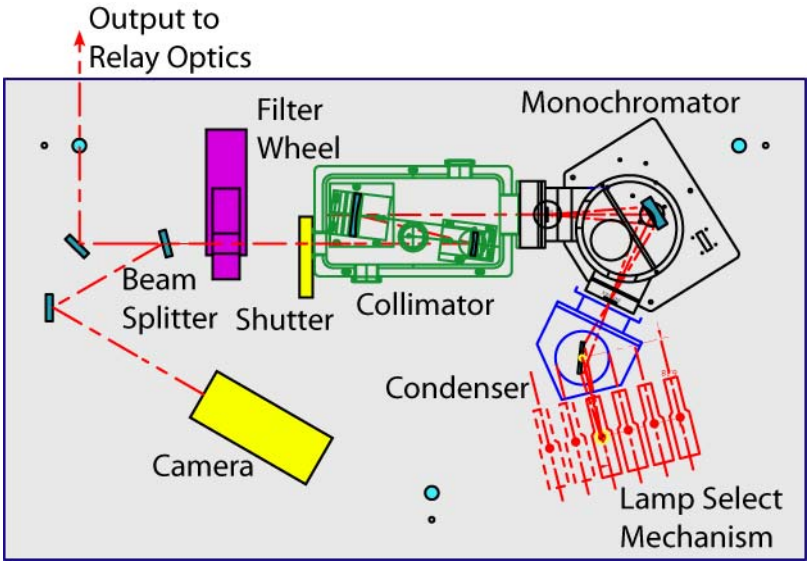

Figure 4.2-4: Vacuum compatible calibration delivery system (CDS) layout. Not to scale.

5. INSTRUMENT PERFORMANCE

5.1 WAVELENGTH SOLUTIONS AND RANGES

5.1.1 CEI Requirements

Tables 4.1 and 4.2 of the CEI list the specific requirements on wavelength coverage.

5.1.2 Description

The wavelength solutions for the NUV and FUV channels are presented below. The wavelength solutions presented were derived using the wavelength calibration spectra. Subsequently, the offsets ($\Delta\lambda$) between the wavelength calibration spectra and the science spectra were measured. This offset must be applied to the y-intercept of the wavelength calibration solution to get the correct wavelength solution for the science spectrum.

Tests: 1160 - CDS Pt-Ne spectra G185M
1170 - CDS Pt-Ne spectra G225M

1180 - CDS Pt-Ne spectra G285M
1190 - CDS Pt-Ne spectra G230L
1110 - FUV CDS Pt-Ne Group 1
1120 - FUV CDS Pt-Ne Group 2

5.1.3 Results from 2003 Appendix B Tests

The tables below present the NUV and FUV wavelength solutions and bandpass values for each wavelength setting and channel. The file names listed and the wavelength solutions given (aside from the $\Delta\lambda$ term) correspond to the internal PtNe calibration exposures . For Table 5.1-1 and Table 5.1-2, λ (min), λ (cen) and λ (max) correspond to the minimum, central and maximum observable wavelengths for that setting, based on the pixel values for the active detector region limits for each segment after thermal and geometric correction. Note that the λ (min) and λ (cen) columns are reversed in Table 5.1-2 relative to Table 5.1-1. These values are approximate wavelengths and may be different in flight due to the final location of the aperture and to repeatability errors within OSM1 and OSM2.

For the FUV channels the wavelengths are computed using

$$\lambda = a_0 (+\Delta\lambda) + a_1 * x + a_2 * x^2$$

where x is in pixels. A first order fit is sufficient for G130M and G160M, so the a_2 values are set to zero for these gratings.

For the NUV channels the wavelengths are computed using

$$\lambda = a_0 (+\Delta\lambda) + a_1 * y + a_2 * y^2$$

where y is in pixels. The $\Delta\lambda$ term is added if the wavelength solution is to be applied to science data as opposed to wavelength calibration spectra.

Table 5.1-1 : FUV Wavelength Solutions

Channel	File	Seg.	λ_c	λ (min)	λ (cen)	λ (max)	a0	a1	a2	$\Delta\lambda$ (Å)
G130M	CSIL03286093403[a]	A	1291	1283.70	1353.80	1423.90	1435.483	-0.0099656	0	0.433
		B		1130.77	1201.52	1272.25	1282.227	-0.0099643	0	0.413
G130M	CSIL03286095158	A	1300	1293.89	1364.00	1434.10	1445.679	-0.0099656	0	0.433
		B		1140.97	1211.72	1282.45	1292.429	-0.0099645	0	0.413
G130M	CSIL03286021646	A	1309	1303.83	1373.94	1444.04	1455.619	-0.0099656	0	0.433
		B		1150.93	1221.68	1292.42	1302.392	-0.0099645	0	0.413
G130M	CSIL03286100953	A	1318	1313.21	1383.32	1453.42	1464.999	-0.0099656	0	0.433

		B		1160.31	1231.05	1301.78	1311.756	-0.0099638	0	0.413
G130M	CSIL03286102748	A	1327	1322.97	1393.08	1463.18	1474.759	-0.0099656	0	0.433
		B		1170.09	1240.83	1311.56	1321.535	-0.0099617	0	0.413

G160M	CSIL03286080403	A	1577	1576.67	1662.50	1748.33	1762.780	-0.012244	0	0.529
		B		1388.50	1472.29	1560.08	1574.523	-0.012238	0	0.513
G160M	CSIL03286082058	A	1589	1588.51	1674.37	1760.18	1774.628	-0.012242	0	0.529
		B		1400.40	1486.17	1571.94	1586.375	-0.012235	0	0.513
G160M	CSIL03286034546	A	1600	1600.06	1685.85	1771.64	1786.080	-0.012238	0	0.529
		B		1411.87	1497.66	1583.45	1597.891	-0.012238	0	0.513
G160M	CSIL03286083753	A	1611	1612.17	1697.95	1783.72	1798.162	-0.012236	0	0.529
		B		1423.98	1509.77	1595.56	1609.997	-0.012238	0	0.513
G160M	CSIL03286085448	A	1623	1624.31	1710.10	1795.89	1810.330	-0.012238	0	0.529
		B		1436.10	1521.94	1607.72	1622.162	-0.012237	0	0.513

G140L	CSIL03286120659	A	1105	1120.64	1686.82	2256.13	2336.657	-0.08047	3.114e-08	3.411
G140L	CSIL03286051016	A	1230	1260.89	1827.55	2396.78	2477.245	-0.08041	2.548e-08	3.411

[a] Exposure names from the thermal vacuum tests are automatically generated and indicate the date and time of the file creation; e.g., CSIL03286093403 indicates that the file was written in year [20]03, day 286, hour 09, minute 34, second 03 (UT time).

Table 5.1-2 : NUV Wavelength Solutions

Channel	File	Stripe	λ_c	λ (cen)	λ (min)	λ (max)	a0	a1	a2	Δλ (Å)
		a		1795.67	1776.49	1814.69	1814.695	-0.03711	-2.23E-07	0.561
G185M	CSIL03265222615	b	1900	1898.72	1880.04	1917.25	1917.247	-0.03613	-2.36E-07	0.470
		c		2003.61	1985.83	2021.57	2021.569	-0.03491	-3.22E-07	0.391
		a		1712.47	1693.12	1731.68	1731.678	-0.03748	-2.06E-07	0.699
G185M	CSIL03266010953	b	1817	1816.56	1797.67	1835.30	1835.300	-0.03655	-2.21E-07	0.593
		c		1922.71	1904.39	1940.86	1940.861	-0.0354	-2.47E-07	0.521
		a		1747.25	1728.00	1766.39	1766.392	-0.03738	-1.48E-07	0.659
G185M	CSIL03266012647	b	1850	1850.92	1832.13	1869.57	1869.567	-0.03638	-2.13E-07	0.567
		c		1956.57	1938.34	1974.63	1974.629	-0.03522	-2.47E-07	0.486
		a		1778.94	1759.78	1798.04	1798.044	-0.03723	-1.67E-07	0.602
G185M	CSIL03266014341	b	1882	1882.21	1863.53	1900.81	1900.816	-0.03623	-2.09E-07	0.517
		c		1987.39	1969.28	2005.39	2005.387	-0.03502	-2.72E-07	0.431
		a		1818.03	1798.97	1837.05	1837.045	-0.03705	-1.73E-07	0.583
G185M	CSIL03266020035	b	1921	1920.8	1902.2	1939.3	1939.298	-0.03599	-2.69E-07	0.505
		c		2025.39	2007.38	2043.29	2043.285	-0.03482	-2.74E-07	0.419
		a		1850.53	1831.51	1869.48	1869.484	-0.03690	-2.12E-07	0.522
G185M	CSIL03266021729	b	1953	1952.88	1934.35	1971.28	1971.284	-0.03579	-3.09E-07	0.448

		c		2056.95	2039.06	2074.77	2074.770	-0.03468	-2.22E-07	0.361
		a		1884.67	1865.74	1903.52	1903.524	-0.03672	-2.07E-07	0.546
G185M	CSIL03266023423	b	1986	1986.54	1968.13	2004.81	2004.879	-0.03568	-2.37E-07	0.438
		c		2090.1	2072.29	2107.8	2107.804	-0.03444	-2.73E-07	0.370
		a		1682.93	1663.56	1702.21	1702.212	-0.03755	-2.25E-07	0.790
G185M	CSIL03266025117	b	1786	1787.37	1768.46	1806.21	1806.207	-0.03667	-2.22E-07	0.674
		c		1893.92	1875.57	1912.2	1912.198	-0.03558	-2.20E-07	0.578
		a		1730.75	1711.46	1749.91	1749.914	-0.03741	-1.79E-07	0.676
G185M	CSIL03266030811	b	1835	1834.62	1815.77	1853.30	1853.302	-0.03644	-2.36E-07	0.602
		c		1940.51	1922.24	1958.61	1958.609	-0.03529	-2.56E-07	0.504
		a		1760.29	1741.07	1779.39	1779.391	-0.03728	-1.72E-07	0.630
G185M	CSIL03266032505	b	1864	1863.82	1845.06	1882.41	1882.408	-0.03626	-2.43E-07	0.549
		c		1969.25	1951.06	1987.27	1987.274	-0.03513	-2.64E-07	0.446
		a		1788.3	1796.16	1807.34	1807.343	-0.03707	-2.53E-07	0.588
G185M	CSIL03266034159	b	1890	1891.45	1872.77	1910.02	1910.019	-0.03613	-2.76E-07	0.471
		c		1996.48	1978.4	2014.47	2014.473	-0.03502	-2.36E-07	0.352
		a		1810.58	1791.5	1829.61	1829.612	-0.03707	-1.83E-07	0.515
G185M	CSIL03266035853	b	1913	1913.45	1894.85	1931.98	1931.979	-0.03610	-1.86E-07	0.419
		c		2018.15	2000.14	2036.08	2036.082	-0.03491	-2.22E-07	0.309
		a		1838.15	1819.1	1857.1	1857.099	-0.03689	-2.44E-07	0.495
G185M	CSIL03266041547	b	1941	1940.64	1922.11	1959.12	1959.121	-0.03601	-1.61E-07	0.377
		c		2044.92	2026.98	2062.77	2062.767	-0.03473	-2.49E-07	0.311
		a		1868.57	1849.62	1887.47	1887.469	-0.03681	-1.84E-07	0.455
G185M	CSIL03266043241	b	1971	1970.68	1952.2	1989.04	1989.035	-0.03570	-2.96E-07	0.366
		c		2074.48	2056.61	2092.23	2092.234	-0.03453	-2.86E-07	0.281
		a		1909.63	1890.79	1928.47	1928.471	-0.03677	-6.42E-08	0.408
G185M	CSIL03266044935	b	2010	2011.17	1992.82	2029.46	2029.459	-0.03560	-2.12E-07	0.348
		c		2114.32	2096.59	2131.96	2131.96	-0.03432	-2.50E-07	0.279

Channel	File	Stripe	λ_c	λ (cen)	λ (min)	λ (max)	a0	a1	a2	Δλ (Å)
		a		2087.85	2069.39	2106.15	2106.1463	-0.035691	-2.36E-07	0.241
G225M	CSIL03266121900	b	2186	2186.78	2168.89	2204.51	2204.5096	-0.034568	-2.48E-07	0.106
		c		2286.92	2269.70	2303.97	2303.9665	-0.033232	-2.60E-07	0.033
		a		2119.01	2100.67	2137.23	2137.2289	-0.035557	-1.78E-07	0.204
G225M	CSIL03266103736	b	2217	2217.45	2199.66	2235.08	2235.0776	-0.034363	-2.57E-07	0.090
		c		2317.02	2299.89	2333.97	2333.9691	-0.033016	-2.90E-07	-0.007
		a		2136.31	2117.99	2154.49	2154.4911	-0.035473	-2.08E-07	0.146
G225M	CSIL03266075357	b	2233	2234.47	2216.73	2252.05	2252.0485	-0.034265	-2.52E-07	0.061
		c		2333.73	2316.66	2350.62	2350.6155	-0.032895	-2.90E-07	-0.079

		a		2153.21	2134.94	2171.31	2171.3134	-0.035313	-2.38E-07	0.119
G225M	CSIL03266105430	b	2250	2251.09	2233.40	2268.62	2268.6245	-0.034214	-2.13E-07	0.050
		c		2350.03	2333.00	2366.84	2366.8427	-0.032714	-3.56E-07	-0.027
		a		2171.97	2153.76	2190.05	2190.0491	-0.035279	-1.89E-07	0.149
G225M	CSIL03266123554	b	2268	2269.56	2251.92	2287.01	2287.0108	-0.034006	-2.87E-07	0.043
		c		2368.15	2351.20	2384.91	2384.9140	-0.032664	-2.89E-07	-0.059
		a		2187.55	2169.35	2205.58	2205.5757	-0.035141	-2.64E-07	0.101
G225M	CSIL03266111124	b	2283	2284.86	2267.29	2302.28	2302.2787	-0.033956	-2.41E-07	0.035
		c		2383.16	2366.26	2399.88	2399.8832	-0.032586	-2.79E-07	-0.055
		a		2208.37	2190.25	2226.33	2226.3299	-0.035025	-2.42E-07	0.089
G225M	CSIL03266125248	b	2306	2305.34	2287.82	2322.68	2322.6808	-0.033803	-2.72E-07	0.002
		c		2403.23	2386.41	2419.87	2419.8699	-0.032411	-2.87E-07	-0.108
		a		2228.74	2210.70	2246.66	2246.6594	-0.034979	-1.71E-07	0.093
G225M	CSIL03266112818	b	2325	2325.38	2307.91	2342.64	2342.6425	-0.033616	-3.26E-07	-0.048
		c		2422.87	2406.12	2439.43	2439.4329	-0.032252	-3.06E-07	-0.095
		a		2242.21	2224.21	2260.05	2260.0539	-0.034780	-2.56E-07	0.059
G225M	CSIL03266130942	b	2339	2338.60	2321.20	2355.91	2355.9071	-0.033828	-9.20E-08	-0.030
		c		2435.85	2419.15	2452.37	2452.3653	-0.032172	-2.93E-07	-0.119
		a		2262.78	2244.83	2280.58	2280.5788	-0.034731	-2.09E-07	0.043
G225M	CSIL03266114512	b	2357	2358.82	2341.48	2375.98	2375.9796	-0.033426	-2.94E-07	-0.054
		c		2455.65	2439.03	2472.09	2472.0909	-0.032033	-2.81E-07	-0.158
		a		2278.28	2260.37	2296.02	2296.0209	-0.034597	-2.49E-07	0.023
G225M	CSIL03266100434	b	2373	2374.04	2356.75	2391.15	2391.1522	-0.033352	-2.74E-07	-0.049
		c		2470.56	2453.96	2486.95	2486.9514	-0.031912	-3.31E-07	-0.173
		a		2295.54	2277.70	2313.24	2313.2361	-0.034533	-1.95E-07	-0.009
G225M	CSIL03266120206	b	2390	2391.00	2373.75	2408.05	2408.0460	-0.033180	-3.37E-07	-0.100
		c		2487.18	2470.66	2503.49	2503.4944	-0.031770	-3.23E-07	-0.191
		a		2316.09	2298.31	2333.72	2333.7245	-0.034402	-2.13E-07	-0.028
G225M	CSIL03266132636	b	2410	2411.19	2394.00	2428.15	2428.1539	-0.033012	-3.63E-07	-0.090
		c		2506.93	2490.51	2523.19	2523.1907	-0.031682	-2.61E-07	-0.212

Channel	File	Stripe	λ_c	λ (cen)	λ (min)	λ (max)	a0	a1	a2	Δλ (Å)
		a		2498.34	2476.19	2520.33	2520.334	-0.04286	-2.83E-07	0.281
G285M	CSIL03266212736	b	2617	2617.21	2595.74	2638.53	2638.530	-0.04154	-2.85E-07	0.213
		c		2737.53	2716.86	2758.04	2758.042	-0.03995	-3.00E-07	0.057
		a		2519.60	2497.50	2541.54	2541.537	-0.04275	-2.89E-07	0.222
G285M	CSIL03266145158	b	2637	2638.13	2616.70	2659.37	2659.367	-0.04133	-3.69E-07	0.129
		c		2758.07	2737.47	2778.50	2778.497	-0.03975	-3.49E-07	0.014
		a		2538.93	2516.90	2560.81	2560.811	-0.04265	-2.63E-07	0.220
G285M	CSIL03266214430	b	2657	2657.16	2635.81	2678.37	2678.369	-0.04134	-2.57E-07	0.116

		c		2776.74	2756.20	2797.11	2797.113	-0.03967	-3.17E-07	0.011
		a		2558.02	2536.03	2579.85	2579.846	-0.04253	-2.97E-07	0.266
G285M	CSIL03266200306	b	2676	2675.94	2654.64	2697.04	2697.042	-0.04108	-3.60E-07	0.151
		c		2795.18	2774.71	2815.49	2815.493	-0.03956	-2.94E-07	0.065
		a		2578.44	2556.56	2600.25	2600.247	-0.04256	-1.36E-07	0.167
G285M	CSIL03266155716	b	2695	2696.05	2674.82	2717.12	2717.120	-0.04105	-2.97E-07	0.055
		c		2814.91	2794.50	2835.14	2835.138	-0.03935	-3.60E-07	-0.027
		a		2593.01	2571.12	2614.75	2614.746	-0.04236	-2.78E-07	0.216
G285M	CSIL03266202000	b	2709	2710.37	2689.15	2731.38	2731.380	-0.04087	-4.01E-07	0.105
		c		2828.96	2808.59	2849.14	2849.141	-0.03928	-3.47E-07	0.000
		a		2601.00	2579.13	2622.71	2622.706	-0.04229	-3.01E-07	0.147
G285M	CSIL03266170234	b	2719	2718.23	2697.04	2739.20	2739.196	-0.04079	-4.02E-07	0.064
		c		2836.66	2816.31	2856.81	2856.806	-0.03920	-3.81E-07	-0.072
		a		2622.00	2600.21	2643.66	2643.657	-0.04222	-2.50E-07	0.172
G285M	CSIL03266220124	b	2739	2738.87	2717.77	2759.80	2759.798	-0.04074	-3.30E-07	0.031
		c		2856.91	2836.67	2877.04	2877.042	-0.03926	-2.03E-07	-0.002
		a		2736.60	2715.14	2757.91	2757.911	-0.04153	-2.73E-07	-0.005
G285M	CSIL03266221818	b	2850	2851.50	2830.79	2872.07	2872.065	-0.04006	-2.81E-07	-0.132
		c		2967.29	2947.43	2986.96	2986.963	-0.03826	-3.76E-07	-0.236
		a		2840.02	2818.90	2861.00	2861.002	-0.04088	-2.67E-07	-0.130
G285M	CSIL03266180752	b	2952	2953.04	2932.72	2973.23	2973.232	-0.03934	-2.52E-07	-0.202
		c		3066.69	3047.22	3085.98	3085.983	-0.03753	-3.51E-07	-0.332
		a		2866.53	2845.52	2887.44	2887.435	-0.04078	-1.89E-07	-0.075
G285M	CSIL03266203654	b	2979	2979.06	2958.76	2999.14	2999.138	-0.03905	-4.13E-07	-0.230
		c		3092.14	3072.77	3111.31	3111.305	-0.03726	-4.08E-07	-0.310
		a		2884.75	2863.77	2905.55	2905.554	-0.04049	-3.49E-07	-0.141
G285M	CSIL03266223512	b	2996	2996.91	2976.72	3016.95	3016.946	-0.03902	-2.97E-07	-0.243
		c		3109.62	3090.31	3128.73	3128.734	-0.03718	-3.70E-07	-0.382
		a		2906.44	2885.52	2927.20	2927.196	-0.04042	-3.13E-07	-0.170
G285M	CSIL03266205348	b	3018	3018.19	2998.06	3038.14	3038.135	-0.03881	-3.50E-07	-0.232
		c		3130.41	3111.20	3149.45	3149.445	-0.03703	-3.47E-07	-0.337
		a		2923.99	2903.18	2944.70	2944.698	-0.04037	-2.11E-07	-0.172
G285M	CSIL03266225206	b	3035	3035.41	3015.37	3055.30	3055.301	-0.03875	-2.82E-07	-0.280
		c		3147.23	3128.21	3166.22	3166.221	-0.03711	-4.42E-08	-0.422
		a		2947.63	2926.85	2968.23	2968.228	-0.04010	-3.34E-07	-0.284
G285M	CSIL03266211042	b	3057	3058.57	3038.59	3078.38	3078.376	-0.03856	-3.19E-07	-0.361
		c		3169.89	3150.80	3188.70	3188.696	-0.03647	-5.60E-07	-0.479
		a		2965.13	2944.43	2985.66	2985.655	-0.03994	-3.53E-07	-0.254
G285M	CSIL03266191310	b	3074	3075.73	3055.81	3095.44	3095.437	-0.03834	-3.91E-07	-0.371
		c		3186.64	3167.63	3205.43	3205.429	-0.03652	-4.24E-07	-0.423

		a		2984.08	2963.45	3004.57	3004.567	-0.03992	-2.69E-07	-0.233
G285M	CSIL03266230900	b	3094	3094.30	3074.47	3113.91	3113.910	-0.03815	-3.93E-07	-0.367
		c		3204.80	3185.83	3223.47	3223.473	-0.03623	-5.54E-07	-0.446

Channel	File	Stripe	λ_c	λ (cen)	λ (min)	λ (max)	a0	a1	a2	Δλ (Å)
		a		1539.56	1343.61	1738.14	1739.14	-0.39334	6.92E-06	20.06
G230L	CSIL03267064458	b	2635	2630.13	2430.46	2828.98	2828.98	-0.38869	-8.43E-07	19.30
		c		1883.88	1784.68	1982.66	1982.66	-0.19311	-4.06E-07	8.51[a]
		a		1852.23	1652.14	2051.69	2051.69	-0.39009	-4.58E-07	19.32
G230L	CSIL03267091836	b	2950	2942.43	2742.98	3141.13	3141.13	-0.38850	-6.80E-07	18.17
		c		2039.71	1940.50	2138.18	2138.18	-0.19215	-1.05E-06	8.18[a]
		a		1911.58	1711.55	2110.82	2110.82	-0.38950	-7.63E-07	19.06
G230L	CSIL03267074616	b	3000	3001.69	2802.13	3200.20	3200.20	-0.38784	-1.25E-06	18.95
		c		2069.68	1972.95	2168.29	2168.29	-0.19498	3.95E-06	5.75[a]
		a		2279.03	2079.17	2478.33	2478.33	-0.38985	-3.23E-07	18.99
G230L	CSIL03267084734	b	3360	3368.69	3169.24	3566.85	3566.85	-0.38692	-1.71E-06	18.18
		c		2252.22	2153.36	2350.83	2350.83	-0.19294	-8.50E-08	8.25[a]

[a] Second-order light.

5.1.4 Results of 2006 measurements

The measurements of the wavelength solutions for all of the COS spectroscopic modes were repeated in Appendix C. The relevant test numbers are given below. Between 2003 and 2006, the 'tag-flash' observing mode was implemented to correct for spectral drifts in the data caused by motions of the OSM1 and OSM2 mechanisms (see Section 5.9). When tag-flash is used, the internal PtNe wavelength calibration lamp is exposed periodically during a science exposure. The Appendix C observations used tag-flash, eliminating the need for the separate internal wavecal exposures that were obtained in the 2003 tests. Accordingly, the tests listed below are equivalent to their 2003 complements (e.g., Tests 1160 and 1161 are paired) in execution, except for the removal of separate internal wavecals and the use of tag-flash during the external exposures.

Tests: 1161 - CDS Pt-Ne spectra G185M
1171 - CDS Pt-Ne spectra G225M
1181 - CDS Pt-Ne spectra G285M
1191 - CDS Pt-Ne spectra G230L
1111 - FUV CDS Pt-Ne Group 1
1121 - FUV CDS Pt-Ne Group 2

There were only minor changes in the wavelength solutions between the 2003 and 2006 measurements. The spectral dispersions remained the same for all of the gratings. The zero points of the science and calibration stripes changed slightly: about 0.5 Å for G130M and G160M, and 4.7 Å for G140L in the FUV modes, for example, and 0.85 Å and 2 Å for G225M on the NUV side. The change in the zero points of the science frames is most likely attributable to a different placement of the COS aperture block relative to RASCAL in the two test setups, except for the larger offset in G225M, which is the result of a change in the flight software commanding for the central wavelength of the grating between 2003 and 2006.

5.2 SPECTRAL RESOLUTION

5.2.1 CEI Requirements

Section 4.2.2 and Table 4-4 of the CEI present the spectral resolution requirements for COS. In short, the G130M, G160M, G225M, and G285M channels shall support a spectral resolution $(\lambda/\Delta\lambda) > 20{,}000$, the G185M shall support $R > 16{,}000$, and the G140L and G230L shall support $R>2000$. The spectral resolution must also be achieved over 80% of the usable bandpass.

5.2.2 Description

The resolutions of the FUV channels were computed using drift corrected exposures with exposure times of 6500 seconds to give accurate representations of the expected instrument resolution. In addition, for the FUV spectra care was taken to extract only those lines identified as narrow and isolated, to remove the potential for naturally broad or multiple lines to appear as degraded resolution.

For the NUV channels the large number of wavelength settings made collecting long exposures and drift correcting all the data impractical, so short exposures were used to measure the spectral resolution. Also, the sheer number of lines and wavelength settings for the NUV channel made it inefficient to hand-select isolated, narrow emission lines, so all the emission lines were measured. This means there appear to be a certain number of lines that do not meet the spectral resolution requirements. It is highly likely that these lines do not reflect poor resolution and should be ignored. Finally, the G185M and G225M resolutions were measured at GN2 to minimize a thermal distortion between the COS thermal balance fixture and RAS/Cal. Thus some of the shortest lines in the G185M channel were not measured, as the GN2 blocked those lines.

Tests: 2300 – FUV Grating Stability

1155 – G185M NUV Pt-Ne Spectra in GN2
1156 – G225M NUV Pt-Ne Spectra in GN2
1180 – G285M NUV Spectra of Pt-Ne Lamp
1190 – G230L NUV Spectra of Pt-Ne Lamp

Relevant Exposures:

Table 5.2-1: Exposure list for 2003 Spectral Resolution Measurements

File	Channel/λ_C	Comments
CSIL03285043406	G130M/1309	t_{exp}=6500
CSIL03285081037	G160M/1600	t_{exp}=6500
CSIL03285101309	G140L/1240	t_{exp}=6500
CSIL03295043202	G185M/2010	GN2 environment
CSIL03295044431	G185M/1986	"
CSIL03295045701	G185M/1971	"
CSIL03295050931	G185M/1953	"
CSIL03295052200	G185M/1941	"
CSIL03295053429	G185M/1921	"
CSIL03295054700	G185M/1913	"
CSIL03295055931	G185M/1900	"
CSIL03295061201	G185M/1890	"
CSIL03295062431	G185M/1882	"
CSIL03295063700	G185M/1864	"
CSIL03295064931	G185M/1850	"
CSIL03295070201	G185M/1835	"
CSIL03295071430	G185M/1817	"
CSIL03295072700	G185M/1786	"
CSIL03295073831	G225M/2410	"
CSIL03295074601	G225M/2390	"
CSIL03295075331	G225M/2373	"
CSIL03295080100	G225M/2357	"
CSIL03295080831	G225M/2339	"
CSIL03295081600	G225M/2325	"
CSIL03295082331	G225M/2306	"
CSIL03295083101	G225M/2283	"

CSIL03295083830	G225M/2268	"
CSIL03295084600	G225M/2250	"
CSIL03295085330	G225M/2233	"
CSIL03295090100	G225M/2217	"
CSIL03295090831	G225M/2186	"
CSIL03266144527	G285M/2637	Vacuum environment
CSIL03266155045	G285M/2695	"
CSIL03266165603	G285M/2719	"
CSIL03266180121	G285M/2952	"
CSIL03266190639	G285M/3074	"
CSIL03266193941	G285M/2637	"
CSIL03266195635	G285M/2676	"
CSIL03266201329	G285M/2709	"
CSIL03266203023	G285M/2979	"
CSIL03266204717	G285M/3018	"
CSIL03266210411	G285M/3057	"
CSIL03266212105	G285M/2617	"
CSIL03266213759	G285M/2657	"
CSIL03266215453	G285M/2739	"
CSIL03266221147	G285M/2850	"
CSIL03266222841	G285M/2996	"
CSIL03266224535	G285M/3035	"
CSIL03266230229	G285M/3094	"
CSIL03267063927	G230L/2635	"
CSIL03267074045	G230L/3000	"
CSIL03267084203	G230L/3360	"
CSIL03267091305	G230L/2950	"

5.2.3 2003 Results - FUV

Figures 4.2-1, 4.2-2, and 4.2-3 show the spectral resolution for the G130M, G160M, and G140L channels respectively. Tables 4.2-1 and 4.2-2 list the wavelengths and measured resolutions in tabular form. The G130M channel does exceed 20,000 over the central portions of the bandpass, but fails to meet the 80% criteria. The G160M just meets the requirement and the G140L easily meets the spectral resolution requirements.

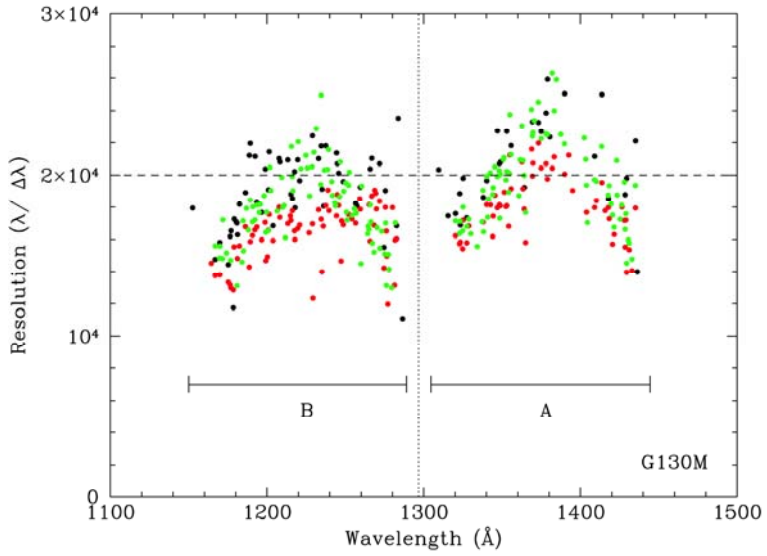

Figure 5.2-1 : G130M spectral resolution. The red dots are the measured spectral resolution BEFORE correcting for mechanism drift. The green dots are the same data AFTER correcting for drift. The black dots show the spectral resolution measured from a short 100 second exposure.

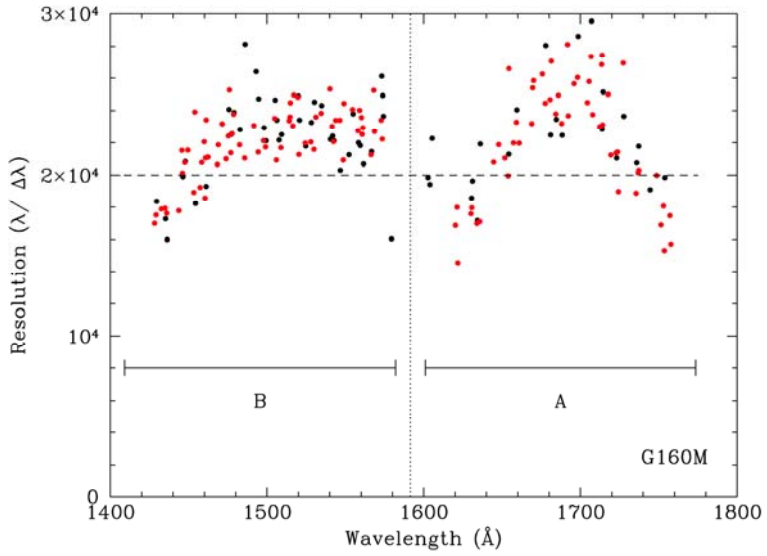

Figure 5.2-2: G160M spectral resolution. In this case the red dots are the spectral resolution as measured from a t_{exp} = 6500 exposure. The black dots are for a 100 second exposure spectrum. No drift correction was required for this data set as there was essentially no drift.

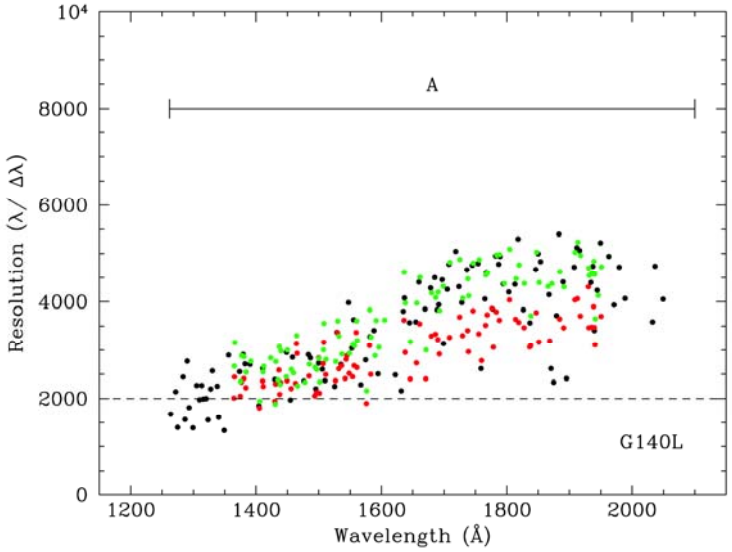

Figure 5.2-3: G140L spectral resolution. The red dots are the measured spectral resolution BEFORE correcting for mechanism drift. The green dots are the same data AFTER correcting for drift. The black dots show the spectral resolution measured from a short 100 second exposure.

Table 5.2-2: Wavelength and Measured Spectral Resolutions for G130M and G160M

G130M-A		G130M-B		G160M-A		G160M-B	
λ (Å)	R (λ/Δλ)	λ (Å)	R (λ/Δλ)	λ (Å)	R (λ/Δλ)	λ (Å)	R (λ/Δλ)
1436.34	13987.45	1286.47	11077.47	1410.14	14316.14	1602.77	19103.34
1435.15	22099.85	1283.69	23519.16	1413.67	13349.1	1605.35	18537.53
1429.53	19796.81	1282.64	16833.88	1417.83	14601.75	1604.74	22957.65
1428.6	18774.01	1275.51	19028.68	1418.38	17171.67	1606.26	20332.41
1417.84	18511.48	1274.63	15512.14	1420.56	14407.3	1610.13	15926.11
1413.69	24988.89	1271.81	20695.52	1421.54	16415.01	1613.98	18319.86
1409.05	21146.65	1266.91	21024.81	1428.57	16767.25	1614.41	19687.93
1389.89	25053.41	1265.74	20365.71	1429.52	17079.09	1620.68	19959.11
1383.29	23986.98	1259.53	19247.95	1432.92	16489.3	1621.65	16927.45
1380.52	22355.84	1257.23	18084.29	1435.13	15481.45	1630.51	17996.8
1379.02	25927.98	1256.57	18231.42	1436.32	18250.57	1631.1	17652.6

1378.07	23855.24	1248.63	19588.24	1446.28	18807.28	1634.23	17497.11
1374.95	22705.05	1245.69	20107.58	1447.8	19485.87	1636.15	17669.01
1373.23	23250.27	1244.84	20692.67	1454.28	18862.26	1644.46	17797.19
1369.42	23303.7	1244.37	21356.79	1461.08	21144.43	1652.12	19857.21
1364.17	19236.6	1237.5	21797.78	1461.49	21429.47	1654.27	22086.38
1355.76	21814.14	1236.09	18064.82	1462.67	20091.62	1659.47	21220.84
1353.02	22716.67	1235.12	19107.55	1464.14	18509.99	1669.23	24692.75
1348.88	20803.39	1234.58	21784.54	1475.64	22290.63	1676.02	23473.67
1348.32	20699.3	1232.9	21016.1	1482.83	22777.73	1677.85	24674.27
1347.02	22729.85	1229.05	22436.04	1494.72	23138.08	1679.19	25365.41
1340.21	19643.62	1220.82	19643.02	1498.12	22393.42	1680.88	22087.78
1337.94	18605.42	1219.53	20930.45	1499.38	22213.04	1681.69	25364.86
1327.49	17331.93	1217.82	17954.67	1505.24	21783.5	1684.58	23139.84
1325.16	19798.86	1217.52	20205.19	1506.29	23138.09	1686.25	21985.01
1323.36	16882.77	1216.14	18528.5	1507.63	19554.21	1688.36	23065.03
1322.91	18840.03	1215.27	18800.54	1509.3	21842.26	1692.15	24666.91
1320.26	17603.71	1213.25	20929.93	1524.73	21844.27	1696.29	23141.75
1315.62	17449.19	1208.23	20807.53	1528.29	22310.8	1698.49	25388.49
1309.58	20322.1	1207.68	21014.32	1530.2	23433.38	1707.08	24111.3
		1203.78	16833.11	1534.9	24957.72	1712.66	24054.21
		1201.32	21423.57	1540.5	20761.46	1713.83	23704.43
		1200.84	19077	1541.83	22026.14	1714.47	22150.78
		1198.81	20365.82	1542.71	21249.45	1723.14	20489.18
		1196.59	17667.55	1546.83	21909.77	1727.67	20518.64
		1193.48	18322.21	1552.32	20697.6	1737.18	20129.55
		1192.3	21150.04	1554.93	22276.94	1737.59	21061.7
		1189.34	21950.72	1559.4	22865.1	1744.43	17035.45
		1188.73	21199.01	1561.55	22024.68	1746.45	21246.35
		1186.26	18905.08	1566.73	19657.84	1753.83	18403.25
		1182.4	18179.99	1568.89	21550.69	1758.12	16824.12
		1181.15	16289.71	1573.18	22002.52	1764.6	107597.57
		1180.77	17008.71	1573.83	19896.71	1766.02	17983.91
		1180.29	17075.38	1574.31	22426.07	1767.15	17410.34
		1179	17255.67	1579.45	19993.04	1776.57	19206.16
		1178.47	11749.81	1581.41	15973.84	1777.08	17560.08
		1177.02	16527.96				
		1176.45	16180.43				
		1175.19	14424.29				
		1169.8	15807.51				

		1166.9	14755.56				
		1152.45	17939.24				

Table 5.2-3: Wavelength and Measured Spectral Resolution for G140L

λ (Å)	R (λ/Δλ)	λ (Å)	R (λ/Δλ)	λ (Å)	R (λ/Δλ)	λ (Å)	R (λ/Δλ)
2049.52	4050.98	1826.44	3833.79	1669.68	3846.19	1429.98	2392.47
2036.56	4734.84	1813.11	4360.98	1644.97	3566.37	1410.52	2622.51
2032.59	3582.43	1803.26	4200.22	1636.79	4077.77	1404.34	1846.62
1988.78	4065.58	1794.45	4366.37	1634.74	3800.65	1390.36	2701.26
1979.47	4715.86	1789.48	4939.32	1631.61	2156.77	1382.49	2711.17
1971.18	3933.36	1786.98	4774.67	1622.2	2488.16	1379.5	2910.27
1962.84	4939.16	1782.21	4951.97	1594.68	2507.33	1373.76	2550.39
1949.54	5220.15	1777.52	3847.1	1588.2	3402.09	1356.18	2895.18
1944.25	4237.22	1767.64	4605.18	1581.96	3276.69	1349.17	1334.4
1939.76	3404.45	1765.14	4058.64	1574.93	2795.47	1340.45	1607.43
1937.28	4732.3	1758.69	2614.32	1567.22	2283.64	1338.15	2250.85
1934.18	4398.89	1754.35	4789.63	1555.47	3629.81	1330.39	2568.8
1916.12	5065.72	1745.03	4753.83	1552.87	3040.55	1327.73	2195.01
1911.73	5118.91	1736.42	4659.44	1547.38	3981.66	1323.32	1552.71
1907.56	4714.85	1728.24	3981.1	1535.42	2702.37	1320.43	1996
1895.31	2411.24	1723.66	4311.34	1528.92	3367.21	1315.78	1986.57
1889.69	4409.74	1718.56	5043.54	1525.32	2246.1	1313.16	2266.61
1883.24	5400.34	1707.66	4776.61	1510.02	2365.31	1309.8	1972.78
1879.32	3714.57	1705.25	4256.79	1505.87	2602.83	1305.34	2265.61
1874.69	2330.6	1699.13	3135.83	1500.05	2728.24	1299.54	1389.5
1870.7	2616.33	1696.86	4457.84	1495.38	2199.42	1293.17	1806.59
1867.3	4148.88	1691.42	3939.72	1486.67	2835.6	1290.17	2768.41
1853.81	4829.67	1688.8	3833.86	1483.5	2904.72	1286.54	1562.22
1850.01	4996.36	1685.09	4502.43	1476.27	2356.64	1283.65	2440.96
1846.12	4664.17	1678.42	4283.67	1458.14	2850.61	1274.84	1397.68
1836.92	3563.31	1660.05	4407.33	1454.75	1968.68	1271.74	2136.27
1818.15	5298.56	1654.82	3581.54	1448.38	2951.24	1263.66	1675.7

5.2.4 2003 Results – NUV

Figure 4.2-4 shows the spectral resolution for the NUV channels. It is apparent that the G225M, G285M, and G230L channels all meet specifications. However, the G185M appears to have lower resolution than specified at the shortest wavelengths. This is thought to be due to residual misalignment between RASCAL and COS.

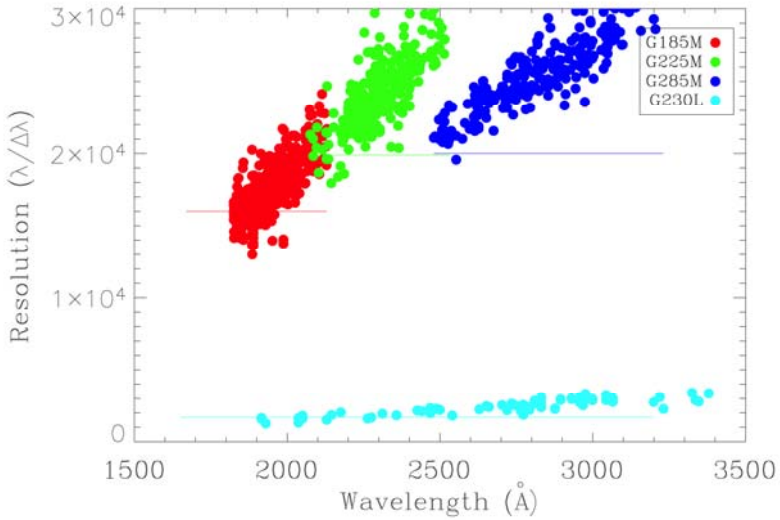

Figure 5.2-4: Measured spectral resolution for the four NUV channels. The solid lines indicate the bandpass of each channel. The filled circles represent the measured spectral resolution for individual emission lines. The G225M, G285M, and G230L channels all clearly meet their respective spectral resolution requirements. The G185M data indicates that the spectral resolution may not meet requirements at the shortest wavelengths, where data do not exist due to absorption of the shortest wavelenghs by the GN2. This is thought to be due to a slight misalignment between COS and RASCAL. Also note that the G185M and G225M data were acquired with the instrument at GN2, not vacuum, in order to minimize the misalignment between COS and RASCAL.

5.2.5 2006 Test Results

Analysis of the spectral resolution of the COS data was repeated in 2006. The external wavecal spectra used to determine the wavelength solutions were also used to find spectral resolutions. Unlike in 2003, all the data analyzed were acquired in vacuum. No corrections were made for drifts, but the exposure times of the data (300 sec) were shorter than the exposures analyzed in 2003. The alignment between the COS thermal balance fixture and RASCAL was much better in

2006 than in 2003, leading to the expectation that some of the low spectral resolutions measured in Appendix B would be improved in 2006.

Tests: 1111 - FUV CDS Pt-Ne Group 1
1161 - CDS Pt-Ne spectra G185M
1171 - CDS Pt-Ne spectra G225M
1181 - CDS Pt-Ne spectra G285M
1191 - CDS Pt-Ne spectra G230L

Figure **5.2-5**, Figure **5.2-6**, and Figure **5.2-7** show the measured spectral resolutions for the FUV gratings from the 2006 tests. The 2006 version of the CDS delivered fewer FUV counts to COS than in 2003, so there were fewer external calibration lines of sufficient signal to measure the FWHM for spectral resolution determinations. This was particularly true for G130M, where the number of measured lines is small and the scatter on the measurements relatively large. However, there is enough data to show that the G130M spectral resolutions are higher in the 2006 data than in 2003. The more recent measurements indicate that G130M meets the spectral resolution requirement of R≥20,000 over 80% of the active waveband. (We don't have measurements <1180 Å, but there is no reason to expect the spectral resolution to decline more than the linear drop with wavelength.) The G160M and G140L measurements are consistent with the 2003 results.

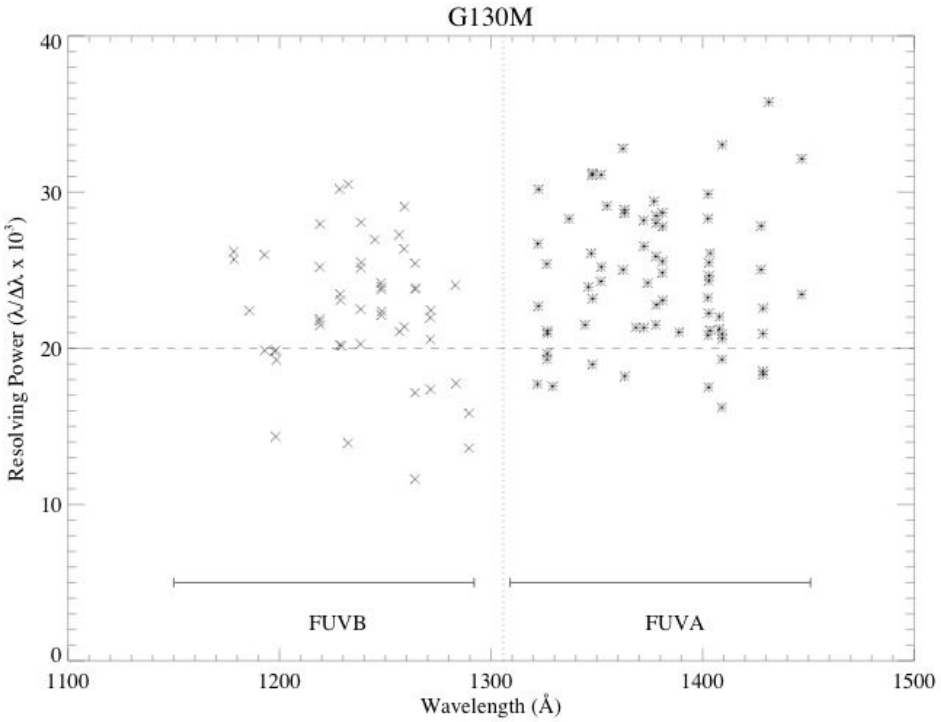

Figure 5.2-5: The measured spectral resolutions for the G130M grating from the 2006 thermal vacuum tests. The solid lines show the active bandpasses for the two grating segments while the dotted line shows the spectral resolution requirement for the grating.

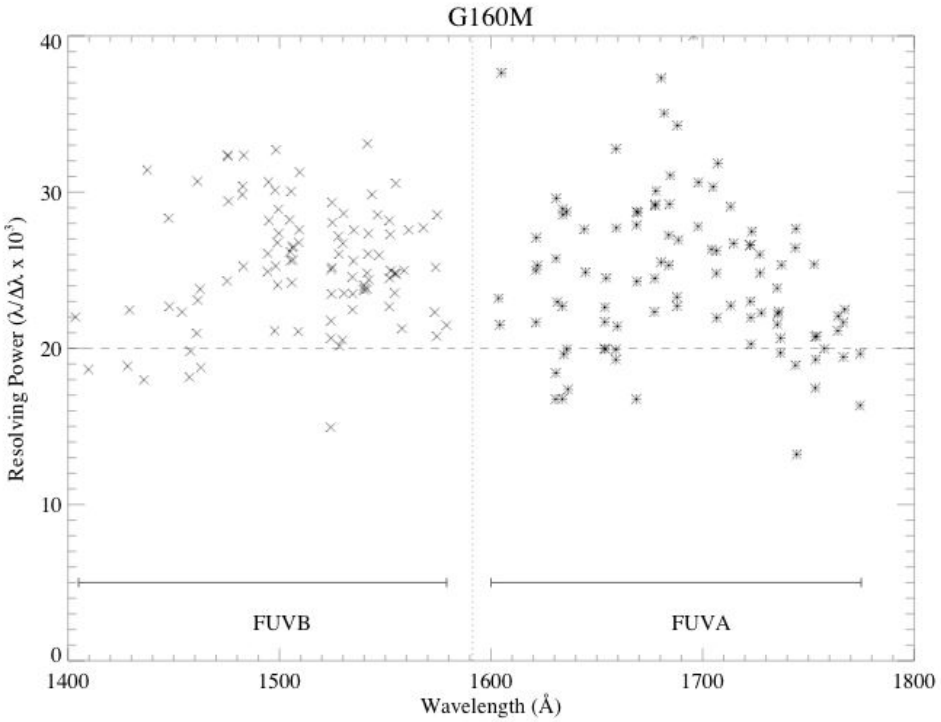

Figure 5.2-6: The measured spectral resolutions for the G160M grating from the 2006 thermal vacuum tests. The solid lines show the active bandpasses for the two grating segments while the dotted line shows the spectral resolution requirement for the grating.

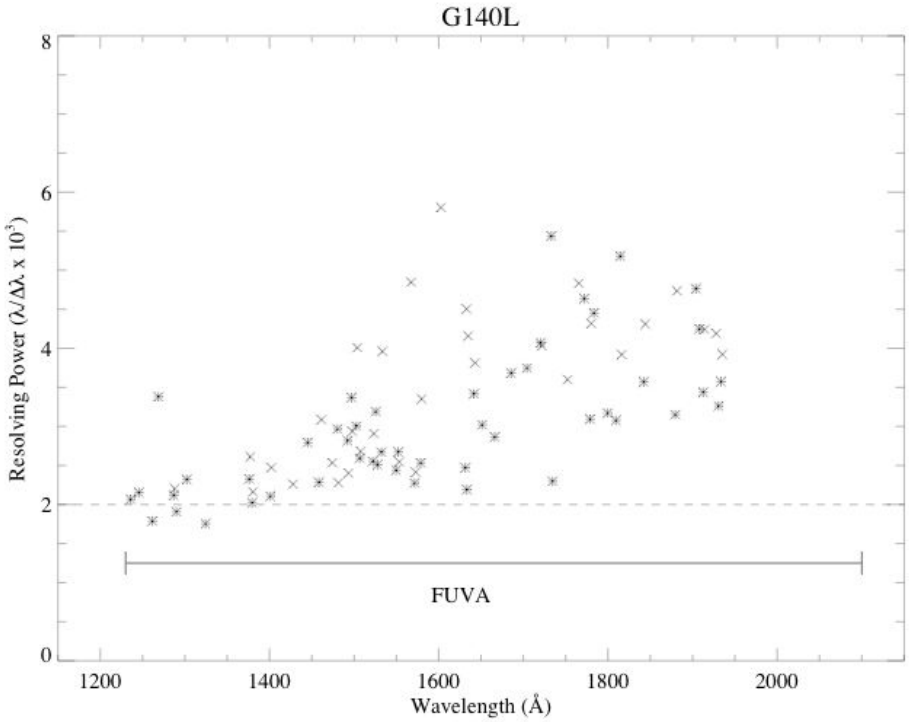

Figure 5.2-7: The measured spectral resolutions for the G140lM grating from the 2006 thermal vacuum tests. The solid line shows the active bandpass for the grating segment while the dotted line shows the spectral resolution requirement for the grating.

Figure 5.2-8 shows the resolution as a function of wavelength for the NUV gratings. As expected, the measured spectral resolutions are higher in 2006 than in 2003, due to the improved alignment in the test configuration. In particular, G185M now meets the spectral resolution requirement over the full bandpass. As with the 2003 data, the highest and lowest spectral resolution points are likely artifacts: in the former case, caused by poor detections of faint features with anomalously narrow spreads and in the latter case, by poor fits to lines or line blends.

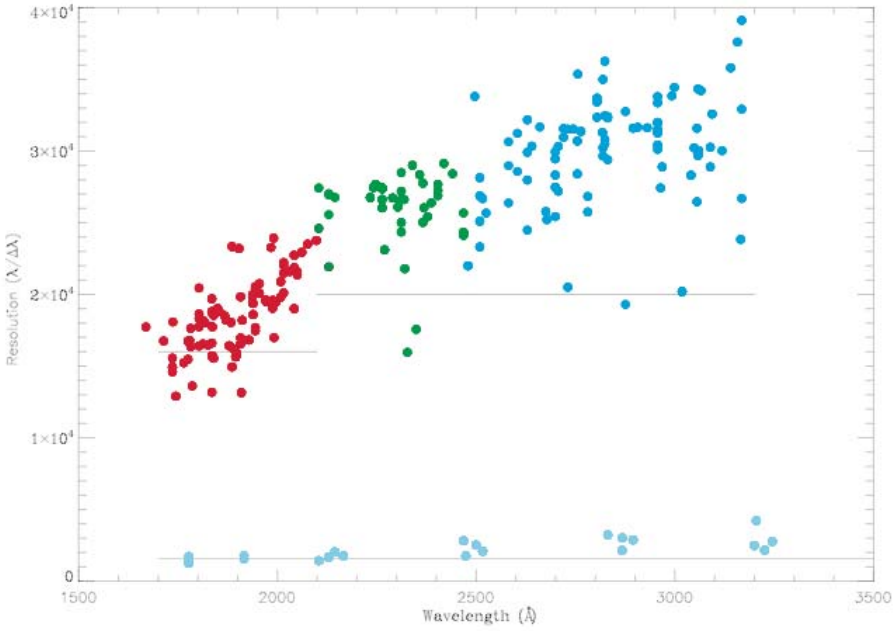

Figure 5.2-8: Spectral resolution as a function of wavelength for the NUV modes. G185M is in red, G225M is in green, G285M is in blue, and G230L is in light blue. The solid lines indicate the bandpass and spectral resolution requirement for each channel.

5.2.6 BOA Spectral Resolution

When COS was first assembled and tested in a GN_2 environment it was discovered that the image quality through the BOA was severely degraded. The BOA is a 2 mm diameter piece of a MgF_2 neutral density that is 2 mm thick. The BOA was fabricated by taking a far larger neutral filter and reshaping it to meet the needs of the COS project.

When the poor image quality was first identified two potential causes of the degradation were investigated: wedge within the BOA and a tilt of the BOA due to installation error. Tilt of the BOA was quickly ruled out. Ray-trace modeling of the COS TA1 channel including a 15 arc-minute wedge successfully reproduced the observed point spread function (see Figures 4.2-9 and 4.2-10). An attempt was made to directly measure the wedge in the spare BOA, however, the small dimensions of the BOA made a direct measurement impossible. As a side note, when the

optic was procured there was no specification on the wedge of the part; wedge being defined as the angle between the front and back surfaces of the filter. Therefore, in the absence of any other empirical data the cause of the degradation in image quality is assumed to be due to a 15 arc-minute wedge between the front and back surfaces of the BOA.

5.2.6.1 Description

During Appendix B testing data were acquired to measure the BOA transmission function (see section 4.5) using the NUV and FUV low resolution modes, G230L and G140L. These data sets can be used to determine the spectral resolution for these channels, which is presented in this section.

The performance of the medium resolution channels can be estimated using empirical data and theoretical models, as discussed below.

Tests: 3300 – FUV BOA transmission & resolution
3310 – NUV BOA transmission & resolution

Relevant Exposures:

Table 5.2-4: Exposures for 2003 BOA spectral resolution tests.

File	Channel/λ_C	Comments
xp=1800 s C104	G140L/ 1320Å	t_{exp}=1800 s
CSIL03267212608	G285M/3000	t_{exp}=1800 s
CSIL03267223054	G285M3360	t_{exp}=1800 s
CSIL03267233540	G285M2635	t_{exp}=1800 s

5.2.6.2 2003 Results

Figure **5.2-9** and Figure 5.2-10 show the measured BOA spectral resolution and the spectrum used to measure the resolution for the FUV G140L channel. Figure 5.2-11 and Figure 5.2-12 present the same information for the NUV G230L channel. The FUV BOA resolution is ~1500, about 0.75 times that of the PSA, which has a spectral resolution requirement of ≥ 2000. The NUV BOA resolution is ~500, about 3 times lower than the spectral requirement of ≥ 1700.

The resolution of the NUV M modes can be estimated from a TA1 image, because the NUV gratings are planar and are inserted into a collimated beam. Figure 5.2-13 shows the point spread

function for a point source taken through the BOA, the corresponding dispersion (vertical profile) and cross-dispersion (horizontal profile) line profiles, and Gaussian fits to the profiles. Figure 5.2-14 shows the predicted results from a ray-trace model of the TA1 channel assuming a 15 arc-minute wedge in the BOA. Because the resolution of the NUV channel is dispersion limited, it is possible to estimate the spectral resolution for the medium resolution channels using the known image size and measured dispersion. Figure **5.2-15** shows the predicted resolutions based on the measured image size of 14.26 pixels FWHM (based on the TA1 image shown in Figure 5.2-13).

Finally, Figure **5.2-16** shows the predicted spectral resolution for the FUV G130M and G160M channels based on a ray-trace model of the two channels that includes a 15 arc-minute wedge in the BOA.

Table 5.2-5: BOA 2003 spectral resolutions.

Channel	λ	Δλ	R = λ/Δλ	a0	a1	dispersion
G225M	2250	0.52	3541.34	-0.03642	-2.09E-07	0.0366
G225M	2250	0.49	4582.52	-0.03423	-1.97E-07	0.0344
G285M	2850	0.57	4957.55	-0.04005	-2.58E-07	0.0403
G230L	3000	5.55	540.93	-0.38774	-1.15E-06	0.389

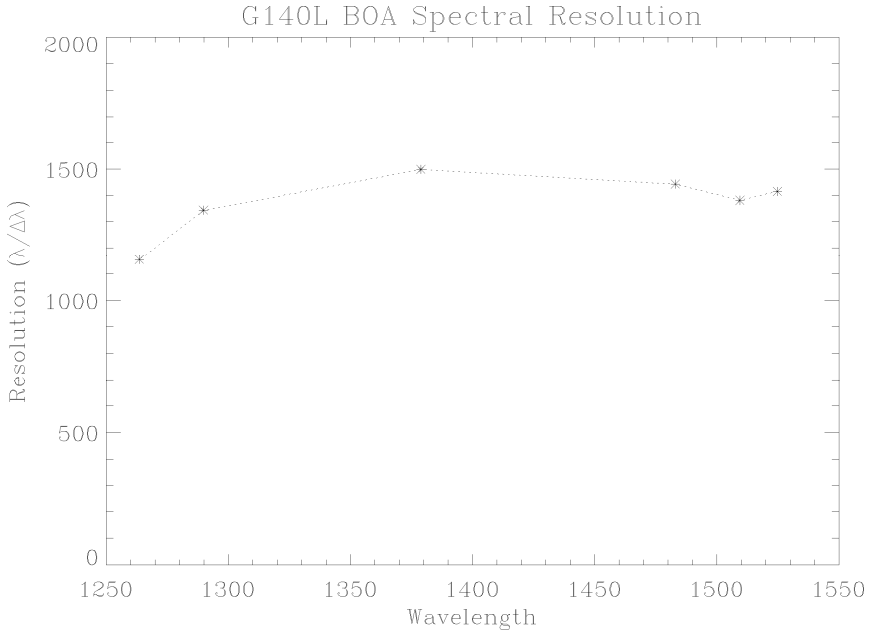

Figure 5.2-9: Measured spectral resolution for the G140L channel.

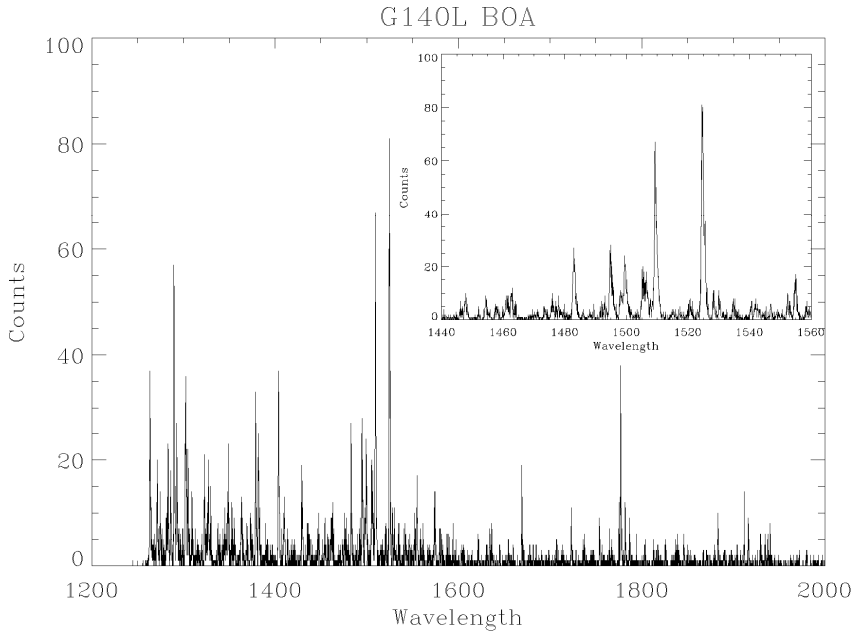

Figure 5.2-10: The PtNe spectrum acquired through the BOA. The data is from file CSIL03285213104.

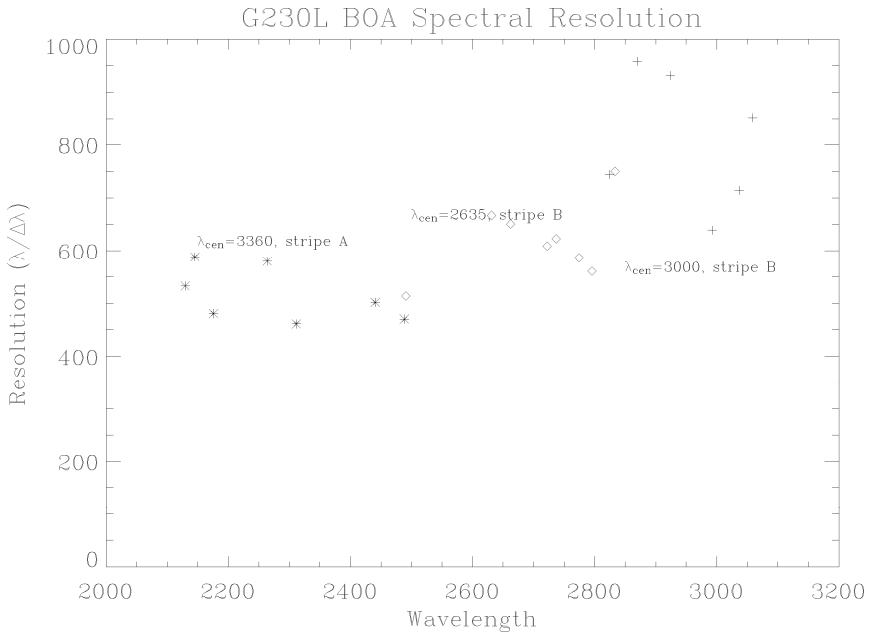

Figure 5.2-11: Measured BOA spectral resolution for the G230L channel.

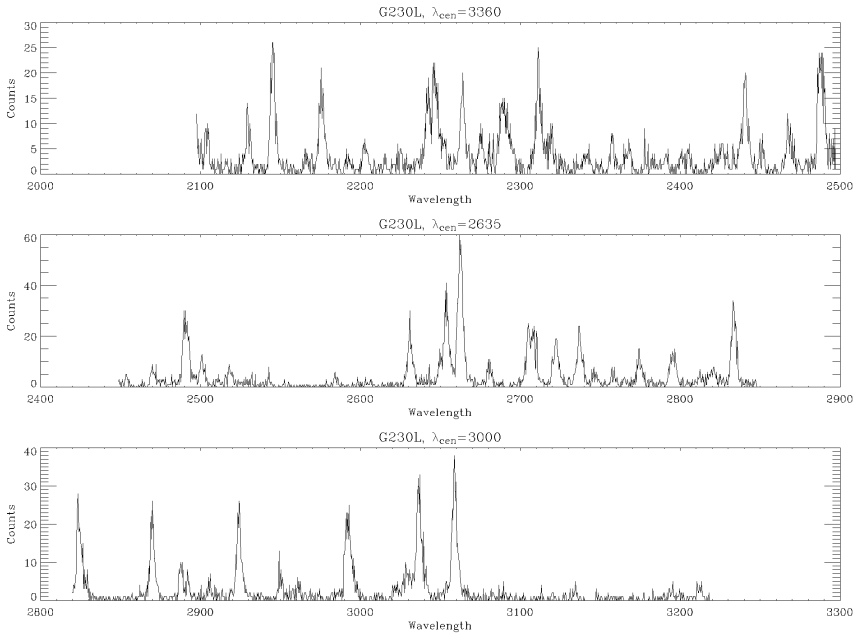

Figure 5.2-12: The PtNe spectra acquired through the BOA used to determine the spectral resolution. The spectra were extracted from CSIL03267212608, CSIL03267223054, and CSIL03267233540.

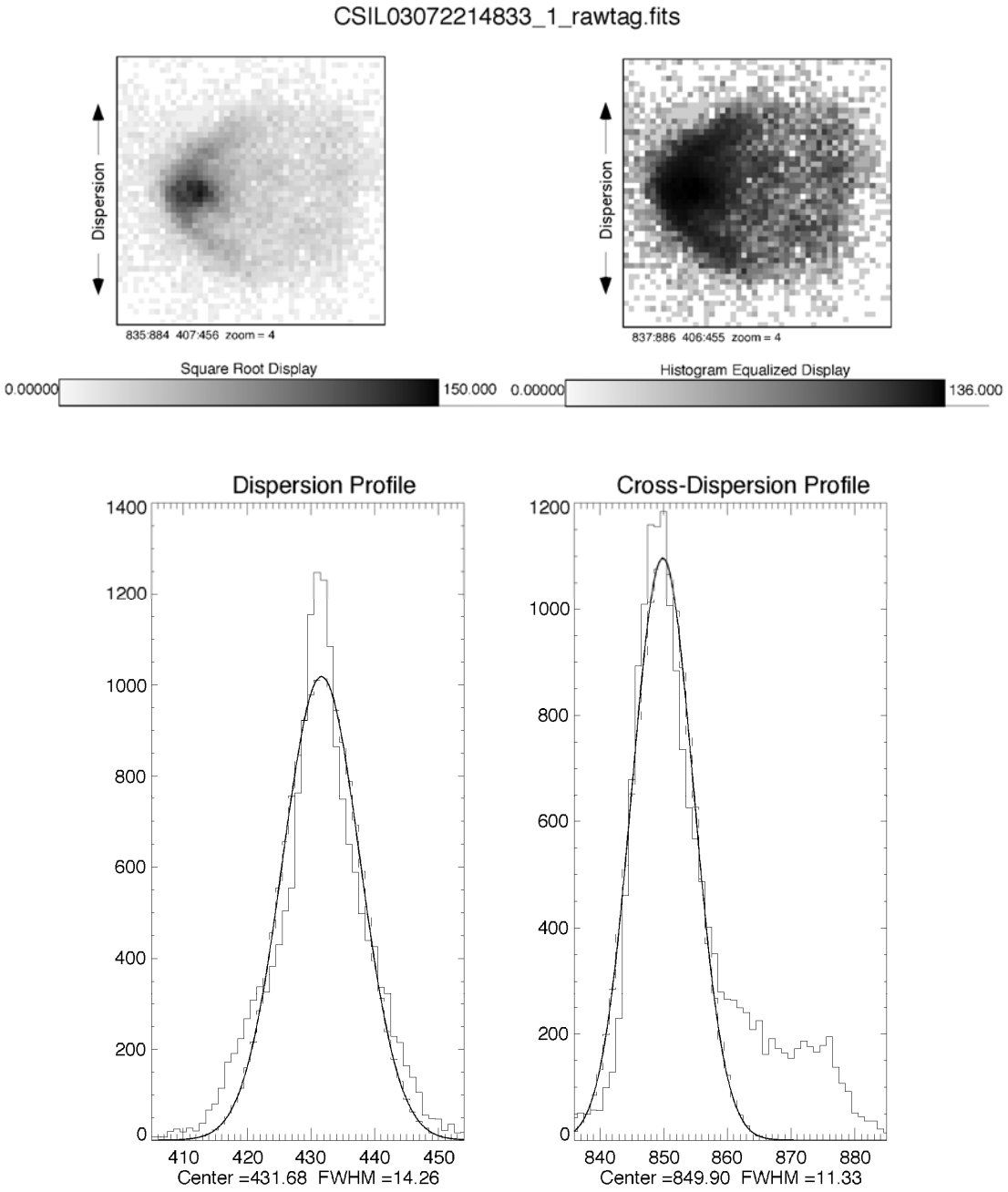

Figure 5.2-13: The upper two panels show a TA1 image through the BOA of a single point source produced by the CAOS HST optical simulator. The images are displayed with two different stretches to high-light structures within the image. The lower panels show the line spread functions in the dispersion and cross-dispersion directions.

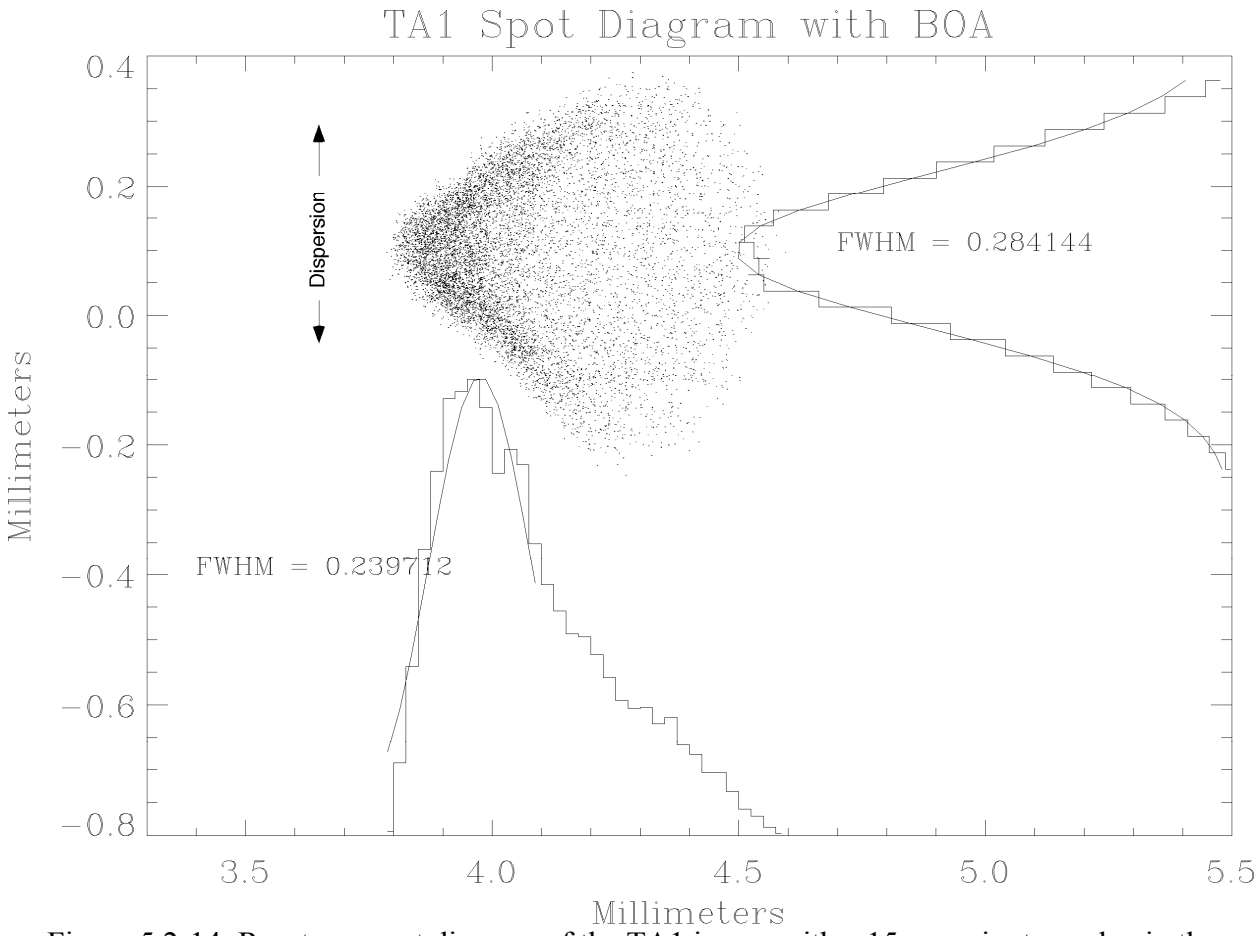

Figure 5.2-14: Ray-trace spot diagram of the TA1 image with a 15 arc-minute wedge in the BOA. Divide the FWHM by 0.025 to get the units in pixels.

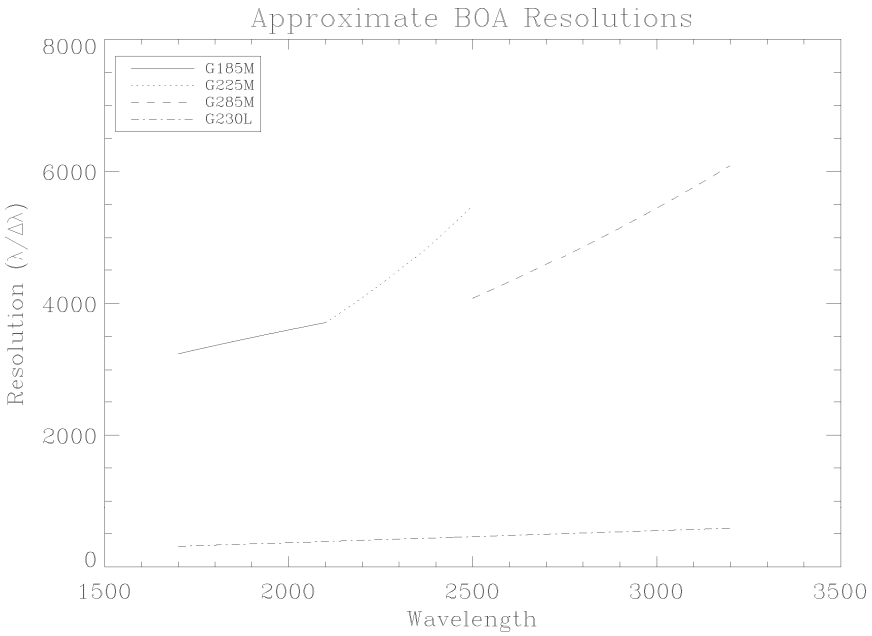

Figure 5.2-15: Predicted spectral resolutions for the NUV channels through the BOA. These predictions are based on the measured dispersion for the central wavelength setting and the measured FWHM in the dispersion direction shown in Figure 4.2-9.

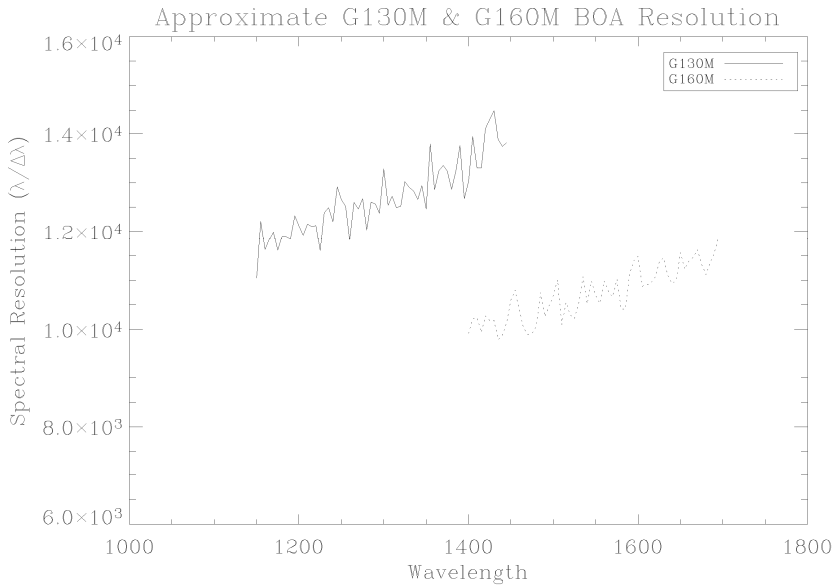

Figure 5.2-16: Predicted FUV spectral resolution assuming a 15 arc-minute wedge between the front and back surfaces of the BOA. These results are based on ray-trace simulations of the

spectral performance; however, the model does not taken into account wavelength dependence in the index of refraction of MgF_2.

5.2.6.3 Results of 2006 Tests

Tests: 3300 – FUV BOA transmission & resolution
3310 – NUV BOA transmission & resolution

The same tests executed in Appendix B were repeated in Appendix C. There are no strict CEI specification requirements for BOA spectral resolution, therefore our aim here is only to show that no changes have occurred since Appendix B testing.

For the NUV, there were three G230L BOA exposures used for BOA-NUV spectral resolution testing. The results of this analysis are shown in the Figure 5.2-17 below. The Appendix B (2003) points are show in blue, and the Appendix C (2006) points are shown in red. There has been no change in the NUV BOA spectral resolution since Appendix B (2003).

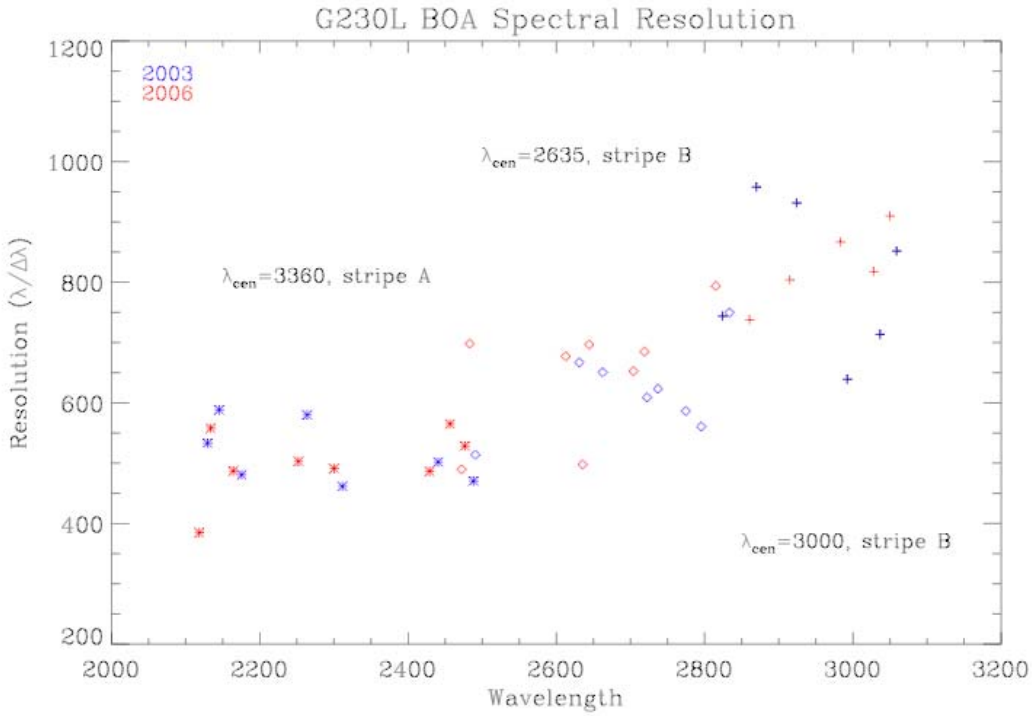

Figure 5.2-17: Measured NUV BOA spectral resolution in 2003 and 2006.

For the FUV, one G140L BOA exposure (CSIL06337025400) was used for BOA-FUV spectral resolution testing. The results of this analysis are shown in Figure 5.2-18 below. The Appendix B (2003) points are shown in blue, and the Appendix C (2006) points are shown in red. The 2003 data points that were presented in Figure **5.2-9** above are connected by the dashed line. The 2006 data points show a lower spectral resolution in the FUV than seen in 2003. However, in Appendix C testing no effort was made to optimally focus COS with the BOA (as was done in Appendix B). The Appendix C FUV-BOA observations were made with OSM1 at the PSA focus position. While this has little impact on NUV resolution, its effect on the FUV resolution is noticeable (as the index of refraction of MgF_2 rises at shorter wavelengths). As a result, there is no reason to believe that the FUV-BOA resolution has actually changed since Appendix B.

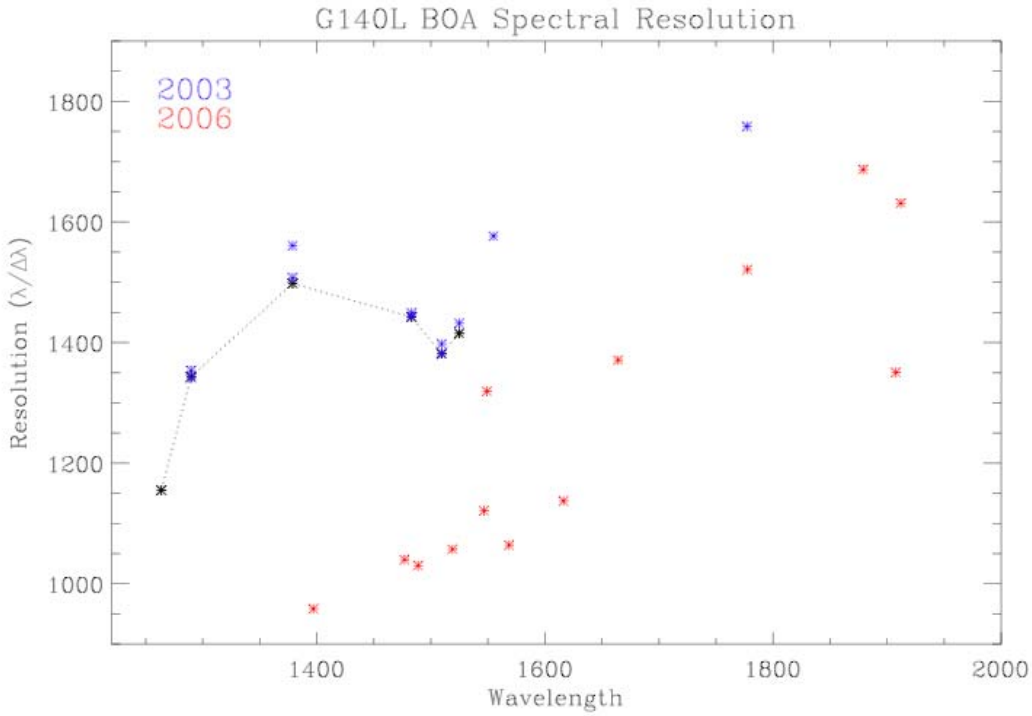

Figure 5.2-18: FUV BOA spectral resolution in 2003 and 2006.

5.3 SPATIAL RESOLUTION

5.3.1 CEI Requirements

Section 4.2.3 of the CEI lists the specific requirements pertaining to spatial resolution. In part the specification reads, "The spectrum of a single point source centered in the Primary Science Aperture (PSA) shall contain 90% of the energy within a range of 300 μm or less in the direction perpendicular to dispersion.

5.3.2 Description

In Appendix B, the spatial resolution of the FUV and NUV channels was measured in separate tests. The FUV spatial resolution was measured as part of the geometric distortion calibration of the FUV detector. In this case the 7x7 pinhole array was used in RASCAL to produce distinct spectra separated by 1". The individual pinholes are separated by 380 μm in the spatial dimension and 100 μm in the spectral dimension. The original purpose of this pinhole array was to sample at a fine scale localized geometric distortions, hence the multiple columns in the spectral dimension. Fortunately, the separation of the rows in the spatial dimension are sufficient to demonstrate spatial imaging.

One thing that was overlooked was the need to demonstrate the spatial resolution in all three FUV channels. Therefore, we only have sufficient data to demonstrate performance in the G160M channel.

The NUV spatial imaging was measured using a column of pinholes, each separated by 1". In this case the spatial imaging was demonstrated for all NUV modes.

5.3.3 FUV spatial resolution

Tests: 2731 – Geometrical Correction PSA 7x7 pinhole array

Relevant Exposures:

Table 5.3-1: Exposure list for 2003 FUV spatial resolution test.

File	Channel/λ_C	Comments
430L03288074030	G160M/1600 Å	15 mA, RASCAL TM2 tip = -0.0387
CSIL03288080430	G160M/1600 Å	15 mA, RASCAL TM2 tip = -0.0397
CSIL03288082630	G160M/1600 Å	15 mA, RASCAL TM2 tip = -0.0407
CSIL03288084830	G160M/1600 Å	15 mA, RASCAL TM2 tip = -0.0437

The exposures listed above are all essentially the same. The RASCAL TM2 mirror was adjusted to direct flux through the pinholes. These files represent the only high quality information we have regarding the FUV spatial imaging.

5.3.3.1 2003 Results

Figure 4.3-1 shows the FUV detector image and extracted line profiles in the spatial dimension. The FUV detector has 24 μm y- pixels, therefore, 12.5 pixels represents 300 μm. The 1σ widths for each Gaussian in the spatial direction range from 1.05 to 1.33 pixels, so 99% of the counts fall within 11.97 pixels in the worst case, meeting the CEI specification.

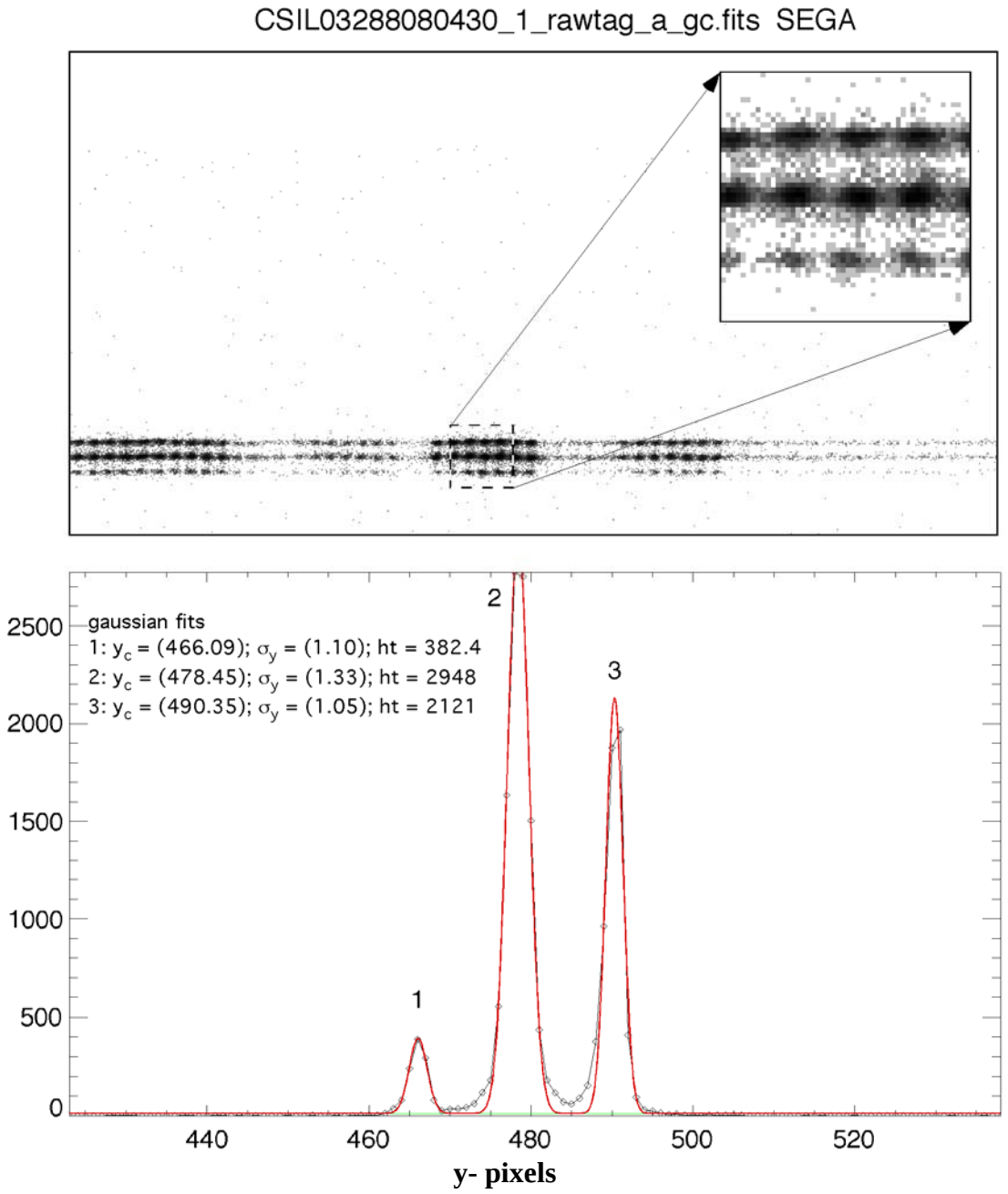

Figure 4.3-1: The upper panel shows an expanded view of the 2D pinhole array image. Only 3 pinholes in the cross-dispersion direction are evident because the PSA blocks the other pinholes.

The lower panel shows the profiles in the cross dispersion direction including the Gaussian parameters for each peak.

5.3.4 NUV spatial resolution

Tests: 2250 – NUV Spatial Resolution

Relevant Exposures:

Table 5.3-2: Exposure list for 2003 NUV spatial resolution test.

File	Channel/λ_C	Comments
CSIL03265180906	G185M / 1850 Å	T_{exp} = 300 sec
CSIL03265183936	G225M / 2250 Å	T_{exp} = 300 sec
CSIL03265185935	G285M / 2850 Å	T_{exp} = 300 sec
CSIL03265192007	G230L / 3000 Å	T_{exp} = 300 sec

5.3.4.1 2003 Results

The nature of the NUV optical path makes it possible to characterize the imaging performance with a single grating. Figure 4.3-2 shows the G225M spectra acquired as part of Test 2250. Clearly evident are the 3 pinhole sources. The measured cross dispersion profiles suggest that 99% of the total counts fall within 342 μm (3σ width) and that 95% falls within 152 μm (2σ width). Thus the CEI specification is met.

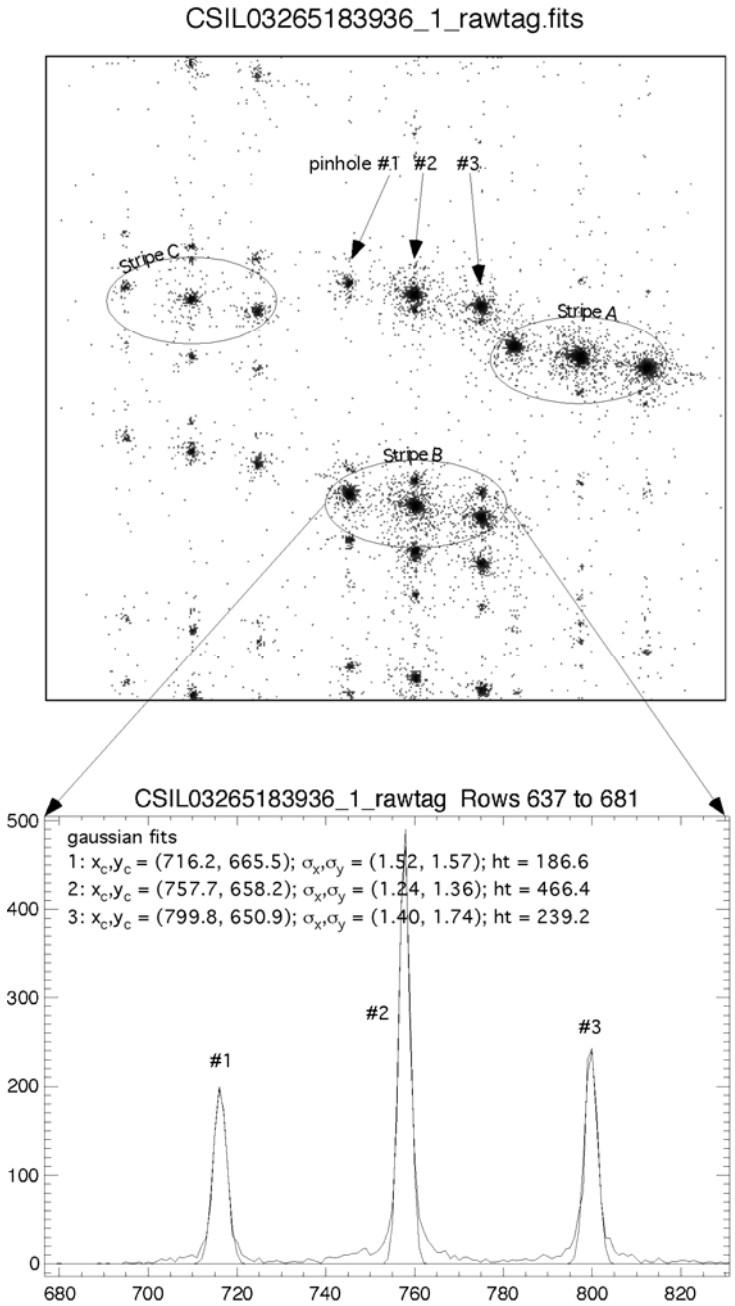

Figure 4.3-2: The G225M image of 3 pinhole sources. The locations of the NUV stripes are shown by ovals. The lower panel shows the cross dispersion profile and corresponding Gaussian fits to the data.

5.3.5 2006 Test Results

Tests: 3300 – FUV BOA Transmission and Resolution
3310 – NUV BOA Transmission and Resolution

The exposures used to measure BOA transmission and resolution (which also included PSA measurements in each setting) were also examined to verify that point source spectra continue to meet the encircled energy requirements in the cross-dispersion direction.

COS FUV digital elements (DE) are 24 μm in the cross-dispersion ('Y') direction, therefore the CEI specification is that 90% of the counts fall within ± 300/24 = 12.5 DE. As presented below, both PSA and FUV observations exceed the specifications.

Table 5.3-3: Results of 2006 FUV spatial resolution test.

Aperture	Grating	λ_C (Å)	Segment	Filename	% within ± 12 pixels
PSA	G140L	1230	A	CSIL06337021910	99.3
BOA	G140L	1230	A	CSIL06337025400	96.3

Pixels on the NUV MAMA are 25.4 μm on a side, therefore the CEI specification requires that 90% of the counts fall within ± 300/25 = 12 cross-dispersion ('X') pixels. As presented below, both PSA and BOA NUV observations exceed the specification.

Table 5.3-4: Results of 2006 NUV spatial resolution test.

Aperture	Grating	λ_C (Å)	Stripe	Filename	% within ± 12 pixels
PSA	G230L	3000	B	CSIL06337040102	95.5
PSA	G230L	3360	A	CSIL06337045256	95.8
PSA	G230L	2635	B	CSIL06337054450	95.9
BOA	G230L	3000	B	CSIL06337043507	93.2
BOA	G230L	3360	A	CSIL06337052701	93.6
BOA	G230L	2635	B	CSIL06337061855	91.4

5.4 SENSITIVITY

5.4.1 CEI Requirements

Section 4.2.4 and Table 4-4 in the CEI list the requirements for instrument sensitivity. Section 4.2.7 and Table 4-6 place requirements on the second order efficiency.

5.4.2 Description

The approach to the efficiency calibration was to treat COS as a detector, and compare its response to that of a reference detector when both viewed the same flux of light. The reference detector was the RASCAL CsTe PMT. This detector was calibrated at the Laboratory for Atmospheric and Space Physics (LASP) in Boulder, CO relative to a NIST calibrated standard diode in the spring of 2003. The source was a Pt-Ne emission line lamp on the CDS monochromator channel. Lines between 1180Å < λ < 3064 Å were used. The monochromator slits allowed approximately 10 Å to pass, centered on a bright emission line. The RASCAL 100μm circular aperture was used. This provided a healthy signal, and produced a somewhat larger image than a point source to average the COS response over many pixels. During Appendix A only one or two wavelengths were measured for each grating, chosen to sample near the expected peak efficiency. During Appendix B we measured six or more wavelengths for each grating spanning as much of the full wavelength range as possible.

The data-taking procedure included the following steps:

1. Insert the PMT into the optical path using its linear stage
2. Measure the PMT dark count rate with the CDS shutter closed
3. Select the appropriate monochromator grating (FUV or NUV)
4. Select the wavelength of interest with the monochromator
5. Measure the PMT count rate with the lamp current near 10 milliamps
6. Adjust the current to provide at least a few hundred cts/sec, preferably near 1000 cts/sec
7. Measure the scattered light contribution to the gross PMT signal
8. Remove the PMT from the optical path
9. Take a COS exposure with the desired grating and wavelength setting. Exposure times were typically 100 seconds, occasionally longer for faint signals.
10. Reinsert the PMT into the optical path
11. Repeat the PMT count rate measurement
12. Do a quick-look analysis by hand to verify that the data were of good quality
13. Move onto the next wavelength or grating

For each FUV grating a single setup position was used. The images of the different emission lines fell on their appropriate regions of the detector. The same basic exposure was repeated for each wavelength. The NUV gratings used different setup wavelengths and different stripes for the different wavelengths. For the NUV M gratings we always had one wavelength that could be measured in all three stripes using different settings. Once underway we could measure three or four wavelengths per hour.

The data analysis is very simple.

PMT count rate = flux * PMT QE
COS count rate = flux * COS efficiency

We tried to be sure that the flux was the same for the two measurements, so that…

COS efficiency = (COS count rate / PMT count rate) * PMT QE

The COS count rate was measured by summing the counts within a range of pixels surrounding the emission line image and dividing by the exposure time. The range of pixels was chosen empirically by the data analyst and test conductor to include the entire 10 Å of spectrum provided by the monochromator. In a few cases the NUV spectrum was too near the edge of the detector to ensure that all of the light had been captured by COS. The exposure was repeated with the OSM2 grating nudged a step or two to move the image towards the center of the stripe. There were no corrections made or needed for background counts or count-rate non-linearity effects. The uncertainty in the COS count rate was estimated from photon statistics as 1σ = sqrt(total counts)/exposure time. The flux in the input light and the exposure times were selected to produce thousands of counts in the final image, so that the uncertainty due to this source was negligible.

The PMT count rate was the average of the measurements made before and after the COS exposure. The rate for each measurement was the gross count rate with the dark count rate (very low) or scattered light (if measured) subtracted. The count rates and 1σ uncertainties reported by the Labview PMT control software were used. The Labview program uses the actual standard deviation of the 100 one second integrations (or however many we requested) as the reported 1σ. Checking a few test cases showed that it is very close to the value estimated from 1σ = sqrt(total counts)/exposure time.

The gratings in the monochromator are not of extremely high quality, and some scattered light is present. Most of the Pt-Ne lines we used are bright enough that the background is small. The FUV lines at the short wavelength end are not bright, and the signal measured by the PMT contained a significant number of longer wavelength photons not recorded by the COS

measurement. We did not realize this during the Appendix A tests, and no correction for this effect was made. During the Appendix B phase we estimated this scattered component by making measurements with the monochromator set for λ = 1050Å, a wavelength for which no light should be passing through CDS due to the MgF_2 window on the lamp and coatings on all of the optics. The PMT count rate measured with this setting was subtracted from the reading obtained with the monochromator set for the wavelength of the emission line being used for calibration. This correction increased the formal uncertainties in the derived COS efficiency, but should be a better estimate.

The PMT QE was the value derived by LASP after adjustment for the annular profile of the RASCAL illumination. The PMT calibration data is recorded in COS-11-0042 entitled "Calibration Report for the RAS/Cal CsTe Photo-Multiplier Tube." The uncertainties resulting from that adjustment were used for the QE errors. These fractional uncertainties range from 7% to 10% of the value of the QE, and dominate the overall errors for all except the faint FUV wavelengths.

The uncertainties in the resulting COS efficiencies were propagated using standard formulas, such as…

$$X = u + v \quad \text{or} \quad X = u - v, \text{ then } \sigma^2 x = \sigma^2 u + \sigma^2 v$$

$$X = u*v, \text{ or } X = u/v, \text{ then } \sigma^2 x/x^2 = \sigma^2 u/u^2 + \sigma^2 v/v^2$$

The sum and difference formulas are used for taking averages and subtracting backgrounds. The product and quotient formulas for calculating count rates, comparing COS count rates to that of the PMT and multiplying by the PMT QE.

Tables 4.4-1 and 4.4-2 present all of the high quality measurements made during the science calibration. Figure 4.4-1 show the efficiencies and the values expected from the most current component measurements.

Tests:
- 1210 G130M Sensitivity
- 1220 G160M Sensitivity
- 1230 G140L Sensitivity
- 1250 G185M Sensitivity
- 1255 G185M/G225M Sensitivity
- 1260 G225M Sensitivity
- 1270 G285M Sensitivity
- 1280 G230L Sensitivity
- 1290 TA1 Sensitivity

1295 TA1-BRT Sensitivity

Relevant Exposures:

Numerous files were taken by the COS team, but not all were used to compute the net system efficiency. The list below is a comprehensive list of all files that were taken during the efficiency testing. The data files NOT used to compute the system efficiency are in *italic*s text and were included in the list for future reference. The dates and test # can be used to cross reference the exposure list and the electronic history files for a more thorough understanding of how the test was conducted or issues that were being explored.

Table 5.4-1: Exposure list for 2003 sensitivity tests.

File	Date	Test #	Channel	λ_c	Test λ
CSIL03265000336	9/21/03	1270	G285M	2657	2659
CSIL03265002706	9/21/03	1270	G285M	2657	2540
CSIL03265004706	9/21/03	1270	G285M	2739	2734
CSIL03265010907	9/21/03	1270	G285M	2952	2830
CSIL03265011906	*9/21/03*	*1270*	*G285M*	*2850*	*2830*
CSIL03265012936	*9/21/03*	*1270*	*G285M*	*2719*	*2830*
CSIL03265014006	*9/21/03*	*1270*	*G285M*	*2850*	*2830*
CSIL03265014735	9/21/04	1270	G285M	2850	2830
CSIL03265020536	9/21/03	1270	G285M	2998	2996
CSIL03265023007	9/21/03	1270	G285M	3064	3057
CSIL03265025305	9/21/03	1260	G225M	2186	2085
CSIL03265030831	9/21/03	1260	G225M	2250	2144
CSIL03265032335	9/21/03	1260	G225M	2268	2262
CSIL03265033807	9/21/03	1260	G225M	2357	2357
CSIL03265035032	9/21/03	1260	G225M	2339	2440
CSIL03265040336	9/21/03	1260	G225M	2390	2487
CSIL03265041406	*9/21/03*	*1260*	*G225M*	*2186*	*2290*
CSIL03265042305	*9/21/03*	*1260*	*G225M*	*2283*	*2290*
CSIL03265044236	9/21/03	1260	G225M	2186	2290
CSIL03265045136	9/21/03	1260	G225M	2283	2290
CSIL03265050037	9/21/03	1260	G225M	2390	2290
CSIL03265052106	9/21/03	1250	G185M	1817	1723
CSIL03265053236	9/21/03	1250	G185M	1817	1723
CSIL03265054437	9/21/03	1250	G185M	1882	1777
CSIL03265060235	9/22/03	1250	G185M	1850	1846
CSIL03265061336	9/22/03	1250	G185M	1835	1937
CSIL03265062807	9/22/03	1250	G185M	1971	1972

CSIL03265064106	9/22/03	1250	G185M	1953	2050
CSIL03265070206	9/22/03	1250	G185M	1786	1883
CSIL03265071506	9/22/03	1250	G185M	1882	1883
CSIL03265072706	9/22/03	1250	G185M	1986	1883
CSIL03265074236	*9/22/03*	*1255*	*G185M*	*2010*	*NST*
CSIL03265074806	*9/22/03*	*1255*	*G185M*	*2010*	*NST*
CSIL03265075237	*9/22/03*	*1255*	*G185M*	*2010*	*NST*
CSIL03265082135	*9/22/03*	*1280*	*G230L*	*2950*	*1723*
CSIL03265084906	*9/22/03*	*1280*	*G230L*	*2950*	*1723*
CSIL03265090105	9/22/03	1280	G230L	2950	1723
CSIL03265092607	9/22/03	1280	G230L	3000	1846
CSIL03265094036	9/22/03	1280	G230L	3000	2050
CSIL03265095807	9/22/03	1280	G230L	3000	2085
CSIL03265101606	9/22/03	1280	G230L	3360	2262
CSIL03265103135	9/22/03	1280	G230L	2635	2487
CSIL03265104435	9/22/03	1280	G230L	2635	2659
CSIL03265110136	9/22/03	1280	G230L	2950	2830
CSIL03265111606	9/22/03	1280	G230L	3000	2998
CSIL03265112736	9/22/03	1281	G230L	3000	2085
CSIL03265113636	9/22/03	1281	G230L	2635	2085
CSIL03265114606	9/22/03	1281	G230L	3360	2085
CSIL03265121336	9/22/03	1290	TA-1	-	1723
CSIL03265123506	9/22/03	1290	TA-1	-	1846
CSIL03265125307	9/22/03	1290	TA-1	-	2262
CSIL03265131106	9/22/03	1290	TA-1	-	2487
CSIL03265132337	9/22/03	1290	TA-1	-	2830
CSIL03265134736	9/22/03	1290	TA-1	-	2998
CSIL03265143906	9/22/03	1290	TA-1	-	1248
CSIL03265150436	9/22/03	1290	TA-1	-	1524
CSIL03265153406	*9/22/03*	*1295*	*TA-1 BRT*	-	*1723*
CSIL03265154636	9/22/03	1295	TA-1 BRT	-	1723
CSIL03265160906	9/22/03	1295	TA-1 BRT	-	2262
CSIL03265163235	9/22/03	1295	TA-1 BRT	-	2487
CSIL03265165406	9/22/03	1295	TA-1 BRT	-	2998
CSIL03265171837	9/22/03	1295	TA-1 BRT	-	1248
CSIL03265174306	9/22/03	1295	TA-1 BRT	-	1524
CSIL032841542545	*10/11/03*	*1210*	*G130M*	*1309*	*1249*

CSIL03284160055	10/11/03	1210	G130M	1309	1249
CSIL03284161725	10/11/03	1210	G130M	1309	1216
CSIL03284163452	10/11/03	1210	G130M	1309	1180
CSIL03284165624	10/11/03	1210	G130M	1309	1327
CSIL03284171253	10/11/03	1210	G130M	1309	1379
CSIL03284173055	10/11/03	1210	G130M	1309	1430
CSIL03284174424	10/11/03	1210	G130M	1309	1430
CSIL03284182126	10/11/03	1220	G160M	1600	1430
CSIL03284183555	10/11/03	1220	G160M	1600	1482
CSIL03284185255	10/11/03	1220	G160M	1600	1524
CSIL03284190655	10/11/03	1220	G160M	1600	1621
CSIL03284191855	10/11/03	1220	G160M	1600	1669
CSIL03284193526	10/11/03	1220	G160M	1600	1723
CSIL03284200425	10/11/03	1230	G140L	1230	1723
CSIL03284202226	10/11/03	1230	G140L	1230	1524
CSIL03284203755	10/11/03	1230	G140L	1230	1430
CSIL03284205327	*10/11/03*	*1230*	*G140L*	*1230*	*1248*
CSIL03284210956	10/11/03	1230	G140L	1230	1327
CSIL03284212626	10/11/03	1230	G140L	1230	1937
CSIL03284215057	10/11/03	1230	G140L	1230	1248
CSIL03284222027	10/11/03	1240	G130M	1309	1216
CSIL03284223956	10/11/03	1240	G130M	1309	1379
CSIL03284225425	10/11/03	1240	G160M	1600	1482
CSIL03284230556	10/11/03	1240	G160M	1600	1669
CSIL03285154919	10/12/03	1265	G225M	2390	1249
CSIL03285160951	10/12/03	1265	G285M	2617	1249
CSIL03285163550	10/12/03	1265	G230L	2635	1249
CSIL03285170051	10/12/03	1265	G225M	2357	1180
CSIL03285172421	10/12/03	1265	G225M	2339	1216
CSIL03285175220	10/12/03	1265	G285M	3057	1524
CSIL03285181320	10/12/03	1265	G230L	3000	1524
CSIL03285184320	10/12/03	1265	G285M	3035	1574
CSIL03285190250	10/12/03	1265	G230L	3000	1574

5.4.3 2003 Results – 1st Order Efficiencies

Table 5.4-2: COS FUV Efficiency Measurements during 2003 science calibration in vacuum

Appendix	Channel	λ_c (Å)	segment	Test λ (Å)	COS efficiency cts/ph	rel. uncertainty	1 σ
B	G130M	1309	B	1180	0.1686	0.245	0.041
B	G130M	1309	B	1216	0.1975	0.248	0.049
A	G130M	1309	B	1248	0.1748	0.075	0.013
B	G130M	1309	B	1248	0.1917	0.214	0.041
A	G130M	1309	A	1327	0.1128	0.094	0.011
A	G130M	1309	A	1327	0.1091	0.111	0.012
B	G130M	1309	A	1327	0.1159	0.192	0.022
B	G130M	1309	A	1379	0.1042	0.286	0.030
B	G130M	1309	A	1430	0.0903	0.169	0.015
A	G160M	1600	B	1430	0.1204	0.062	0.007
B	G160M	1600	B	1430	0.1167	0.141	0.016
B	G160M	1600	B	1482	0.1114	0.133	0.015
B	G160M	1600	B	1524	0.1071	0.128	0.014
A	G160M	1600	A	1621	0.0746	0.081	0.006
B	G160M	1600	A	1621	0.0639	0.161	0.010
B	G160M	1600	A	1669	0.0581	0.127	0.007
B	G160M	1600	A	1723	0.0487	0.141	0.007
B	G140L	1230	A	1248	0.1066	0.096	0.010
A	G140L	1230	A	1327	0.0827	0.093	0.008
B	G140L	1230	A	1327	0.0652	0.244	0.016
B	G140L	1230	A	1430	0.0642	0.195	0.013
B	G140L	1230	A	1524	0.0528	0.142	0.007
B	G140L	1230	A	1723	0.0309	0.137	0.004
B	G140L	1230	A	1937	0.0065	0.091	0.001

Table 5.4-3: COS NUV Efficiency Measurements during 2003 science calibration in vacuum

Appendix	Channel	λ_c (Å)	stripe	Test λ (Å)	COS efficiency cts/ph	rel. uncertainty	1 σ

B	G185M	1817	A	1723	0.0320	0.123	0.004
B	G185M	1882	A	1777	0.0394	0.103	0.004
A	G185M	1850	B	1846	0.0355	0.084	0.003
B	G185M	1850	B	1846	0.0377	0.117	0.004
B	G185M	1986	A	1883	0.0364	0.083	0.003
B	G185M	1882	B	1883	0.0372	0.083	0.003
B	G185M	1786	C	1883	0.0360	0.083	0.003
B	G185M	1835	C	1937	0.0322	0.075	0.002
B	G185M	1971	B	1972	0.0292	0.087	0.003
B	G185M	1953	C	2050	0.0255	0.085	0.002
B	G185M	1986	C	2085	0.0230	0.074	0.002
B	G185M	2010	C	2129	0.0196	0.075	0.001
B	G225M	2186	A	2085	0.0140	0.077	0.001
B	G225M	2186	A	2085	0.0137	0.075	0.001
B	G225M	2010	C	2129	0.0165	0.074	0.001
B	G225M	2250	A	2144	0.0169	0.076	0.001
A	G225M	2268	B	2262	0.0231	0.065	0.002
B	G225M	2268	B	2262	0.0266	0.074	0.002
B	G225M	2390	A	2290	0.0263	0.075	0.002
B	G225M	2283	B	2290	0.0271	0.075	0.002
B	G225M	2186	C	2290	0.0266	0.075	0.002
B	G225M	2357	B	2357	0.0301	0.067	0.002
A	G225M	2357	C	2440	0.0254	0.064	0.002
B	G225M	2339	C	2440	0.0292	0.067	0.002
A	G225M	2390	C	2487	0.0248	0.070	0.002
B	G225M	2390	C	2487	0.0288	0.074	0.002
A	G285M	2676	A	2540	0.0181	0.066	0.001
B	G285M	2657	A	2540	0.0200	0.068	0.001
A	G285M	2657	B	2659	0.0189	0.063	0.001
B	G285M	2657	B	2659	0.0218	0.070	0.002
B	G285M	2739	B	2734	0.0205	0.086	0.002
A	G285M	2952	A	2830	0.0152	0.098	0.001

A	G285M	2952	A	2830	0.0153	0.098	0.001
A	G285M	2952	A	2830	0.0149	0.098	0.001
B	G285M	2952	A	2830	0.0174	0.102	0.002
B	G285M	2850	B	2830	0.0172	0.102	0.002
B	G285M	2719	C	2830	0.0170	0.102	0.002
B	G285M	2996	B	2998	0.0105	0.115	0.001
B	G285M	3057	B	3064	0.0089	0.105	0.001
B	G230L	2950	A	1723	0.0235	0.128	0.003
B	G230L	3000	A	1846	0.0303	0.119	0.004
B	G230L	3000	A	2050	0.0306	0.086	0.003
B	G230L	3360	A	2085	0.0303	0.078	0.002
A	G230L	3360	A	2262	0.0246	0.065	0.002
B	G230L	3360	A	2262	0.0273	0.076	0.002
B	G230L	2635	B	2487	0.0232	0.075	0.002
B	G230L	2635	B	2659	0.0204	0.066	0.001
B	G230L	2950	B	2830	0.0143	0.103	0.001
B	G230L	3000	B	2998	0.0079	0.116	0.001
B	TA1		A	1248	4.88E-05	0.154	0.000
B	TA1		A	1524	6.17E-05	0.130	0.000
B	TA1		A	1723	0.0483	0.131	0.006
B	TA1		A	1846	0.0594	0.116	0.007
B	TA1		A	2262	0.0512	0.076	0.004
A	TA1		A	2487	0.0424	0.070	0.003
B	TA1		A	2487	0.0473	0.075	0.004
B	TA1		A	2830	0.0323	0.103	0.003
B	TA1		A	2998	0.0198	0.124	0.002
B	TA1-BRT		A	1248	0.0008	0.110	0.000
B	TA1-BRT		A	1524	0.0023	0.078	0.000
B	TA1-BRT		A	1723	0.0043	0.101	0.000
B	TA1-BRT		A	2262	0.0028	0.078	0.000
A	TA1 BRT		A	2487	0.0031	0.070	0.000

B	TA1-BRT	A	2487	0.0032	0.077	0.000
B	TA1-BRT	A	2998	0.0012	0.114	0.000

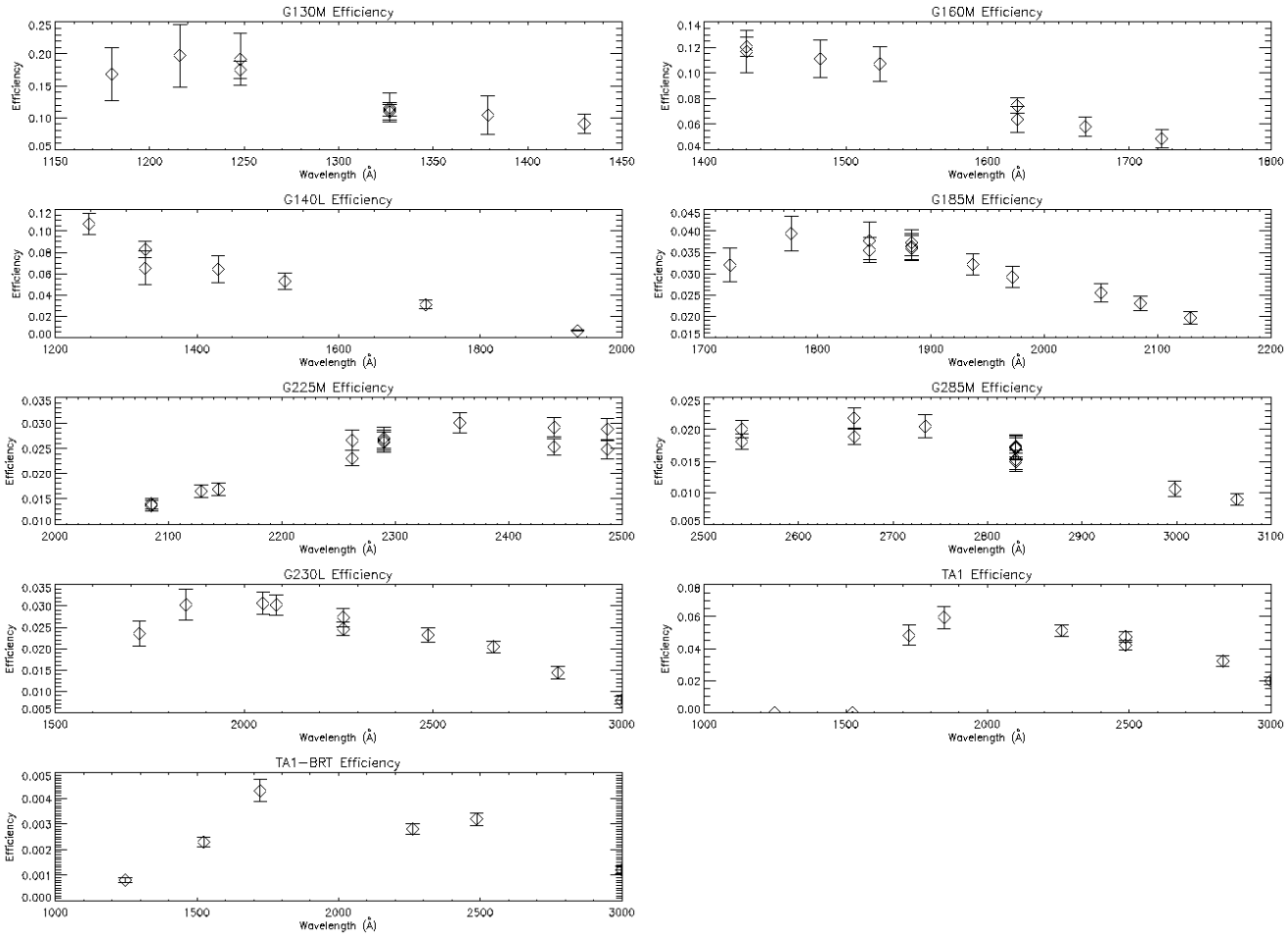

Figure 5.4-1: Efficiency plots for each channel representing the data in Tables Table 5.4-2 and Table 5.4-3.

5.4.4 2003 Results – 2nd Order Efficiencies

The light that falls on a given pixel of the detector satisfies the condition that $m\lambda$ = constant, where m is the order of diffraction and λ is the wavelength of light. The numerical value of the constant is determined by the groove spacing of the grating and the angles of incidence and diffraction. All of the spectroscopic modes of COS were designed to operate in the first order of diffraction, m=1. Wavelengths whose products with m=2, m=3 etc. equal the same constant will overlap the m=1 spectra at the same pixel locations. If these wavelengths can be transmitted by the optical system and registered by the detector they will create a confusing mixture of spectral features. This effect is known as 2nd order overlap. COS minimizes this problem using several factors.

The FUV channel is not susceptible to higher order overlap. The optics of COS and HST are coated with Al and MgF_2. These surfaces do not reflect wavelengths $\lambda < 1150$Å with significant efficiency. Multiple reflections essentially eliminate these short wavelengths. The FUV detector is used between $1150\text{Å} < \lambda < 1775\text{Å}$ for the M gratings, and is only required to work between $1230\text{Å} < \lambda < 1800\text{Å}$ for G140L. The longest wavelength that could overlap is 900Å, which is not reflected by the optical system.

The HST optics reflect all wavelengths longward of 1150Å with good efficiency. The NUV MAMA detector responds well to light in the range $1150\text{Å} < \lambda < 3200\text{Å}$. Therefore the NUV modes designed for $m\lambda \geq 2300$Å when m=1 will be vulnerable to 2nd order overlap when m=2 and $\lambda > 1150$Å. COS is not susceptible to 3rd order light, since it is not intended to observe $\lambda \geq 3450$Å. No second order light can reach G185M. Modes G225M, G285M and G230L are susceptible to overlap, and two means were provided to attenuate the second order light. All of the NUV optics were coated with a version of Al + MgF_2 whose reflectivity decreases strongly shortward of 1650Å. The net throughput for four reflections is less than 1% for wavelengths $\lambda <$ 1250Å. All second order light within the required wavelength range of G225M is attenuated, but not extinguished, this way. Gratings G285M and G230L operate at longer wavelengths where the reflectivity of the optics and the sensitivity of the NUV detector are both high. A 2mm thick fused silica order sorter was placed in front of the gratings, so that the light makes two passes through the filter before reaching the detector. UV grade fused silica transmits well for $\lambda >$ 1700Å, but is almost totally opaque for $\lambda < 1600$Å. We therefore expect no significant second order overlap for these gratings for $\lambda < 3200$Å.

Test number 1265 was run during the Appendix B phase to measure the 2nd order throughput of G225M, G285M and G230L. The experimental setup and data reduction was the same as for the normal sensitivity measurements. An FUV line from the Pt-Ne lamp was isolated by the monochromator, its flux was measured by the RASCAL PMT, and its count rate was recorded with the appropriate COS NUV mode where it might show up in 2nd order. Exposure times were all 10 minutes. All data were of high quality. Of the nine measurements made, positive detections of the 2nd order image were obtained only for two wavelengths with G225M.

No 2nd order light was detected for G285M or G230L, confirming that the order sorter filter performed properly. One complication in the data analysis was that the 1st order spectrum of the Pt-Ne lamp appears faintly in the data. The FUV grating in the monochromator is not of very high quality, and light of all wavelengths from the lamp gets scattered into the exit slit at low levels. We compared the spectrum of the region expected to contain the 2nd order image with high quality 1st order spectra of the Pt-Ne lamp obtained with other tests, and unambiguously identified the features due to overlapping 2nd order light.

5.4.4.1 Results for G225M:

Light with wavelength 1219Å was detected in 2nd order with a throughput of 1.12×10^{-4}. Light with wavelength 1249Å was detected in 2nd order with a throughput of 3.73×10^{-4}.
The measured response of G225M to 1st order light at 2440Å was 0.03 (270 and 80 times higher). The FUV grating G130M detected 1219Å and 1248Å in 1st order with efficiencies near 0.12 (over 1000 and 300 times higher).

5.4.4.2 Results for G285M and G230L:

No 2nd order images were detected. Judging from the quality of the NUV spectra a very generous upper limit of 10 counts in 600 seconds can be allowed. This gives an upper limit 10^{-6} for any 2nd order throughput for these gratings.

5.4.4.3 Conclusions:

The Appendix B calibration results confirm that the design of COS avoided any problems with spectral contamination from higher orders of diffraction. None of the FUV gratings are susceptible, nor is G185M. G225M has a small throughput between 2300Å < λ < 2500Å, which was agreed to be acceptable during the trade studies that led to its design. The order sorters of G285M and G230L block all higher order light within their required wavelength bands.

5.4.5 2003 Results – 1st Order Efficiencies w/ FUV Detector QE Grid Off

Two data sets were acquired where the sensitivity of the FUV channel was measured with the FUV detector QE grid off. In test 1240 monochromatic emission lines were used. In tests 1110 and 2750 full spectra were acquired. This test was run for informational purposes, not to demonstrate a CEI requirement.

Tests: 1240 – FUV sensitivity with QE Grid Off
1110 – PtNe Group 1 Spectra (grid on)
2750 – PtNe Group 1 Spectra (grid off)

Relevant Exposures:

Table 5.4-4: Exposure list for 2003 FUV detector QE tests.

File	Date	Test #	Channel	λ_c	Test λ
CSIL03284222027	10/11/03	1240	G130M	1309	1216
CSIL03284223956	10/11/03	1240	G130M	1309	1379
CSIL03284225425	10/11/03	1240	G160M	1600	1482
CSIL03284230556	10/11/03	1240	G160M	1600	1669
CSIL03286020938	10/12/03	1110	G130M	1309	PSA
CSIL03286021646	10/12/03	1110	G130M	1309	WCA
CSIL03286033938	10/12/03	1110	G160M	1600	PSA
CSIL03286034546	10/12/03	1110	G160M	1600	WCA
CSIL03286050338	10/12/03	1110	G140L	1230	PSA
CSIL03286064155	10/13/03	2750	G130M	1309	WCA
CSIL03286064903	10/13/03	2750	G130M	1309	PSA
CSIL03286072355	10/13/03	2750	G160M	1600	WCA
CSIL03286073003	10/13/03	2750	G160M	1600	PSA
CSIL03286060155	10/13/03	2750	G140L	1230	WCA

Note: where PSA or WCA is called out for the wavelength the entire detector image was used to compute the count rate. PtNe spectra were used in all cases.

Should the situation arise where the FUV DQE enhancement grid must be turned off due to anomalous operating conditions, e.g. excessive coronal emission, the sensitivity of COS was measured at 4 wavelengths with the DQE grid off. The DQE enhancement grid forces photoelectrons generated between MCP pores back onto the MCP, thus increasing the probability of initiating an electron cascade in the stack. Thus, the DQE is increased by 30-40%.

The sensitivities of COS with the DQE grid off were measured as follows:

FUV DQE Measurement Notes with QE GRID OFF

G130M_A: 6712 counts in 200 sec in spectral region on FUV detector
PMT rate = (54.0+51.4)/2 = 52.7 cps
PMT QE at 1379Å is 0.068
QE = 33.56/((52.7-19.9)/0.068) = 0.0696
The 19.9 cps represents out of band light as measured with a CaF filter in place

G130M_B: 19379 counts in 100 seconds
PMT rate = (239.0+234.8)/2 = 236.9 cps
PMT QE at 1216Å is 0.117
QE = 193.79/((236.9-39.0)/0.117) = 0.1146
The 39 cps represents out of band light as measured with a CaF filter in place

G160M_A: 2152 counts in 100 seconds
PMT rate = (62.8+71.3)/2 = 67.06 cps
PMT QE at 1669Å is 0.138
QE = 21.52/(67.06/0.138) = 0.0443

G160M_B: 6002 counts in 100 seconds
PMT rate = (60.8+62.7)/2 = 61.75 cps
PMT QE at 1482Å is 0.0803
QE = 60.02/(61.75/0.0802) = 0.0780

Now, the QE as measured for those wavelengths with the QE grid ON (see previous sections) are....

G130M_A: 1379Å -> 0.1042
G130M_B: 1216Å -> 0.1975
G160M_A: 1669Å -> 0.0581
G160M_B: 1482Å -> 0.1114

Forming the ratio of (ON-OFF)/ON measures the QE contribution from the web:

G130M_A: 0.33
G130M_B: 0.42
G160M_A: 0.24
G160M_B: 0.30

Evaluating the data acquired during tests 1110 and 2750 yields a similar result. In this case the total counts in each PSA or WCA were used to calculate the contribution from the web. The results are shown Table 4.4-3 below. All results are consistent with expectations.

Table 5.4-5: Raw Data and Final Results for FUV DQE with the FUV Detector QE Grid ON and OFF.

File	Channel	λ_c	Aperture	Seg.	Count Rate
QE GRID ON					
CSIL03286020938_1_rawtag_a_gc.fits	G130M	1309	PSA-FUV	FUVA	382.587
CSIL03286020938_1_rawtag_b_gc.fits	G130M	1309	PSA-FUV	FUVB	607.517
CSIL03286021646_1_rawtag_a_gc.fits	G130M	1309	WCA-FUV	FUVA	242.05

CSIL03286021646_1_rawtag_b_gc.fits	G130M	1309	WCA-FUV	FUVB	167.017
CSIL03286033938_1_rawtag_a_gc.fits	G160M	1600	PSA-FUV	FUVA	179.777
CSIL03286033938_1_rawtag_b_gc.fits	G160M	1600	PSA-FUV	FUVB	723.68
CSIL03286034546_1_rawtag_a_gc.fits	G160M	1600	WCA-FUV	FUVA	238.35
CSIL03286034546_1_rawtag_b_gc.fits	G160M	1600	WCA-FUV	FUVB	710.367
CSIL03286050338_1_rawtag_a_gc.fits	G140L	1230	PSA-FUV	FUVA	1442.03
CSIL03286051016_1_rawtag_a_gc.fits	G140L	1230	WCA-FUV	FUVA	914.833
QE GRID OFF					
CSIL03286064155_1_rawtag_a_gc.fits	G130M	1309	PSA-FUV	FUVA	287.388
CSIL03286064155_1_rawtag_b_gc.fits	G130M	1309	PSA-FUV	FUVB	445.053
CSIL03286064903_1_rawtag_a_gc.fits	G130M	1309	WCA-FUV	FUVA	175.925
CSIL03286064903_1_rawtag_b_gc.fits	G130M	1309	WCA-FUV	FUVB	120.658
CSIL03286072355_1_rawtag_a_gc.fits	G160M	1600	PSA-FUV	FUVA	135.977
CSIL03286072355_1_rawtag_b_gc.fits	G160M	1600	PSA-FUV	FUVB	513.788
CSIL03286073003_1_rawtag_a_gc.fits	G160M	1600	WCA-FUV	FUVA	185.45
CSIL03286073003_1_rawtag_b_gc.fits	G160M	1600	WCA-FUV	FUVB	537.217
CSIL03286060155_1_rawtag_a_gc.fits	G140L	1230	PSA-FUV	FUVA	1078.87
CSIL03286060833_1_rawtag_a_gc.fits	G140L	1230	WCA-FUV	FUVA	708.211

Contribution to DQE by MCP web:	Channel	λ_c	Aperture	Seg.	Web Contrib.
Web contribution = (ON-OFF)/ON	G130M	1309	PSA-FUV	FUVA	0.25
(ON is with QE grid on and	G130M	1309	PSA-FUV	FUVB	0.27
OFF is with QE grid off)	G130M	1309	WCA-FUV	FUVA	0.27
	G130M	1309	WCA-FUV	FUVB	0.28
	G160M	1600	PSA-FUV	FUVA	0.24
	G160M	1600	PSA-FUV	FUVB	0.29
	G160M	1600	WCA-FUV	FUVA	0.22
	G160M	1600	WCA-FUV	FUVB	0.24
	G140L	1230	PSA-FUV	FUVA	0.25
	G140L	1230	WCA-FUV	FUVA	0.23

5.4.6 2006 Sensitivity Measurements

The sensitivity observations made in Appendix B were repeated in Appendix C with the same test execution (but with the new CDS hardware). The analysis of the data was also repeated in

the same manner. The RASCAL CsTe photo-multiplier tube (PMT) used as the reference detector was recalibrated at LASP prior to the 2006 observations. The PMT calibration data is recorded in COS-11-0042 entitled "Calibration Report for the RAS/Cal CsTe Photo-Multiplier Tube." The FUV sensitivity tests with the QE detector grid turned off were not repeated in 2006. The 2006 CDS had better gratings and much lower scattered light which led to reduced uncertainties on the sensitivity measurements.

Tests: 1210 G130M Sensitivity
1220 G160M Sensitivity
1230 G140L Sensitivity
1250 G185M Sensitivity
1255 G185M/G225M Sensitivity
1260 G225M Sensitivity
1270 G285M Sensitivity
1280 G230L Sensitivity
1290 TA1 Sensitivity
1295 TA1-BRT Sensitivity

The sensitivity measurements are given in Table **5.4-6** and Table **5.4-7** for the FUV and NUV, respectively. The sensitivities are shown graphically in Figure 5.4-2 and Figure 5.4-3 for both the 2003 and 2006 data. Figure **5.4-4** shows the percentage change between 2003 and 2006 for each grating.

Figure 4.4-3 shows substantial changes in reported throughputs between the 2003 and 2006 calibrations. We believe that the increase in throughput at shorter wavelengths is at least partially an artifact of the test setup, while the long wavelength performance changes are attributable to changes in the instrument performance.

The ~10-44% increase in reported FUV throughput between 1300Å and 1500Å is probably due to a change in the polarization content in the calibration beam at these wavelengths. While it is difficult to say if the 2006 or 2003 short wavelength data is more reliable, the 44% increase in the G140L 1327Å is not consistent with component level measurements, casting doubt on the 2006 values. Furthermore, the polarization scrambler used to randomize the polarization of the 2006 CDS output was not completely effective at shorter wavelengths, and design constraints imposed by the need to place the CDS in vacuum in 2006 lead to a design which was more prone to polarization than the previous incarnation.

At wavelengths longer than 1600Å we were able to measure the polarization content of the 2006 calibration beam and note that it was effectively unpolarized, while no measurements were made

of the 2003 CDS polarization content. In addition, the instrument sensitivity to polarized light was directly measured in 2007 at wavelengths beyond 2200Å and the unpolarized response was found to match the 2006 thermal vacuum data. Consequently, the 2006 data is considered more reliable than the 2003 data for wavelengths longer than 1600Å.

The general decrease in apparent throughput at longer wavelengths could be due to the change in polarization content of the calibration beam, with the 2003 values being artificially high. The change in the G225M and G285M grating throughputs departs substantially from the G230L and TA1 throughput changes and is believed to be due to a slow oxide growth on the bare aluminum optics. This would change their sensitivity as a function of polarization, effectively reducing sensitivity to unpolarized light. These results are discussed in separate documents: COS-11-0045a, COS-11-048 and COS-11-0049. Note that despite the drop in sensitivity, all the gratings continue to meet their CEI specifications on performance.

Table 5.4-6: 2006 FUV Sensitivity Measurements

					COS efficiency		
Appendix	Channel	λ_c (Å)	Segment	Test λ (Å)	cts/ph	rel. uncertainty	1 σ
C	G130M	1309	B	1216	0.1852	0.081	0.015
C	G130M	1309	B	1248	0.1735	0.098	0.017
C	G130M	1309	A	1327	0.1382	0.047	0.006
C	G130M	1309	A	1379	0.1291	0.047	0.006
C	G130M	1309	A	1430	0.1115	0.048	0.005
C	G130M	1309	A	1430	0.1086	0.056	0.006
C	G160M	1600	B	1430	0.1306	0.054	0.007
C	G160M	1600	B	1482	0.1099	0.056	0.006
C	G160M	1600	B	1524	0.0995	0.049	0.005
C	G160M	1600	A	1621	0.0574	0.056	0.003
C	G160M	1600	A	1669	0.0505	0.053	0.003
C	G160M	1600	A	1723	0.0399	0.060	0.002
C	G140L	1230	A	1248	0.1041	0.137	0.014
C	G140L	1230	A	1327	0.0943	0.135	0.013
C	G140L	1230	A	1430	0.0699	0.083	0.006
C	G140L	1230	A	1524	0.0530	0.054	0.003
C	G140L	1230	A	1723	0.0263	0.066	0.002

C	G140L	1230	A	1937	0.0049	0.052	0.0003

Table 5.4-7: 2006 NUV Sensitivity Measurements

					COS Efficiency		
Appendix	Channel	λ_c (Å)	Stripe	Test λ_c (Å)	cts/ph	rel. uncertainty	1σ
C	G185M	1817	A	1723	0.0293	0.056	0.002
C	G185M	1882	A	1777	0.0338	0.045	0.002
C	G185M	1850	B	1846	0.0327	0.049	0.002
C	G185M	1986	A	1883	0.0299	0.047	0.001
C	G185M	1882	B	1883	0.0303	0.047	0.001
C	G185M	1786	C	1883	0.0294	0.047	0.001
C	G185M	1835	C	1937	0.0283	0.049	0.001
C	G185M	1971	B	1972	0.0238	0.062	0.002
C	G185M	1953	C	2050	0.0219	0.061	0.001
C	G185M	1986	C	2085	0.0191	0.058	0.001
C	G185M	2010	C	2129	0.0173	0.058	0.001
C	G225M	2186	A	2085	0.0127	0.059	0.0007
C	G225M	2186	A	2085	0.0119	0.059	0.0009
C	G225M	2010	C	2129	0.0151	0.058	0.0009
C	G225M	2250	A	2144	0.0147	0.060	0.0009
C	G225M	2268	B	2262	0.0211	0.058	0.001
C	G225M	2390	A	2290	0.0217	0.058	0.001
C	G225M	2283	B	2290	0.0221	0.058	0.001
C	G225M	2186	C	2290	0.0210	0.059	0.001
C	G225M	2357	B	2357	0.0301	0.067	0.002
C	G225M	2339	C	2440	0.0239	0.063	0.002
C	G225M	2390	C	2487	0.0232	0.061	0.001
C	G285M	2657	A	2540	0.0142	0.062	0.0009
C	G285M	2657	B	2659	0.0166	0.059	0.001
C	G285M	2739	B	2734	0.0149	0.064	0.001
C	G285M	2952	A	2830	0.0135	0.094	0.001
C	G285M	2850	B	2830	0.0139	0.094	0.001
C	G285M	2719	C	2830	0.0138	0.094	0.001

C	G285M	2996	B	2998	0.0091	0.089	0.0008
C	G285M	3057	B	3064	0.0078	0.086	0.0007
C	G230L	2950	A	1723	0.0202	0.055	0.001
C	G230L	3000	A	1846	0.0261	0.048	0.001
C	G230L	3000	A	2050	0.0257	0.061	0.002
C	G230L	3360	A	2085	0.0255	0.060	0.0002
C	G230L	3360	A	2262	0.0242	0.061	0.002
C	G230L	2635	B	2487	0.0207	0.061	0.001
C	G230L	2635	B	2659	0.0181	0.060	0.001
C	G230L	2950	B	2830	0.0128	0.094	0.001
C	G230L	3000	B	2998	0.0075	0.157	0.001
C	TA1		A	1248	4.88E-05	0.154	0.000
C	TA1		A	1524	6.17E-05	0.130	0.000
C	TA1		A	1723	0.0401	0.055	0.002
C	TA1		A	1846	0.0491	0.044	0.002
C	TA1		A	2262	0.0466	0.058	0.003
C	TA1		A	2487	0.0420	0.060	0.002
C	TA1		A	2830	0.0314	0.094	0.003
C	TA1		A	2998	0.0198	0.089	0.002
C	TA1-BRT		A	1248	0.0008	0.143	0.0001
C	TA1-BRT		A	1524	0.0032	0.049	0.0002
C	TA1-BRT		A	1723	0.0054	0.056	0.0003
C	TA1-BRT		A	2262	0.0037	0.061	0.0002
C	TA1-BRT		A	2487	0.0034	0.054	0.0002
C	TA1-BRT		A	2998	0.0014	0.091	0.0001

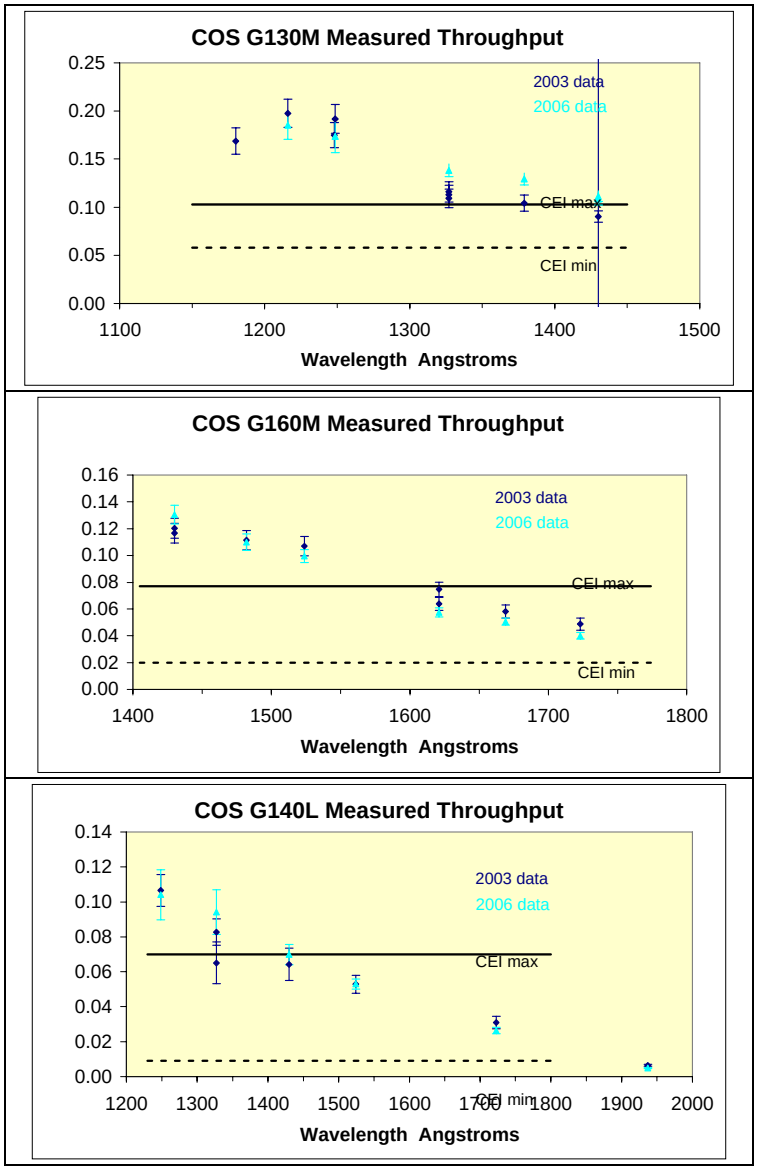

Figure 5.4-2: FUV sensitivity measurements in 2003 and 2006. The 2003 measurements are shown in dark blue and the 2006 measurements in light blue. The CEI specifications are shown as lines on the grating plots: the solid line is the CEI maximum (which must be exceeded at one wavelength) and the dotted line is the CEI minimum (which must be exceeded at all wavelengths).

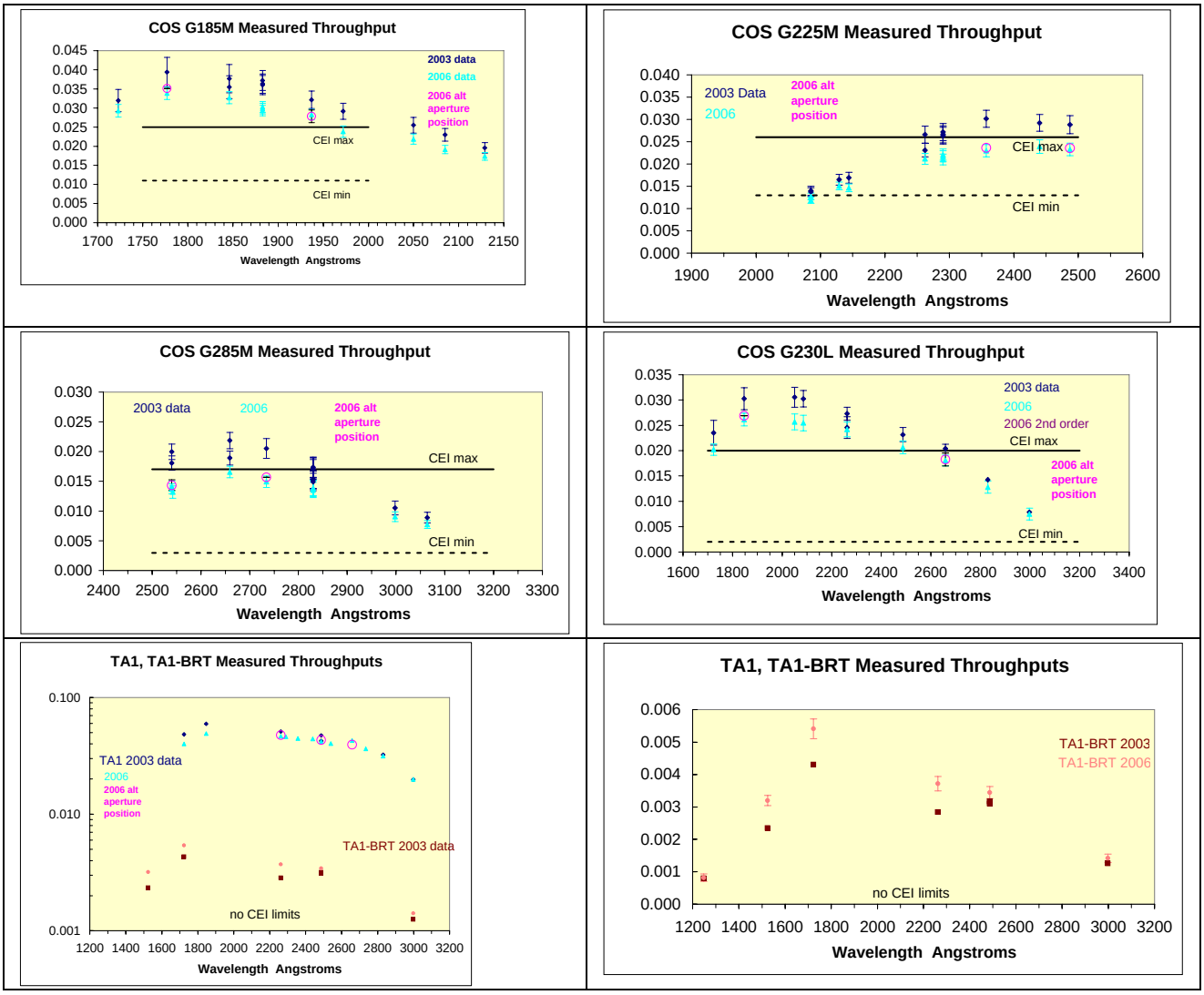

Figure 5.4-3: NUV sensitivity measurements in 2003 and 2006. The 2003 measurements are shown in dark blue and the 2006 measurements in light blue. The points in pink were repeated measurements in 2006. The CEI specifications are shown as lines on the grating plots: the solid line is the CEI maximum (which must be exceeded at one wavelength) and the dotted line is the CEI minimum (which must be exceeded at all wavelengths).

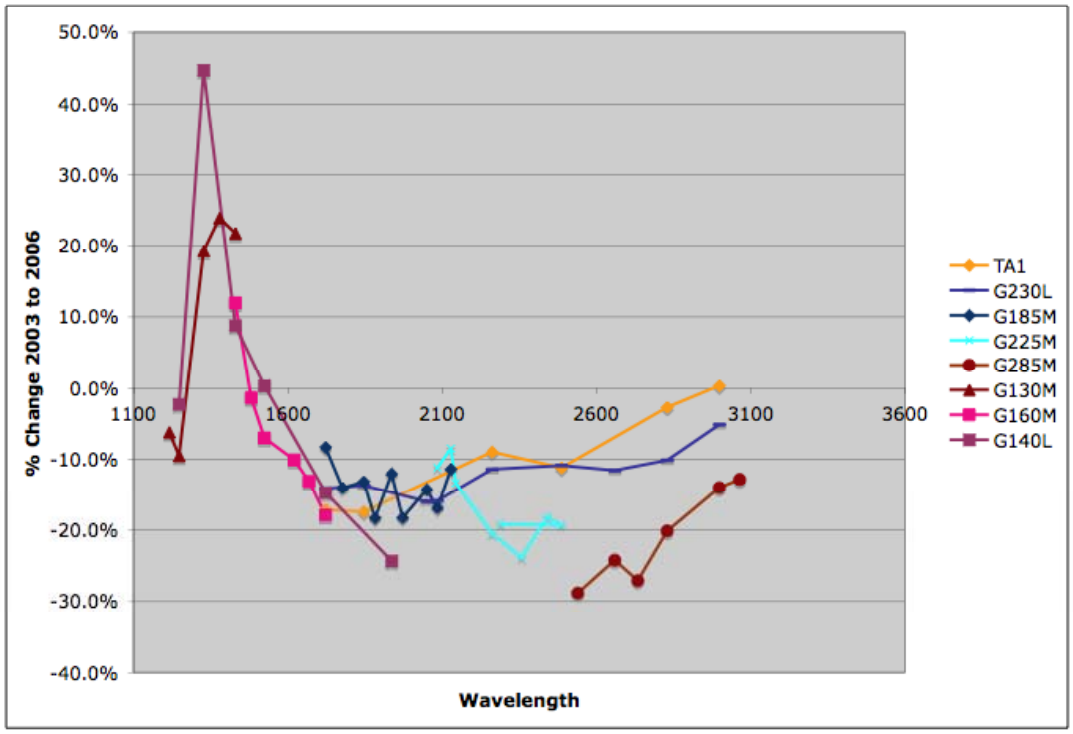

Figure 5.4-4: Percent change in measured COS throughput between 2003 and 2006 observations.

5.5 BRIGHT OBJECT APERTURE TRANSMISSION

5.5.1 CEI Requirement

Section 4.2.6 and Table 4.5 of the CEI specification list the specific requirements for the COS bright object aperture (BOA). For the purposes of this discussion, the BOA must have transmission of no more than 1% across the FUV and NUV band passes (e.g. >ND2).

5.5.2 2003 Test Description & Data Reduction

The transmission of the BOA was computed by dividing the observed counts from an external lamp through the primary science aperture (PSA) into the observed counts of the same light

source through the BOA, with an appropriate scaling for the difference in exposure times (PSA observations consisted of two 120 second exposures and the BOA observation consisted of a single 1800 second exposure). The transmission at FUV wavelengths was measured during Test 3300 using the G140L channel. The NUV transmission was measured during Tests 3310 and 3310A using the three wavelength settings of the G230L channel. Tests 3300 and 3310 were conducted using an external PtNe lamp through the CDS. Test 3310A used an external D2 lamp through the CDS.

Test 3310 was originally thought to be sufficient to characterize the BOA transmission function. However, a preliminary evaluation of the data suggested that differences in the spectral resolution between the PSA and BOA were introducing noise into the calculation. Therefore, Test 3310A was initiated using a D2 continuum lamp instead of the PtNe line lamp, thus eliminating variations in the spectral resolution as a concern. Ultimately both tests produced similar results.

For each test the spectra were extracted and binned from ~14000 spectral bins to 16 bins for the FUV data or 1024 to 16 for the NUV data. This increased the number of counts per bin, decreasing the statistical error in the computation of the transmission. The data were then scaled by 240/1800 to account for the differences in exposure times. PSA data from before and after the BOA exposures were used, thus the 240 or 2x120. The mathematical expressions for the transmission and error in the transmission are as follows;

$$T(\lambda) = \frac{C_{BOA}(\lambda) - C_{bkgnd}}{C_{PSA}(\lambda) - C_{bkgnd}} \cdot \frac{240}{1800}$$

$$\sigma_T(\lambda) = T(\lambda)\sqrt{\frac{C_{PSA}(\lambda) + C_{bkgnd}}{\left(C_{PSA}(\lambda) - C_{bkgnd}\right)^2} + \frac{C_{BOA}(\lambda) + C_{bkgnd}}{\left(C_{BOA}(\lambda) - C_{bkgnd}\right)^2}}$$

In this case C_{BOA} and C_{PSA} are the measured counts in a given spectral bin. C_{bkgnd} is the background counts for a similarly sized spectral bin.

5.5.3 FUV Channel

Tests: 3300 – FUV BOA Throughput and Resolution

Relevant Exposures:

Table 5.5-1: Exposure list for 2003 FUV BOA throughput and resolution tests.

Test 3300	Description

CSIL03285204854	λ_c=1320,PSA,t_{exp}=120 sec
CSIL03285213104	λ_c=1320,BOA,t_{exp}=1800 sec
CSIL03285214514	λ_c=1320,PSA,t_{exp}=120 sec

5.5.3.1 2003 Results

Table 4.5-1 and Figure 4.5-1 (at the end of this section) show the wavelength, transmission (T), and statistical error (σ_T) for Test 3300 in tabular and graphical format respectively.

Table 5.5-2: Results for Test 3300

λ(Å)	T	σ_T
1227.96	0.00726	0.00012
1309.88	0.00916	0.00017
1391.8	0.00634	0.00015
1473.72	0.00636	0.00010
1555.64	0.00762	0.00019
1637.56	0.00645	0.00025
1719.48	0.00624	0.00027
1801.4	0.00583	0.00019
1883.32	0.00638	0.00028
1965.24	0.00630	0.00028
2047.16	0.00604	0.00061
2129.08	0.01102	0.00147
2211	0.01547	0.00420
2292.92	0.03945	0.01454
2374.84	0.02888	0.01466
2456.76	0.00981	0.00275

5.5.4 NUV Channel

Tests: 3310, 3310A – NUV BOA Transmission and Resolution

Relevant Exposures:

Table 5.5-3: Exposure list for 2003 NUV BOA transmission and resolution tests.

Test 3310	Test 3310A	Description
CSIL03267204612	CSIL03273163316	λ_c=3000, PSA, t_{exp}=120 s
CSIL03267212608	CSIL03273171312	λ_c=3000, BOA, t_{exp}=1800 s
CSIL03267213804	CSIL03273172508	λ_c=3000, PSA, t_{exp}=120 s
CSIL03267215058	CSIL03273173802	λ_c=3360, PSA, t_{exp}=120 s
CSIL03267223054	CSIL03273181758	λ_c=3360, BOA, t_{exp}=1800 s
CSIL03267224250	CSIL03273182954	λ_c=3360, PSA, t_{exp}=120 s
CSIL03267225544	CSIL03273184248	λ_c=2635, PSA, t_{exp}=120 s
CSIL03267233540	CSIL03273192244	λ_c=2635, BOA, t_{exp}=1800 s
CSIL03267234736	CSIL03273193440	λ_c=2635, PSA, t_{exp}=120 s

5.5.4.1 2003 Results

Tables 4.5-2 and 4.5-3 present the transmission as computed from Test 3310 and 3310A respectively. Figure 1 shows the wavelength, transmission (T), and statistical error (σ_T) for Test 3310A, while Figure 4.5-2 shows the transmission computed from Test 3310.

Table 5.5-4: Results for Test 3310 – PtNe line lamp spectra

λ_c = 2635, Stripe A			λ_c = 3000, Stripe A		
λ(Å)	T	σ_T	λ(Å)	T	σ_T
2745.14	0.00466	0.00028	2027.06	0.00653	0.00058
2720.18	0.00458	0.00028	2002.03	0.00663	0.00059
2695.21	0.00458	0.00028	1977	0.00573	0.00055
2670.24	0.00462	0.00028	1951.97	0.00585	0.00056
2645.28	0.00434	0.00027	1926.94	0.00587	0.00055
2620.31	0.00457	0.00028	1901.91	0.00780	0.00065
2595.34	0.00441	0.00027	1876.88	0.00653	0.00057
2570.38	0.00425	0.00027	1851.85	0.00621	0.00057
2545.41	0.00446	0.00028	1826.82	0.00557	0.00054
2520.44	0.00443	0.00027	1801.79	0.00618	0.00056
2495.48	0.00439	0.00027	1776.76	0.00615	0.00057

2470.51	0.00409	0.00026	1751.72	0.00603	0.00056
2445.55	0.00438	0.00027	1726.69	0.00679	0.00059
2420.58	0.00429	0.00027	1701.66	0.00538	0.00053
2745.14	0.00466	0.00028	2027.06	0.00653	0.00058
2720.18	0.00458	0.00028	2002.03	0.00663	0.00059

λ_c = 3000, Stripe B			λ_c = 3360, Stripe A		
λ(Å)	T	σ_T	λ(Å)	T	σ_T
3165.37	0.00373	0.00032	2441.51	0.00517	0.00035
3140.42	0.00392	0.00032	2416.49	0.00553	0.00036
3115.46	0.00408	0.00033	2391.48	0.00516	0.00034
3090.51	0.00399	0.00032	2366.46	0.00478	0.00033
3065.56	0.00382	0.00031	2341.44	0.00529	0.00035
3040.6	0.00373	0.00031	2316.42	0.00569	0.00036
3015.65	0.00429	0.00033	2291.41	0.00483	0.00033
2990.69	0.00369	0.00031	2266.39	0.00517	0.00034
2965.74	0.00388	0.00032	2241.37	0.00504	0.00034
2940.79	0.00424	0.00033	2216.35	0.00531	0.00035
2915.83	0.00400	0.00032	2191.34	0.00539	0.00035
2890.88	0.00419	0.00033	2166.32	0.00498	0.00034
2865.93	0.00372	0.00031	2141.3	0.00567	0.00036
2840.97	0.00419	0.00033	2116.28	0.00485	0.00034
2816.02	0.00429	0.00033	2091.27	0.00536	0.00035
2791.07	0.00400	0.00032	2066.25	0.00534	0.00035

Table 5.5-5: Results for Test 3310A – D2 continuum lamp spectra

λ_c = 2635, Stripe A			λ_c = 3000, Stripe A		
λ(Å)	T	σ_T	λ(Å)	T	σ_T
2795.08	0.00455	0.00032	2077.12	0.00619	0.00043
2770.11	0.00436	0.00031	2052.09	0.00660	0.00044
2745.14	0.00490	0.00033	2027.06	0.00627	0.00044
2720.18	0.00494	0.00033	2002.03	0.00604	0.00043
2695.21	0.00455	0.00032	1977	0.00557	0.00041
2670.24	0.00435	0.00031	1951.97	0.00589	0.00042
2645.28	0.00473	0.00032	1926.94	0.00613	0.00043
2620.31	0.00487	0.00033	1901.91	0.00600	0.00042

2595.34	0.00475	0.00033	1876.88	0.00595	0.00043
2570.38	0.00422	0.00031	1851.85	0.00636	0.00043
2545.41	0.00432	0.00031	1826.82	0.00625	0.00044
2520.44	0.00457	0.00032	1801.79	0.00629	0.00044
2495.48	0.00420	0.00031	1776.76	0.00572	0.00042
2470.51	0.00441	0.00031	1751.72	0.00627	0.00044
2445.55	0.00484	0.00033	1726.69	0.00586	0.00042
2420.58	0.00430	0.00031	1701.66	0.00634	0.00044

λ_c = 3000, Stripe B			λ_c = 3360, Stripe A		
λ(Å)	T	σ_T	λ(Å)	T	σ_T
3165.37	0.00525	0.00058	2441.51	0.00486	0.00028
3140.42	0.00356	0.00049	2416.49	0.00527	0.00029
3115.46	0.00362	0.00049	2391.48	0.00560	0.00031
3090.51	0.00426	0.00051	2366.46	0.00499	0.00029
3065.56	0.00473	0.00056	2341.44	0.00548	0.00030
3040.6	0.00514	0.00059	2316.42	0.00524	0.00030
3015.65	0.00404	0.00053	2291.41	0.00526	0.00029
2990.69	0.00486	0.00055	2266.39	0.00532	0.00029
2965.74	0.00469	0.00055	2241.37	0.00505	0.00029
2940.79	0.00418	0.00052	2216.35	0.00532	0.00029
2915.83	0.00471	0.00055	2191.34	0.00523	0.00029
2890.88	0.00442	0.00053	2166.32	0.00515	0.00029
2865.93	0.00496	0.00056	2141.3	0.00537	0.00030
2840.97	0.00445	0.00054	2116.28	0.00538	0.00030
2816.02	0.00486	0.00056	2091.27	0.00569	0.00031
2791.07	0.00425	0.00052	2066.25	0.00541	0.00030

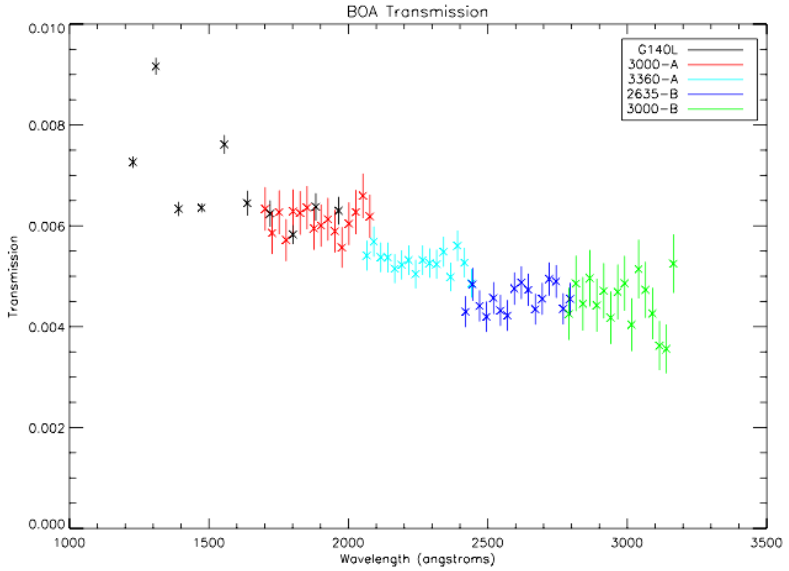

Figure 5.5-1: FUV and NUV BOA transmission computed from data acquired during Tests 3300 and 3310A.

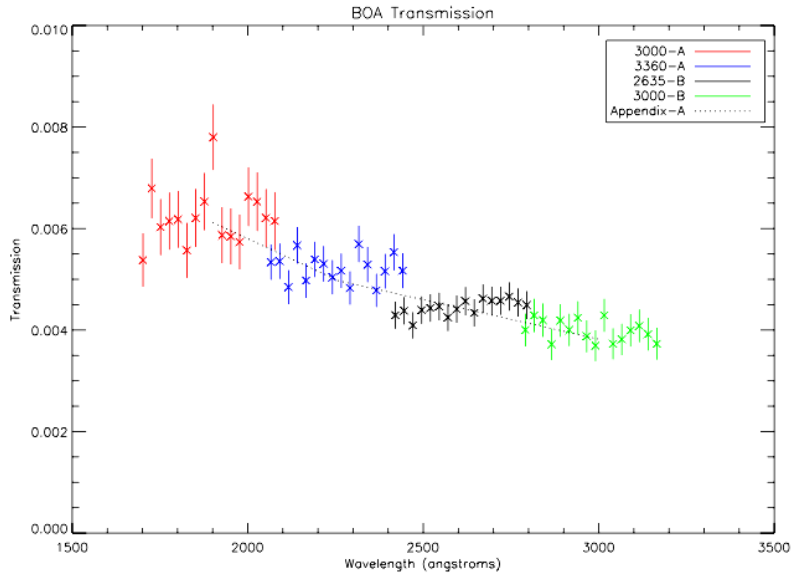

Figure 5.5-2: NUV BOA transmission computed from data acquired from Test 3310.

5.5.5 2006 Test Results

Tests: 3300 – FUV BOA transmission and resolution
3310 – NUV BOA transmission and resolution

5.5.5.1 FUV

One set of G140L exposures (central wavelength = 1230 Å) allow us to quantify the BOA transmission across the FUV bandpass. This set consists of two 120 second PSA exposures (CSIL06337021910 and CSIL06337030547) and one 1800 second BOA exposure (CSIL06337025400). The segment A BOA and PSA spectra were wavelength calibrated, background subtracted, then divided into 16 equal segments.

The table below lists 1) the central wavelength of each segment, 2) the BOA/PSA transmission in percentage, 3) the 1-sigma error of the transmission, 4) the count rate (in counts per second) of the BOA exposure, and 5) the count rate of the merged PSA exposure.

All measured FUV BOA transmissions agree with previous measurements and exceed the requirements.

Table 5.5-6: 2006 FUV BOA transmission and resolution test results.

λ(Å) (1)	Trans (%) (2)	Error (%) (3)	BOA cts/sec (4)	PSA cts/sec (5)
2047.2	0.58	0.02	0.6	104.8
1965.2	0.57	0.01	1.22	214.6
1883.3	0.59	0.02	0.67	112.8
1801.4	0.61	0.02	0.5	81.4
1719.5	0.61	0.02	0.43	69.9
1637.6	0.6	0.02	0.93	154.8
1555.6	0.62	0.01	2.24	359.3
1473.7	0.63	0.02	0.55	86.9
1391.8	0.65	0.03	0.3	46.7
1309.9	0.78	0.04	0.27	34.2
1228	0.78	0.08	0.1	13.1

A comparison with previous results is given in Figure **5.5-3** below. The Appendix C data are plotted with magenta triangles (FUV) and magenta diamonds (NUV). The NUV and FUV measured transmission agree in the overlap region of 1900-2000Å.

5.5.5.2 NUV

Four sets of G230L exposures allow us to quantify the BOA transmission across the NUV bandpass. Each set consists of two 120 second PSA exposures and one 1800 second BOA exposure.

Details of the observations are listed in the table below. Columns in this table are (1) PSA filenames, (2) BOA filenames, (3) Central wavelength setting, (4) NUV stripe measured, (5) Wavelength at the center of the stripe, (6) measured transmission (in percentage) of the BOA relative to the PSA, (7) 1-sigma error of the measured transmission, (8) BOA count rate (in counts per second), and (9) PSA count rate (in counts per second).

All measured NUV BOA transmissions agree with previous measurements and exceed the requirements.

Table 5.5-7: 2006 NUV BOA transmission and resolution results.

PSA filenames (CSILxxxx) (1)	BOA filename (CSILxxxx) (2)	λ_C (Å) (3)	S (4)	λ(Å) (5)	Trans (%) (6)	Error (%) (7)	BOA cts/sec (8)	PSA cts/sec (9)
06337040102 06337044532	06337061855	2635	B	1877	0.56	0.02	0.846	150.0
06337040102 06337044532	06337043507	3000	A	2241	0.51	0.02	2.665	525.4
06337045256 06337053726	06337043507	3000	B	2595	0.42	0.01	3.756	887.8
06337054450 06337062920	06337052701	3360	A	2966	0.36	0.01	2.196	611.7

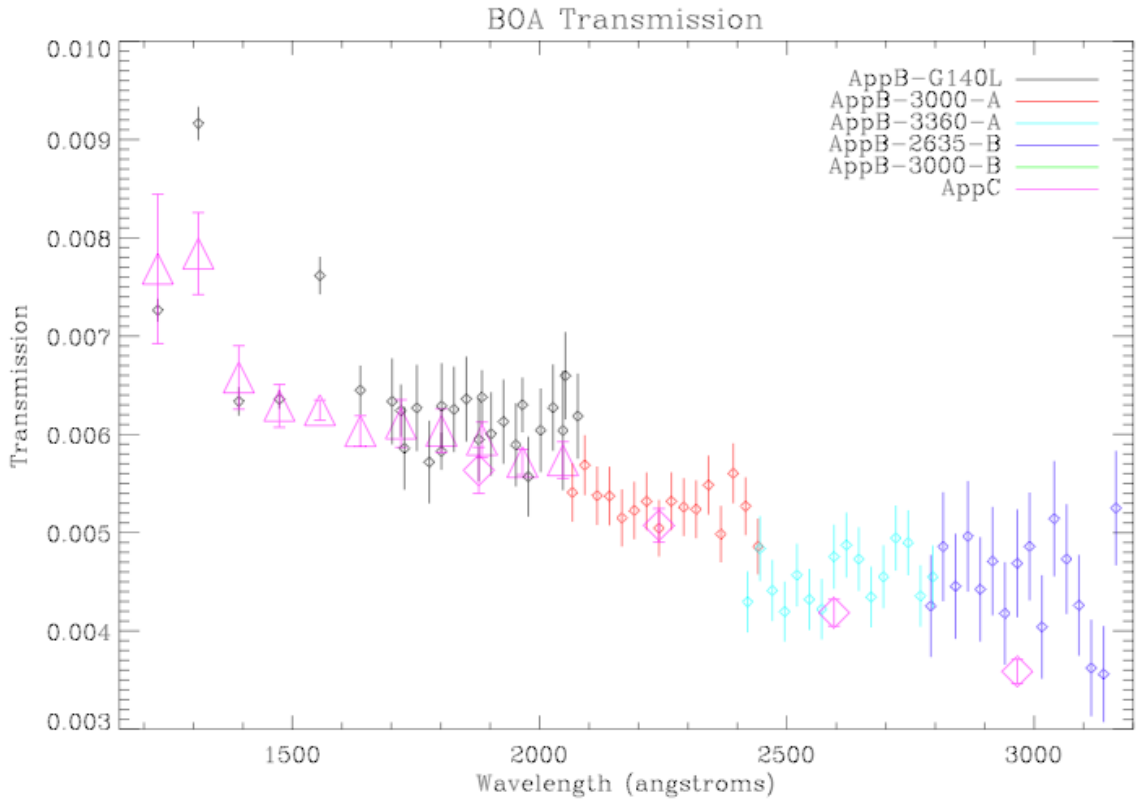

Figure 5.5-3: Comparison of 2003 and 2006 BOA transmission measurements.

5.6 SIGNAL TO NOISE

5.6.1 CEI Requirements

Section 4.2.5 and Table 4-4 of the CEI list the requirements for the COS instrument signal to noise performance. For the purposes of this discussion signal to noise is defined as the "reciprocal of the root-mean-square (RMS) scatter of data points about a smooth function fit to those points." In summary, the COS instrument shall support at least 30:1 signal to noise during routine operations and 100:1 under optimal conditions.

5.6.2 FUV Channel

Five test procedures were used to characterize the flat-field response of the FUV detector. These tests (#850, #1700, #1720, #1730, and #3000) provided 95 internal flat-field calibration lamp exposures per FUV detector segment that were suitable for characterizing the intrinsic efficiency variations of the digital elements (DE). All tests for FUV segment 'A' used the'G130M grating, while all segment 'B' tests used the G160M grating. Tests #1700, #1720, #1730, and #3000 were specifically performed for purposes of obtaining the flat-field, while test #850 "FUV Repeatability Monitor" provided additional exposures as part of stability testing. The illumination of the FUV segments was adjusted throughout the tests to paint the lifetime cross-dispersion science regions of the detectors. In geometrically corrected images, we considered cross-dispersion (XD) 'Y' digital element values 377 to 578, and the dispersion direction (DD) 'Y' digital element values 1130 through 15241 to be the science region of segment 'A' of the FUV detector. For segment 'B', the XD range was taken to be digital values 436 to 636, and the DD range was taken to be 1324 to 15546. We restrict our analysis to these regions. Furthermore, we define a resolution element (RE) to be 6(DD)x10(XD) digital elements (DE), resulting in ~2350 RE per segment.

The combined segment 'A' flat-field image (super-flat) contained 1.84E8 counts, with a median counts/DE over the science region of 276, and a median photon statistic S/N of 17 per DE, or 129 per RE. The combined segment 'B' flat-field image contained 1.79E8 counts, with a median counts/DE over the science region of 296, and a median photon statistic S/N of 18 per DE, or 134 per RE.

5.6.2.1 2003 FUV Flat Field Analysis

The dispersion and cross-dispersion profiles of the FUV 'super-flats' are shown in Figures 4.6-1 (A) and 4.6-2 (B). The strong dips in the upper panels of these figures are shadows from the grid-wires, which are periodic in the DD. Also shown in the bottom (XD) panels are the nominal spectral locations, and the XD extent of the PSA at the FUV detector. To determine the DE-to-DE variations (the P-flat) from the structure associated with the grid-wires and the illumination from the calibration lamps (the L-flat), polynomials were constructed along columns of the super-flats. For each column in the science region, least-squares polynomials of order 1 (linear) to 5 were constructed. These polynomials form the FUV L-flats of varying accuracy. The 3rd order produced the lowest reduced χ^2, and we adopt this as our L-flat. Dividing the FUV super-flat by the L-flat defines the P-flat.

To quantify the variations inherent to the P-flat, we construct histograms of the P-flat values for each segment. The histograms, along with the measured Gaussian widths (σ), are shown in Figure 5.6-4. The FUV P-flat Gaussian widths indicate the maximum achievable S/N without flat-field correction. The FUV P-flat distribution indicates that, at the DE level, the standard

deviations are 15-20%, with a higher standard deviation for segment 'A'. At the RE level, the P-flat distributions show standard deviations of ~5-6%, implying that the maximum S/N per RE achievable without flat-fielding is ~20.

To predict the actual S/N achievable when applying the FUV P-flats, we examined data taken during the 17 science and wavelength calibration exposure pairs of test 2120, "FUV high quality spectra". Each exposure pair consisted of a CO absorption line spectrum (Kr lamp used as the light source) and an internal wavelength calibration exposure. The exposures were taken at a series of OSM offsets to enable the data to be dithered (FP_SPLIT). To determine the dispersion offsets, the wavelength spectra were cross-correlated at the 1/10 of a DE level. Due to characteristics of the CDS, the segment 'A' spectra contained significantly fewer counts than the segment 'B' spectra. Figure 4.6-3 shows the S/N achieved for a line-free region of the segment 'B' spectra for five reduction algorithms;

Raw (thermal correction (TC) only),
Geometric correction (GC) +TC (GC+TC)
FP_SPLIT (FP)+TC+GC (FP+GC),
FP_SPLIT+TC+flatfielding (FF) using TC only (FP+FF-GC+TC), and
fully corrected (FP+FF+GC+TC).

The results are compared to the maximum S/N achievable due to photon statistics (Photon noise = √counts). Extractions not using a flatfield (FF) reach a S/N per RE limit of ~20. The dithering extraction (FP_SPLIT) partially corrects the DE-to-DE variations, and can achieve S/N per RE of ~40. Applying both dithering and the derived P-flats corrects the digital element-to-digital element variations close to the limits of our photon statistics.

Finally, Figure 4.6-5 shows the full G130M Kr lamp spectrum with the CO absorption cell in place for segments A and B.

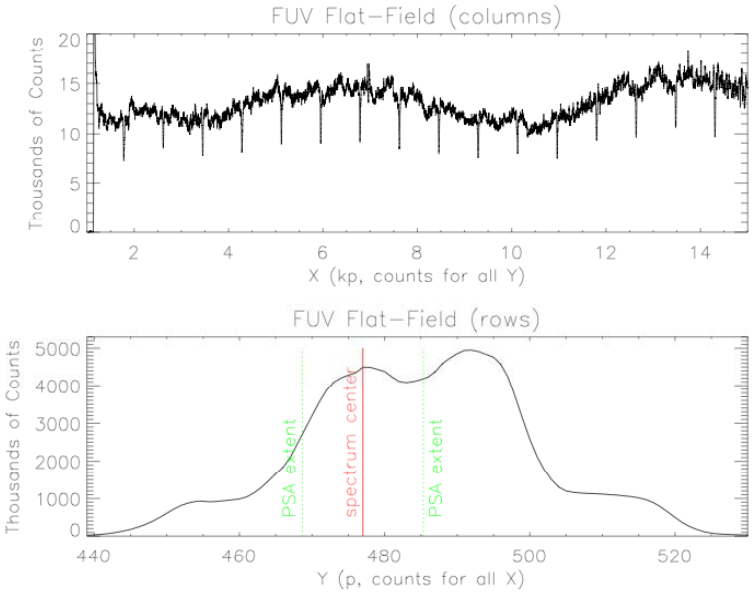

Figure 5.6-1: Histograms in X and Y for FUV02 segment A showing the number and distribution of counts used to generate the flat field image.

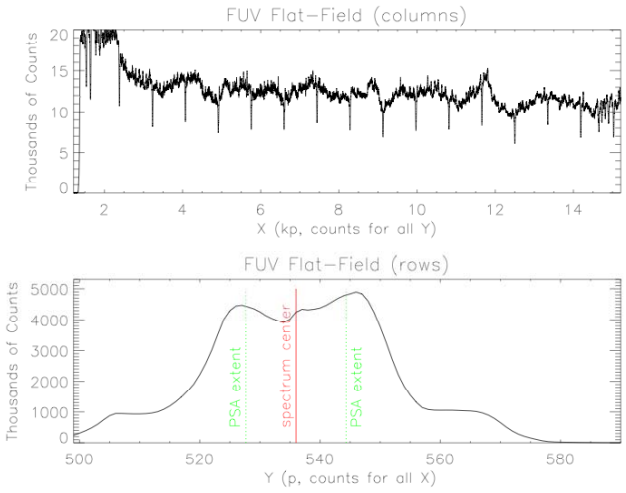

Figure 5.6-2: Histograms in X and Y for FUV02 segment A showing the number and distribution of counts used to generate the flat field image.

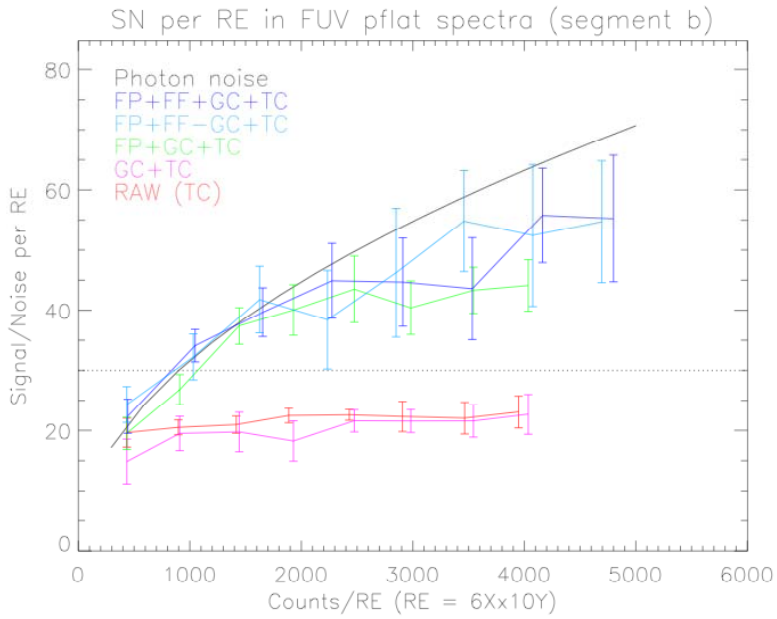

Figure 5.6-3: Measured signal to noise versus counts per resolution element under different correction assumptions.

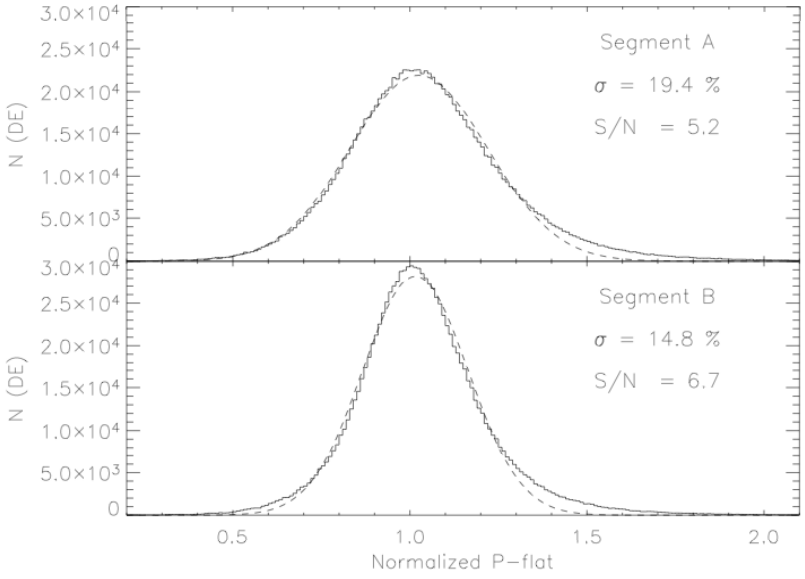

Figure 5.6-4: Distribution of residuals in the final FUV flat fields.

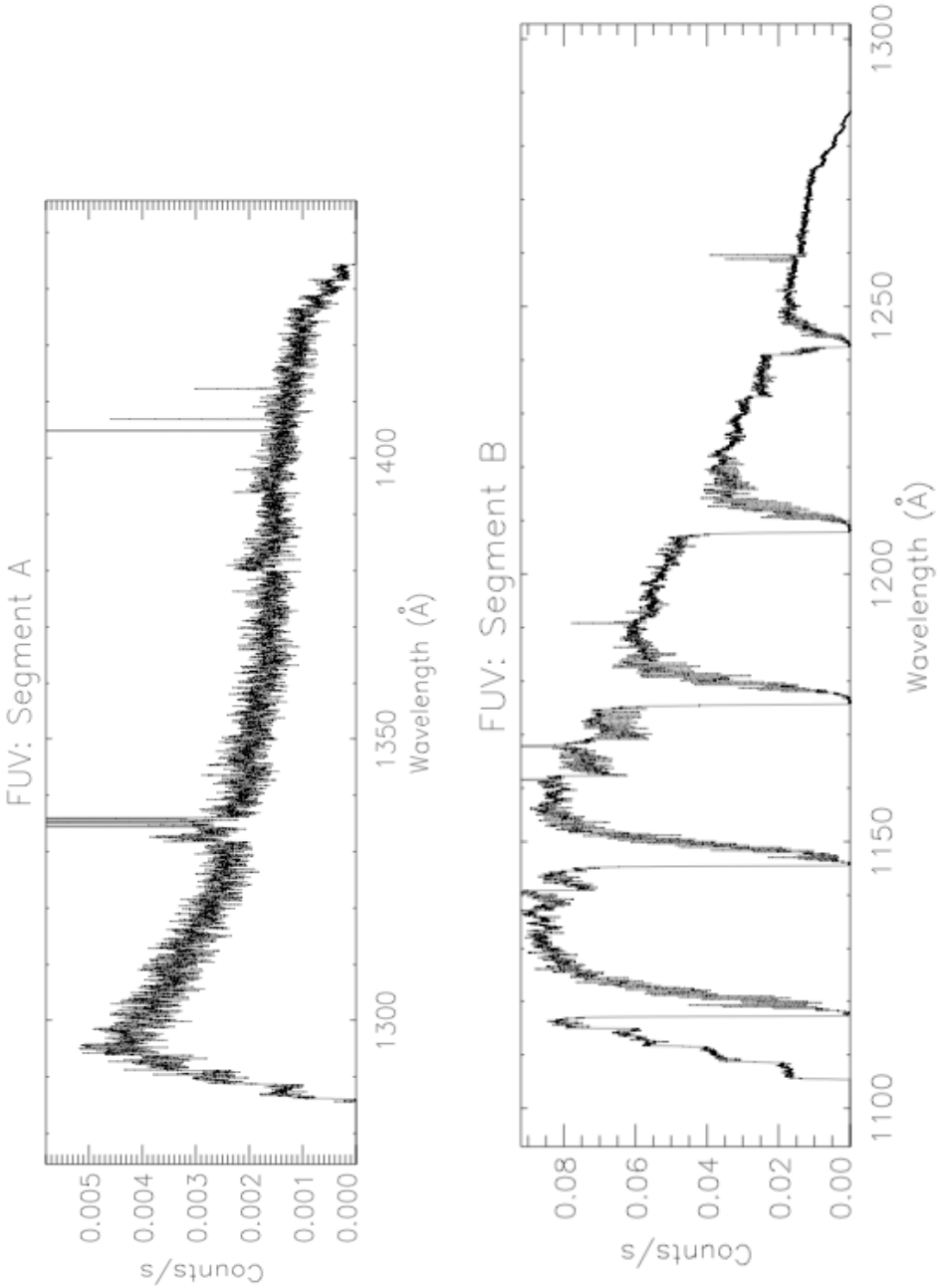

Figure 5.6-5: G130M Kr lamp spectra with a CO absorption cell in place used to evaluate the signal-to-noise performance of COS.

5.6.2.2 2006 FUV Flat Field Analysis

The 2006 CDS was capable of delivering more light from the D2 flat field lamp in the FUV than the 2003 CDS could provide. As a result, in 2006 we obtained external flat field data for the FUV.

Tests: 1301 – FUV CDS lamp brightness
1300 – FUV external flat field S/N=30
1399 – FUV faint source

Test #1301 was a setup test to verify settings for the external deuterium (D2) lamp. Test #1300 acquired D2 observations through the wide open aperture in RASCAL. Test #1399 was similar to #1300 except that the D2 observations were acquired through the 10μm RASCAL aperture to simulate a point source spectrum. The data analysis below concentrates on this final set of observations, as they more closely mimic the type of external flat field source we will be able to acquire on orbit.

Test #1399 was performed on 12/06/06 as part of the COS Appendix C testing to determine whether an external source (a Deuterium lamp, D2) could be used to obtain a flat-field (FF) spectrum for the FUV channel. Previous attempts in Appendix B testing at flat-fielding with a traditional 2-D flat using an internal source did not improve the data quality. During this test, 180 second G160M exposures were taken at each of the twenty central wavelength and FP-OFFSET (FP) position listed in the table below.

Table 5.6-1: Exposure list for 2006 FUV flat field tests.

Dataset	Wavelength Setting (Å)	FP-OFFSET
CSIL06340100500	1577	-1
CSIL06340101249	1577	0
CSIL06340102038	1577	1
CSIL06340102936	1589	-2
CSIL06340103725	1589	-1
CSIL06340104514	1589	0
CSIL06340105303	1589	1
CSIL06340110201	1600	-2
CSIL06340110950	1600	-1
CSIL06340111739	1600	0

Dataset	Wavelength Setting (Å)	FP-OFFSET
CSIL06340112528	1600	1
CSIL06340113426	1611	-2
CSIL06340114215	1611	-1
CSIL06340115004	1611	0
CSIL06340115753	1611	1
CSIL06340120653	1623	-2
CSIL06340121442	1623	-1
CSIL06340122231	1623	0
CSIL06340123020	1623	1

After thermal and geometric correction, the spectra where divided into 'odd' and 'even' samples. These spectra shown in Figure 5.6-6 below. The external D2 lamp produces a continuum only at the longest wavelengths (above ~1600Å, the lower pixel portion of segment 'A'). We focused our flat-fielding efforts on the region of the detector where the spectra are colored blue and red. The ten red regions were added to produce the even flat-field and the ten blue regions were combined to produce the odd flat-field. Because the continuum is very flat in this region, normalization of the flat-field was achieved by a simple linear fit.

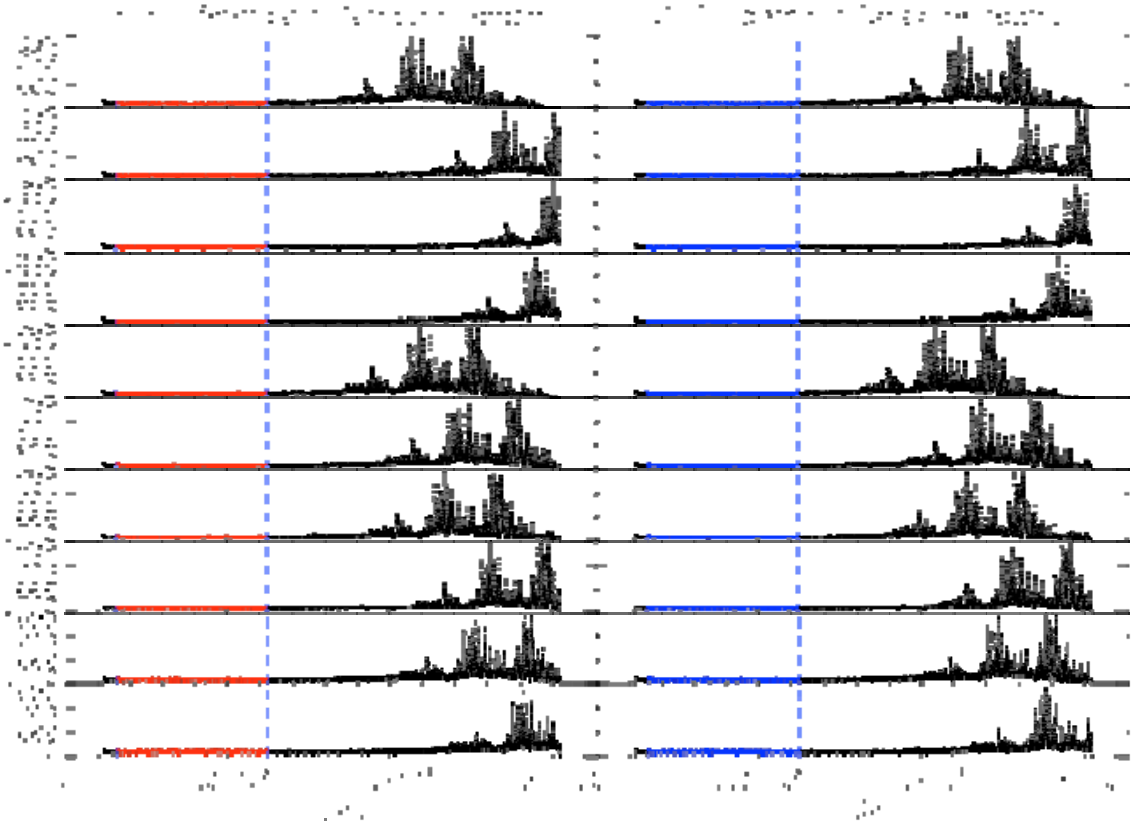

Figure 5.6-6: External D2 spectra from 2006 thermal vacuum testing used for FUV flat field analysis. The spectra have been divided into two samples, "odd" and "even."

The same spectra where then aligned in wavelength space, and the same regions were added to create odd and even test spectra. The wavelength alignment was performed by a cross-correlation of the portion of the D2 spectrum with strong lines (the upper pixel portion of the spectra). The wavelength aligned spectra are shown in Figure 5.6-7 below (with an arbitrary wavelength scale); again, the test portions of the spectra are shown in blue and red.

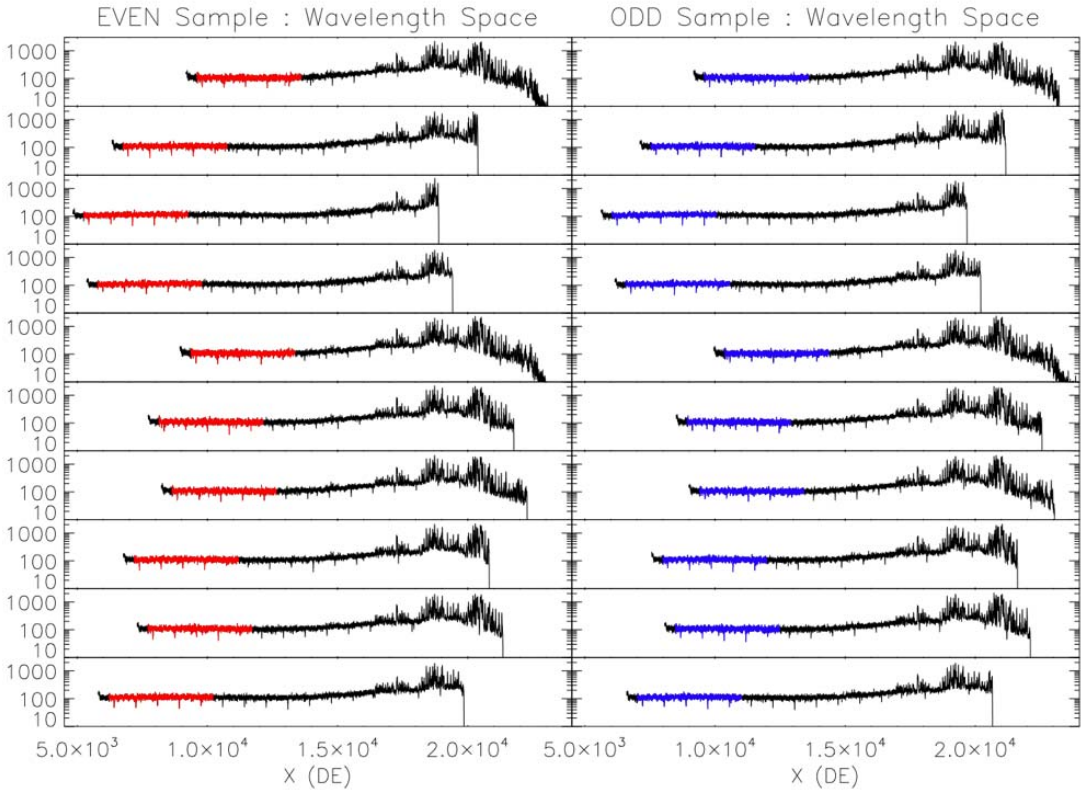

Figure 5.6-7: FUV external D2 spectra for flat-field analysis. The spectra have been aligned in wavelength space.

The odd flat-field was used to correct the merged even test spectra, and vice-versa. In this way, no data was ever flat-fielded by itself, or by data taken at the same wavelength region. Because the spectrum and the flat-field shared the same illumination on the detector (cross-dispersion profile), the flat-fielding was performed in one dimension (the spectral dimension). In other words, each merged data column was used to create the flat-field value for that detector column. The 1D flat-field is shown in Figure 5.6-8 below. Various features such as hex, grid wires, and hot spots are clearly visible.

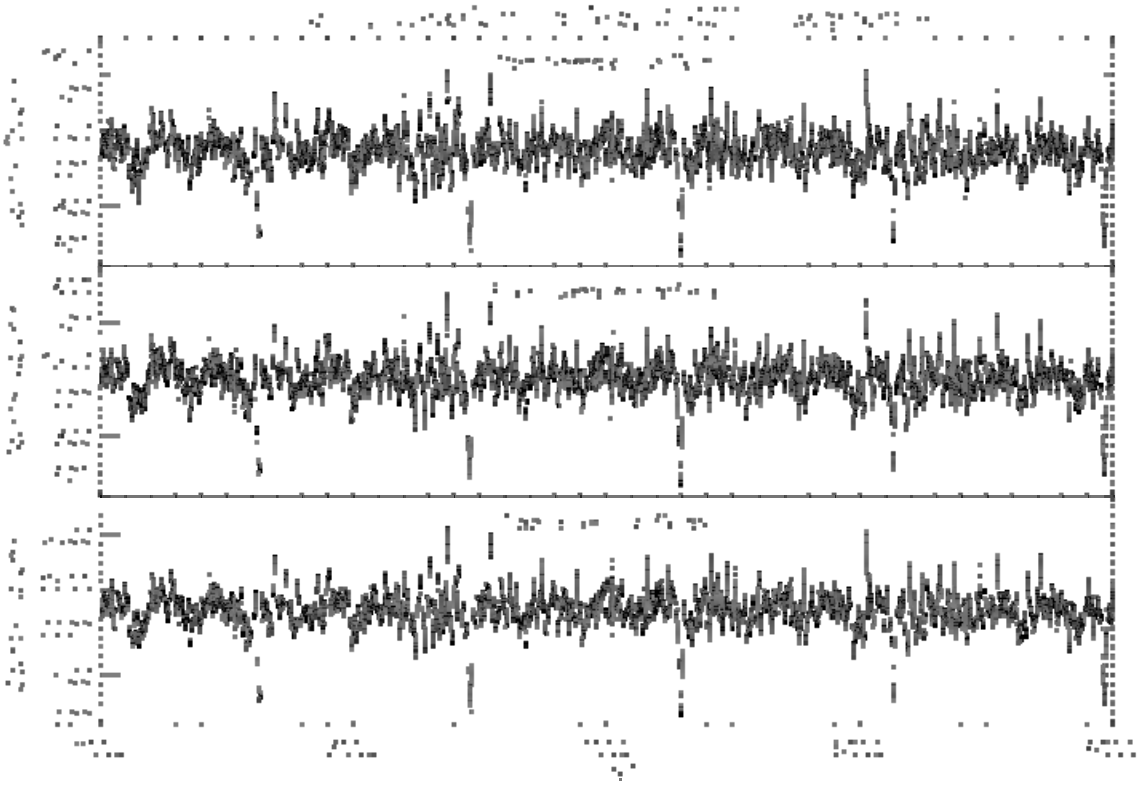

Figure 5.6-8: One dimensional flat-fields created from the odd and even data sets.

In Figure 5.6-9 below, the results of this flat-fielding can be observed. The upper left panel (labeled "noFP, no FF") shows the normalized, odd sample added in detector space (it is the odd flat-field). The distribution at the right shows the column to column variations, and is an indication of the maximum S/N without FP-dithering or flat-fielding (FF). The second row shows the normalized spectra added in wavelength space, and reveals S/N improvement from the FP-dithered positions. The third row shows the normalized spectrum after FP-dithering and the inclusion of the even FF. Finally, the bottom row shows the normalized FP+FF spectrum on a per resolution element basis. The results shown in this figure only use the highest S/N portion of the merged spectra.

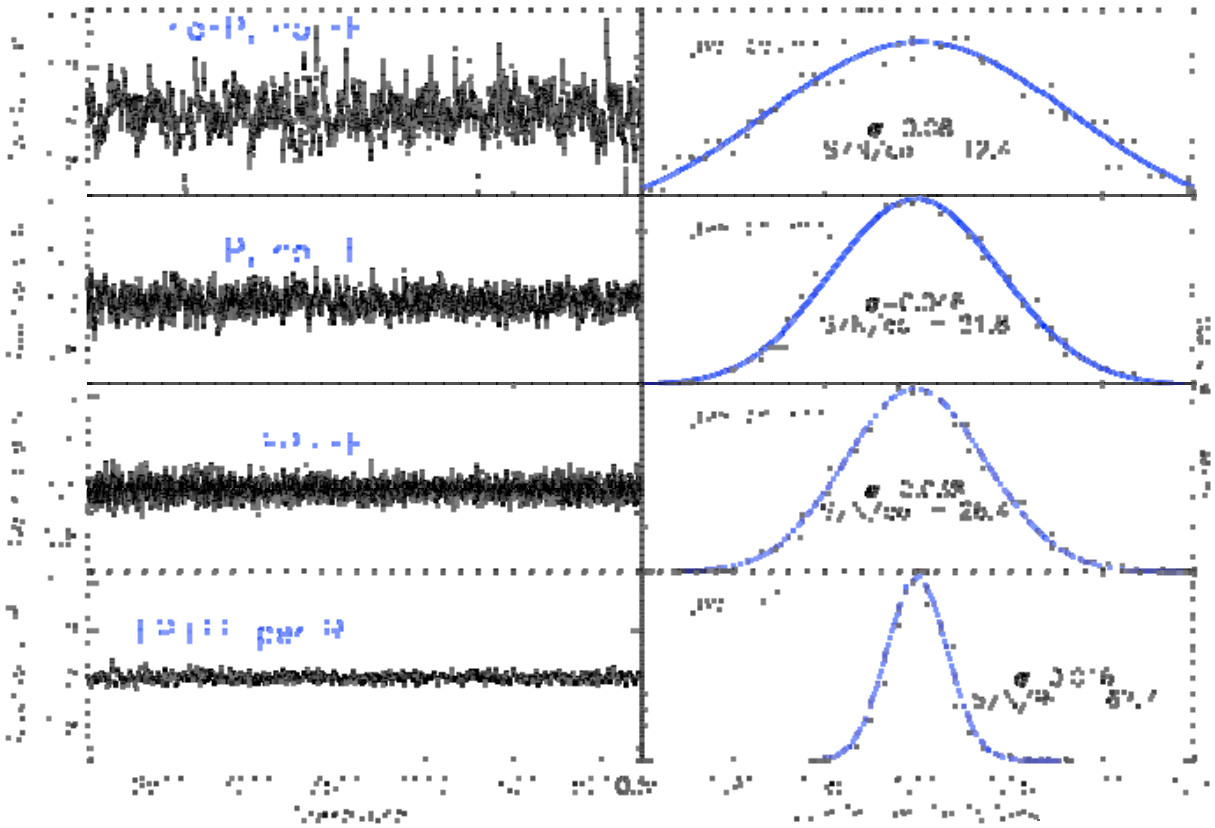

Figure 5.6-9: Results of flat fielding for different combinations of flats plus application of focal plane splits.

To illustrate the effectiveness of the 1D flat-fielding, the above process was repeated after the addition of each of the ten (odd or even) test spectra, and is plotted in Figure 5.6-10 below against the photon limited result and the photon limited result factoring in the quality of our FFs (photon statistics of about +/- 3%). Starting at the top of the figure, the solid line with triangles shows the photon-limited result with a perfect FF. The solid black line without triangles shows the maximum achievable S/N with the FF obtained in this test and ten FP positions. The results to the left of the vertical dashed line are per column values, while results to the right are per RE. The solid blue and red lines are the odd and even test spectra FFd and FP-dithered as previously described. Deviations of the odd and even test spectra from the theoretical maximum are due mixed S/N regions of the merged spectra as more and more spectra and wavelength ranges are added to the test spectra. Just below the test spectra results, the green solid line shows the theoretical maximum if no FP dithering was used, but our FF was still applied. Finally, at the bottom the S/N achieved in our odd and even test spectra are shown with FP dithering, but no

flat-fielding. Unlike the previous figure, the entire merged spectrum was used in the figure, and the final S/N values are lower than the those obtained previously when only using the highest S/N portions. These results indicate that high signal to noise observations will be possible in the FUV with COS on orbit once acquisition of an external "flat" source (such as a nearby white dwarf) is acquired and used to construct a one dimensional spectral flat field correction.

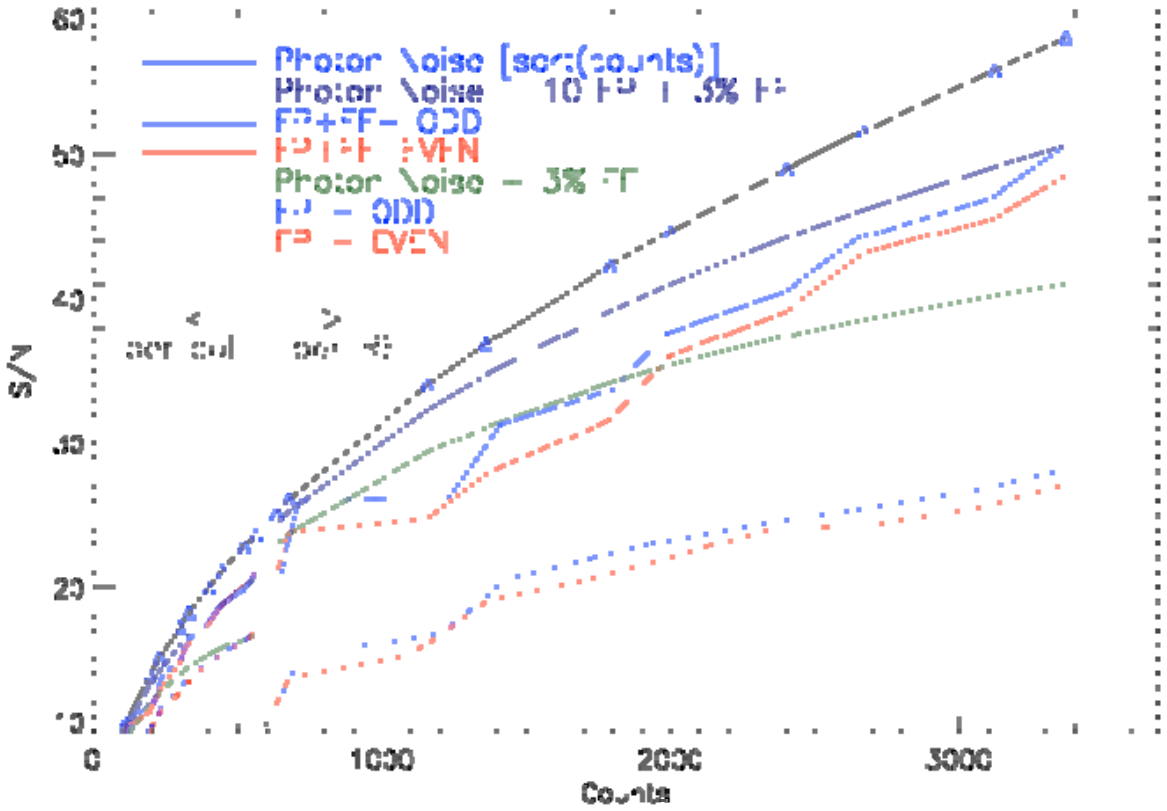

Figure 5.6-10: Measured signal to noise versus counts per resolution element under different correction assumptions for the 2006 FUV flat field data set.

5.6.3 NUV Channel

Three procedures were used to characterize the flat-field response of the NUV detector. The first test (#1750) used the internal calibration lamp Flat #1, while the other two tests (#2505 and #2506) used an external calibration lamp D2. Test #2506 was added to extend the cross-dispersion coverage of test 2505 and is included in this analysis. In this analysis cross-dispersion

(XD) 'X' pixel values 500 through 900, and the dispersion direction (DD) 'Y' pixel values 2 through 1021 were considered to be the science region of the detector. This analysis is restricted to this region. Furthermore, a resolution element (RE) is defined to be 3x3 pixels (p), resulting in 340 RE per spectral stripe. Our fiducial location spectral stripes are: A, X = 861; B, X= 759; and C, X=619. All flat-field exposures were taken with the G185M grating.

Test #1750, "NUV Calibration Sub-System Flat Fields, S/N=30", consisted of 27 exposures with a total exposure time of 64.8 ksec. The combined NUV internal exposure contained 7.54E7 counts. The median counts/p over the science region was 210. The median signal to noise ratio (S/N) was 15 per p, or 44 per RE.

Test # 2505, " NUV Calibration Delivery System, S/N = 100', and its cross-dispersion extension, Test #2506, consisted of 44 exposures with a total exposure time 24.5 ksec. The combined external exposure contained 3.59E9 counts. The median counts/p over the science region was 8707. The median S/N was 94 per p, or 280 per RE.

To create the highest quality NUV flat-field, all data from tests 1750, 2505 and 2506 were combined to create a NUV calibration `super-flat', with most of the counts coming from the external tests. The combined Flat-field image contained 3.62E9 counts. The median counts/p over the science region was 8920. The median S/N was 95 per p, or 284 per RE

5.6.3.1 2003 Results

The dispersion and cross-dispersion profiles of the NUV super-flat are shown in Figure 5.6-11. Also shown in Figure 5.6-11 are the spectral stripe locations. By extracting from the super-flat 1D spectra at the spectral stripe locations, the S/N as a function of spectral location (wavelength) can be derived. Figure 5.6-13 shows the S/N achieved per RE from the NUV super-flat for the three science stripes. To convert to S/N per pixel, simply divide the displayed S/N by 3 ($\sqrt{9}$).

The small scale deviations from a smooth extracted spectrum are the result of pixel-to-pixel variations of the NUV detector response. To extract the pixel-to-pixel variations (the P-flat) from the structure in Figure 5.6-11 associated with the illumination from the calibrations lamps (the L-flat), polynomials were constructed along columns of the super-flat. For each column in the science region, least-squares polynomials of order 1 (linear) to 6 were constructed. These polynomials form the NUV L-flats of varying accuracy. The parabolic (order =2) produced the lowest reduced χ^2, and we adopted this as our final L-flat. Dividing the NUV super-flat by the L-flat defines the P-flat.

To quantify the variations inherent to the P-flat, we extracted flat-field spectra (per RE) at the stripe locations. The histograms of the spectra, along with the measured Gaussian widths (σ), are

shown in Figure 5.6-12. The Gaussian widths define the maximum achievable S/N without flat-field correction of the NUV data. The S/N values are indicated for each stripe in Figure 5.6-12. Without flat-fields, NUV spectra are limited to S/N of ~50.

To predict the S/N achievable when applying the NUV flatfields, we examined data taken during the 54 exposures of test 2170, "NUV high quality spectra". Each of these exposures used the D2 lamp, taken with an internal wavelength calibration exposure. The exposures were taken at a series of OSM offsets to enable the data to be dithered (FP_SPLIT). To determine the dispersion offsets, the internal wavelength spectra were cross-correlated. Figure 5.6-14 shows the S/N achieved for the 'C' stripe for three reduction algorithms; Raw (no corrections), FP_SPLIT, and FP_SPLIT plus flat-fielding (FF). The results are compared to the maximum S/N achievable due to photon statistics (√counts). Due to the Gaussian nature of the P-flat, the raw extraction reaches a S/N limit of 50. The dithering extraction (FP_SPLIT), however, partially corrects the pixel-to-pixel variations, and can achieve high S/N with no limit detected by the calibration tests. Applying both dithering and the derived P-flats fully corrects the pixel-to-pixel variations to the limit of our photon statistics.

Finally, Figure **5.6-15** shows the complete D2 spectrum used for this analysis.

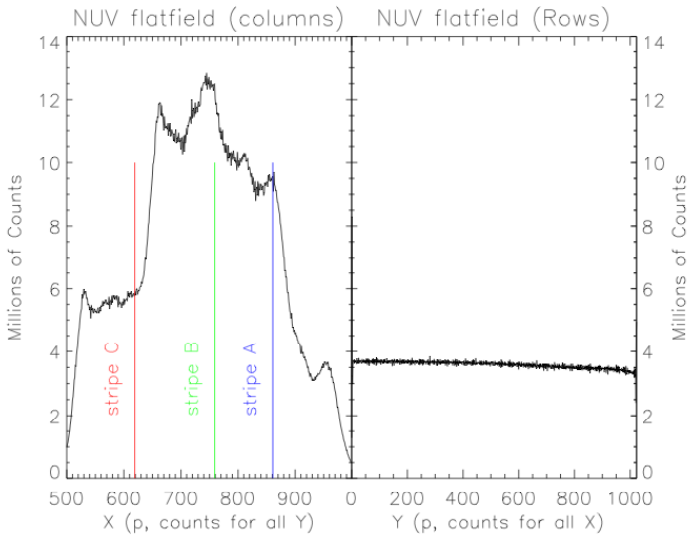

Figure 5.6-11: Counts per pixel used to derive the NUV flat fields and achievable signal to noise.

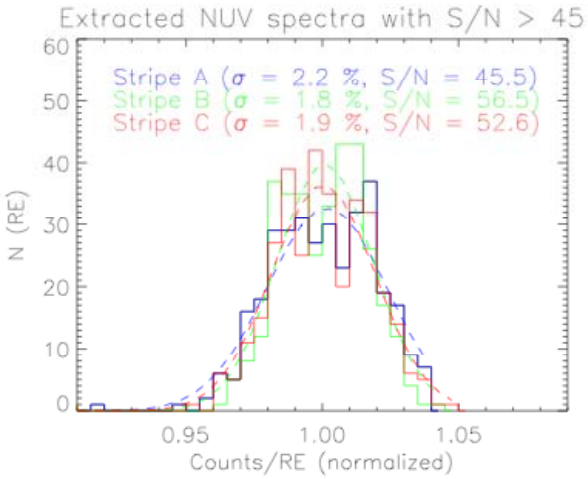

Figure 5.6-12: Histograms of the residual errors for each spectra. The width is an indication of the maximum achievable signal to noise without flat fielding.

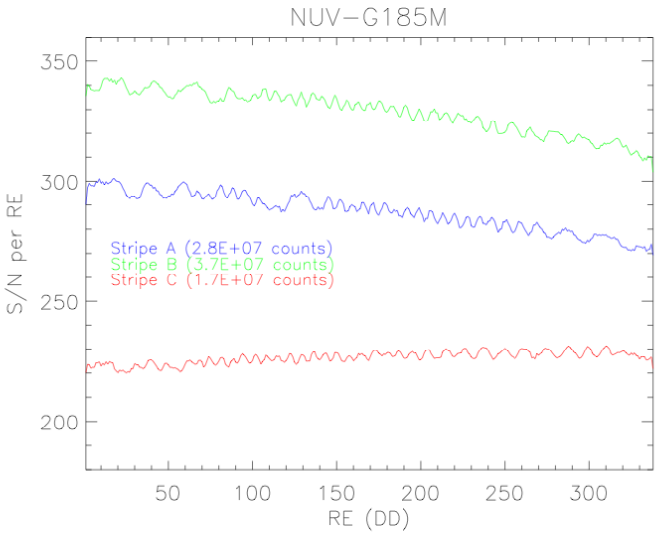

Figure 5.6-13: Signal to noise per resolution element for the data.

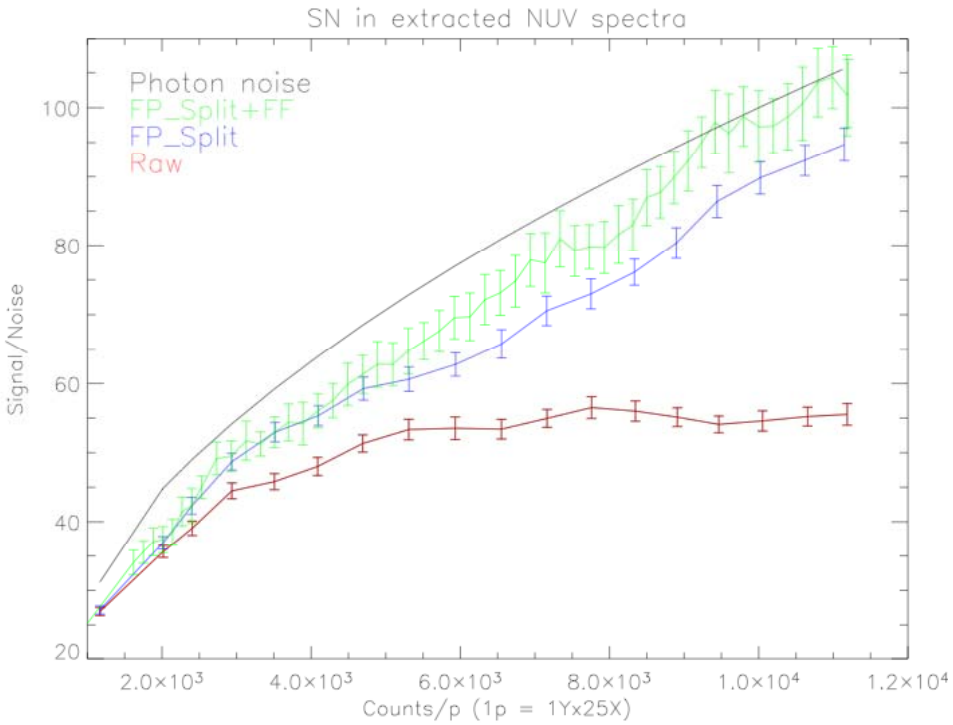

Figure 5.6-14: Signal to noise per resolution element as a function of counts and processing step.

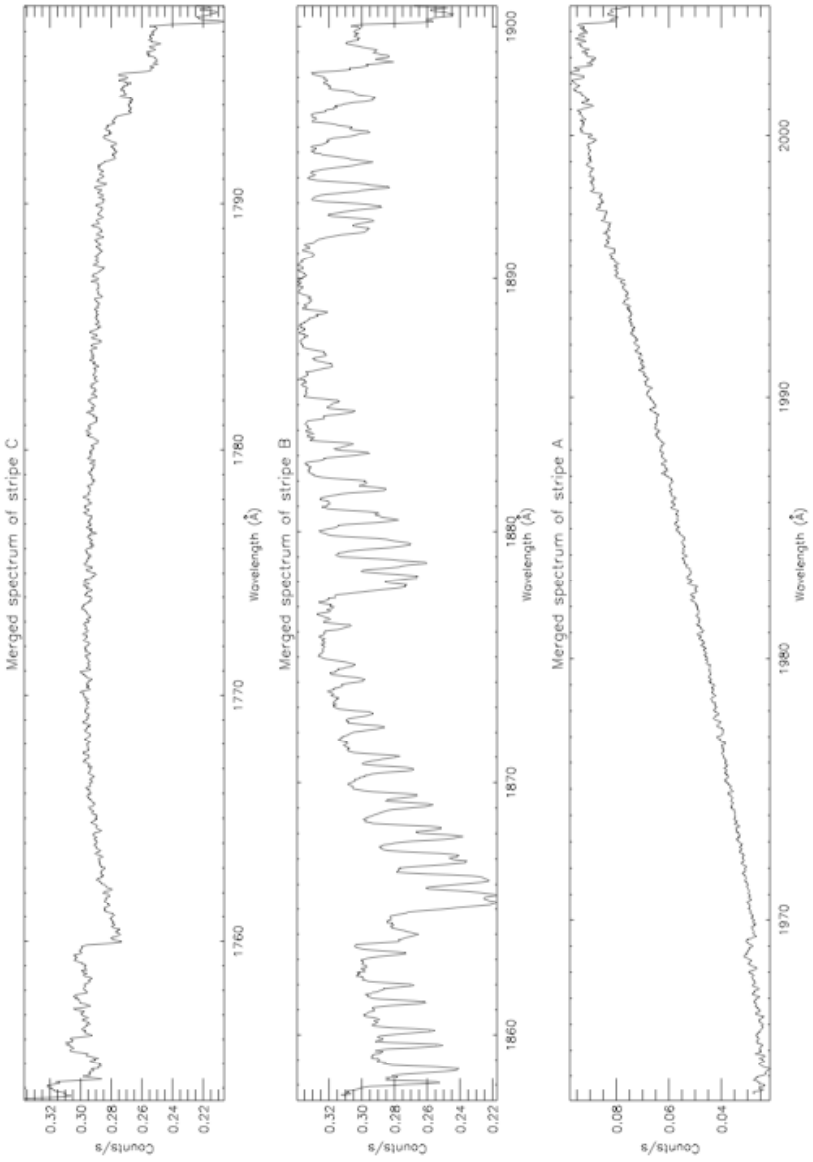

Figure 5.6-15: G185M spectrum of a D2 lamp with an O2 absorption cell used to evaluate the signal-to-noise performance of the COS instrument.

5.6.3.2 2006 Results

The NUV flat-field analysis was not repeated in the 2006 thermal vacuum tests.

5.7 FIELD OF VIEW

5.7.1 CEI Requirements

Section 4.2.6 of the CEI and Table 4-5 list the specifications for the field of view of the COS instrument. In general terms the CEI states that the COS instrument shall have two apertures, a Prime Science Aperture (PSA) and a Bright Object Aperture (BOA). The BOA shall have at least a factor of 100 attenuation compared to the PSA. Each aperture shall have a 2.5" diameter working field of view. These requirements are met by design and implementation.

5.7.2 Description

The 2.5" requirement is satisfied by the physical size of the PSA and BOA and was measured as part of component inspection at delivery. However, during Appendix B the PSA aperture was fully illuminated to measure the offsets from the internal wavelength calibration lamp image center to the center of the science aperture and additionally demonstrate the total field of view and look for potential sources of stray or scattered light. The aberrated nature of the HST PSF allows light from field angles outside the 2.5" diameter of the apertures to enter the instrument. Specifically, ray-trace models predict that objects within a 4" diameter centered on an aperture will be visible in the science data.

To verify the optical performance of the COS apertures the region around the PSA was over-illuminated and an image acquired with the TA-1 mode in Appendix B. These measurements were not repeated in Appendix C.

Tests: 1437 – Image of LINE1 lamp vs. Flooded Aperture
1410 – TA1 Field of View Mapping

Relevant Exposures:

Table 5.7-1: Exposure list for 2003 field of view tests.

File	Channel/λ_C	Comments
CSIL03289175054	TA-1	Fully illuminated PSA image
CSIL03289191553	TA-1	Fully illuminated BOA image

CSIL03269170802	TA-1	Test 1410:
CSIL03269171202	TA-1	PSA scanned across the RAS/Cal image
CSIL03269171602	TA-1	All exposures with D2 lamp for 100 sec.
CSIL03269172002	TA-1	
CSIL03269172402	TA-1	
CSIL03269172802	TA-1	
CSIL03269173201	TA-1	
CSIL03269173600	TA-1	
CSIL03269174001	TA-1	
CSIL03269174401	TA-1	
CSIL03269174809	TA-1	
CSIL03269175332	TA-1	
CSIL03269175731	TA-1	
CSIL03269180131	TA-1	
CSIL03269180532	TA-1	
CSIL03269180931	TA-1	
CSIL03269181331	TA-1	
CSIL03269181731	TA-1	
CSIL03269182131	TA-1	
CSIL03269182531	TA-1	
CSIL03269182930	TA-1	
CSIL03269183340	TA-1	

5.7.3 2003 Results

As stated above, ray-trace models predict that objects within a 4" diameter, corresponding to 167 pixels in the TA-1 mode, will be visible in the science data. Examining the images for the files presented above we see that in each case the size of the image is ~167 pixels, exactly as we would have predicted (see Figure 4.7-1). It is worth noting that the asymmetry in the illumination pattern of the image is likely due to irregularities in the light produced within the lamp and not due to vignetting within the COS instrument. This is because non-uniformity in the image cannot generally be induced by vignetting some portion of a converging, diverging, or collimated beam. This sort of non-uniformity is generally produced either by the object or vignetting at an image plane. Since COS does not form an image plane within the instrument the non-uniformity can only come from the source or vignetting right at the aperture.

In addition, during Test 1410 the COS PSA was scanned across the point source formed by RASCAL and the count rate monitored. The count rates were symmetric about the center of the

aperture, so vignetting at or near the aperture is unlikely, leaving source non-uniformity as the most probable of the observed structure. A comparison of the measured PSA transmission and the predicted transmission from a ray-trace model is shown in Figure 4.7-2.

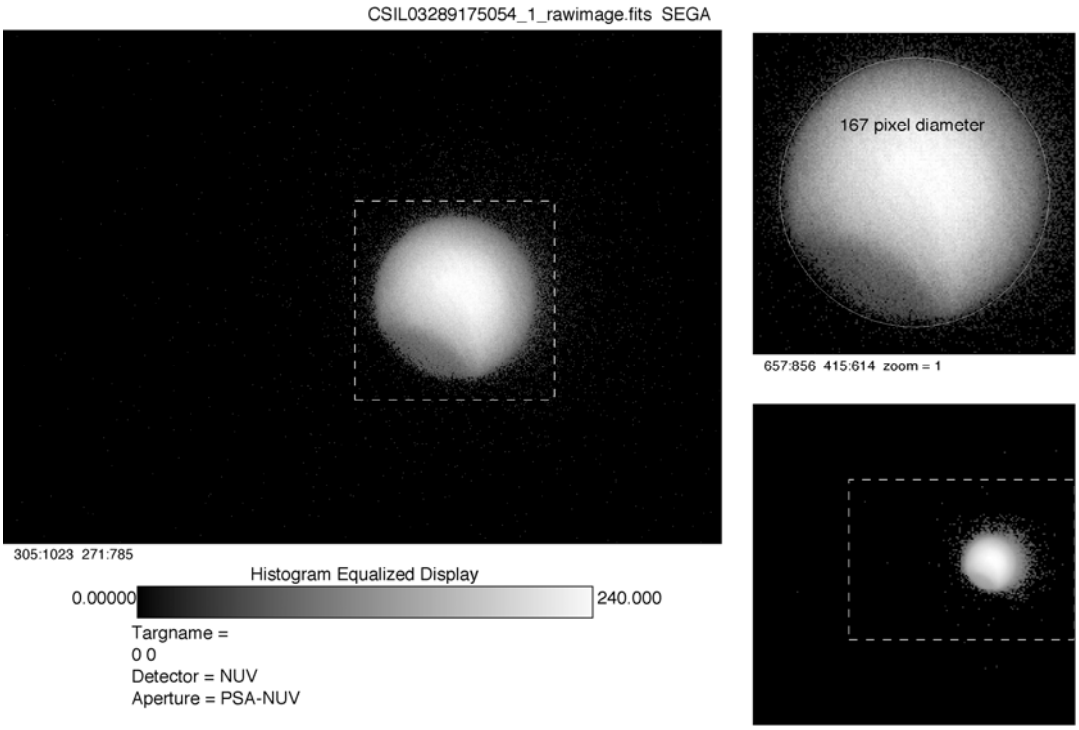

Figure 5.7-1: TA-1 image of a fully illuminated PSA aperture. The circle in the upper right image is 167 pixels in diameter and highlights how the observed image is as large as expected from ray-trace models.

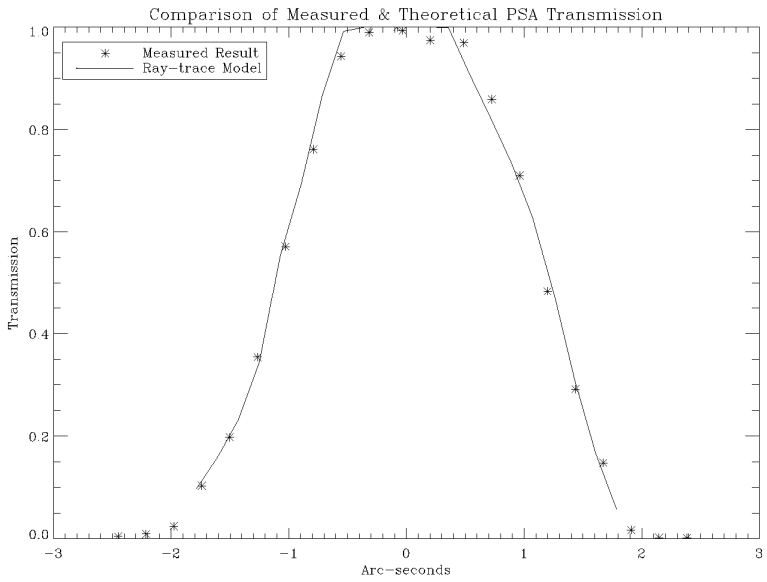

Figure 5.7-2: Comparison of the measured PSA transmission as a function of off-axis angle and the predicted transmission from ray-trace models.

5.8 STRAY AND SCATTERED LIGHT

5.8.1 Requirements

The Contract End Item (CEI) Specification (STE-063) states that diffuse and scattered light shall contribute no more than 2% residual intensity to the signal in the core of a saturated absorption line measured with any of the medium dispersion modes in the spectrum of a point source in the PSA. The residual intensity shall be measured in the net spectra after extraction from the two dimensional gross data and measurement and removal of background light using COS data processing algorithms.

The COS Calibration Requirements and Procedures (AV-03) states that the primary measurement is to obtain a continuum exposure with saturated absorption lines at a signal to noise level of 30:1 per resolution element. Compare the continuum level to the level at the core of the saturated line. A secondary test is to examine a high S/N external Pt-Ne spectrum to search for light between the emission lines. (Note, this secondary test was not run due to potential for significant permanent charge extraction from the FUV detector.)

5.8.2 FUV

The following tests were executed in Appendix B (2003). The CDS did not contain an absorption cell in 2006, so the tests were not repeated in Appendix C (2006).

Tests: 2100 – Initial Absorption Cell Spectra
2110 – FUV Scattered Light

Relevant Exposures:

Table 5.8-1: Exposure list for 2003 FUV stray and scattered light tests.

File	Channel/λ_C	Comments
CSIL03289040431	G130M/1309 Å	A few saturated bands in Å
CSIL03289042300	G160M/1600 Å	Saturated bands in B
CSIL03289050500	G140L/1230 Å	Saturated or nearly so in A
CSIL03289051900	G160M/1600 Å	Saturated in B
CSIL03289053131	G130M/1309 Å	A saturated, B saturated or very close
CSIL03289055131	G130M/1309 Å	A saturated, B close
CSIL03289061831	G160M/1600 Å	B saturated
CSIL03289065031	G140L/1230 Å	A saturated or close to saturated

All of the spectra have nearby unabsorbed or weakly absorbed regions from which to measure the unattenuated flux.

5.8.2.1 Analysis

This analysis focuses on two exposures, one from each medium-resolution grating, which show a nice series of saturated absorption bands: CSIL03289051900 (G160M, segment B only), and CSIL03289053131 (G130M, both segments). For each spectrum and appropriate segment, a one-dimensional spectrum was created by performing a sum in the cross-dispersion direction covering the full width at zero intensity (FWZI) of the external spectrum. A background light spectrum was also created by extracting another one-dimensional spectrum of the same width away from the target spectrum. The FUV spectra are shown in Figure 4.8-1.

5.8.2.2 Results

CSIL03289053131, Seg A: The peak intensity in the unattenuated spectral regions decreases smoothly from 131 counts (near pixel 2000) to 61 counts (near pixel 14250). The first three absorption cores are the widest. They run from pixels 3191 -- 3794, 5929 -- 6386, and 8464 -- 8904. The mean count in these regions is 0.02, with an rms of 0.25 and a maximum count value of 2. Taking the conservative unabsorbed count rate of 61 counts gives a 2% residual level of 1.2 counts, which is easily met in the observed spectrum.

CSIL03289053131, Seg B: The peak unattenuated count rate is roughly 70 counts in the two unattenuated spectral regions around pixels 2700 and 4500. The first two absorption bands only just approach saturation, while the third does not become saturated. In the narrow regions, 2024 - 2087 and 3903 - 3935, the mean counts are 0.23, with a 0.6 pixel rms and a maximum pixel value of 2. The 2% residual level is 1.4 counts, so measured scattered light meets specifications.

CSIL03289051900: The unattenuated counts in the three brightest humps in the spectrum average roughly 190 counts. For the stray and scattered light, the average and deviation were calculated for the four saturated bands near these unattenuated spectral regions: pixels 6763 - 7356, 9459 - 10015, 11866 - 12483, and 14224 - 14753. The average counts over all four regions is 0.04 counts. The rms is 0.3 counts the maximum single count in a pixel is 3. The 2% residual intensity level is 3.8 counts, so again the scattered light is well within specifications.

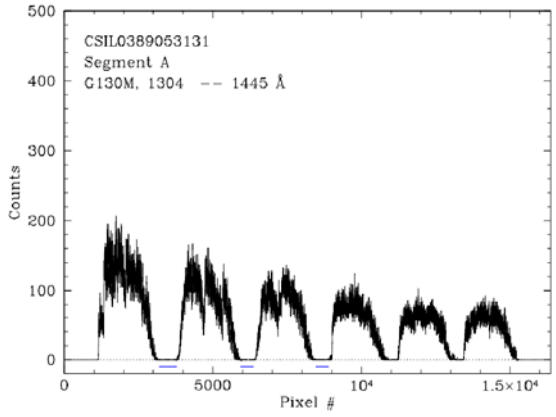

(a)

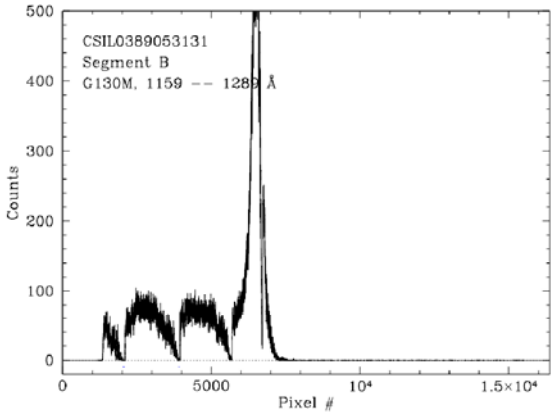

(b)

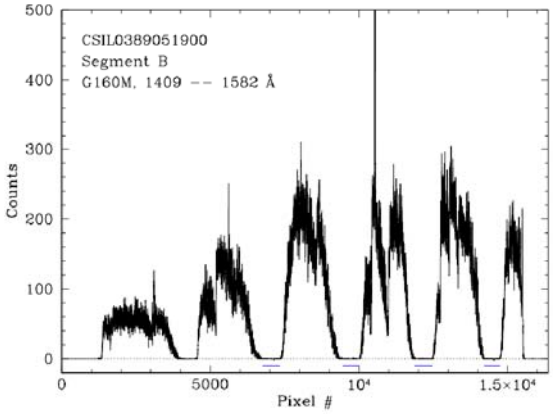

(c)

Figure 5.8-1: FUV absorption spectra acquired during Tests 2100 and 2110. Panels (a) and (b) were acquired with G130M and panel (c) with G160M. The solid bars show the regions used to measure the stray and scattered light.

5.8.3 NUV

The following tests were executed during Appendix B. There was no absorption cell available in 2006, so the tests were not repeated in Appendix C.

Tests: 2150 – NUV O2 Initial Spectra
2160 – NUV Scattered Light

Relevant Exposures:

Table 5.8-2: Exposure list for 2003 NUV stray and scattered light tests.

File	Channel/Stripe/λ_C	Comments
CSIL03270041709	G185M / B/ 1817Å	Absorption cell pressure = 700 Torr
CSIL03270080108 *	G185M / A / 1784Å	Absorption cell pressure = 700 Torr
CSIL03270084139	G185M / B / 1817Å	Absorption cell pressure = 700 Torr
CSIL03270033410 **	G185M / B /1817Å	Continuum reference spectrum

* The central wavelength of Stripe B in this exposure (the nominal wavelength for a given setting) is 1882Å, but Stripe A runs from 1766 – 1801Å.
** This is a reference spectrum for the 1817Å exposures taken at 200 mTorr that gives the count rate in the unabsorbed continuum. The exposure time on this exposure is 600 sec, so its counts need to be multiplied by 3 to give the expected continuum level for the saturated exposures.

There is no reference spectrum for the 1784 Å spectrum.

5.8.3.1 Analysis

For all spectra, a row sum was used to find the centroid of each stripe. A 20 pixel window centered on the middle of each stripe was extracted to obtain 1-D spectra. A 20 pixel wide background spectrum in between stripes B and A in each exposure (centered well away from each stripe) was also measured. The background spectrum was subtracted from the stripe spectrum at the pixel level before analysis.

Regions in the spectra where the absorption line cores appear to be fully saturated were selected for analysis. Most of the saturated regions are narrow, 10 -- 20 pixels wide. However, the A stripe of CSIL03270080108 is completely saturated for pixels >755.

Saturated regions:

CSIL03270041709: pixels 524 -- 547; 840 -- 849; 868 -- 894

CSIL03270084139: pixels 472 -- 481; 501 -- 509; 526 -- 554; 779 -- 790; 816 -- 825; 841 -- 852; 863 -- 897

CSIL03270080108: pixels 155 -- 186; 634 -- 661; 783 – 1024

5.8.3.2 Results

The reference spectrum for the two 1817Å observations shows that the B-stripe unabsorbed intensity (counts multiplied by 3 to give the counts in 1800 sec) is 315 counts for pixels <775 and 293 counts for $775 \leq p \leq 900$. Therefore, 2% residual counts corresponds to 6.3 counts in the first region and 5.9 counts in the second.

It is less clear what the unabsorbed count rate is for the 1784Å spectrum. The A stripe nominally covers 1766 – 1801Å, so we can estimate the long wavelength end of the A stripe based on the short wavelength counts in the 1817Å reference spectrum, which nominally goes just out to 1800Å and has a count total (scaled up by 3) of 215 counts. A stricter limit can be set by the maximum observed counts in the A stripe, which is 158 counts at pixel 9. This is over-conservative, though, since the entire A stripe appears to be absorbed, with no true continuum present.

The counts in the saturated regions are:

CSIL03270041709: The 524 -- 547 region has a mean count value of 2 and an rms of 2.3, below the 6.3 count limit. The maximum counts in a single pixel in this region is 10, but this appears to be due to an unabsorbed region rather than stray or scattered light. The mean residual intensity is 0.6%. The other two regions, which look much flatter, have mean counts of 0.76, an rms of 1.5, and a maximum count of 5. All of these are below the 2% residual intensity limit of 5.9 counts. The mean residual intensity in these regions is 0.3%.

CSIL03270084139: This is the same setup as the previous exposure, but at higher pressure in the absorption cell. The first three regions (pixels in the 400s and 500s; see above) have a mean count of 1.5, an rms of 1.8, and a max of 5. The mean residual intensity is 0.5%. The final four

regions (700s and 800s) have a mean of 0.7, an rms of 1.4, and a max of 5. The mean residual intensity is 0.2%.

CSIL03270080108: The mean counts in the absorbed regions is 0.07. The rms is 0.99 and the max count is 5 (although again, this could be caused be unabsorbed flux rather than scattered light; see near pixel 850). This is well within the 2% residual intensity limit, so long as the unabsorbed counts are >3.5!

Figure 4.8-2 shows the 1-D spectra used for the stray and scattered light analysis for the three cases examined. For the two 1817Å exposures, the reference spectrum (multiplied by 3) is also shown. The red dashed lines indicate the continuum level used in the analysis. The blue bars underneath the spectra show the saturated regions used.

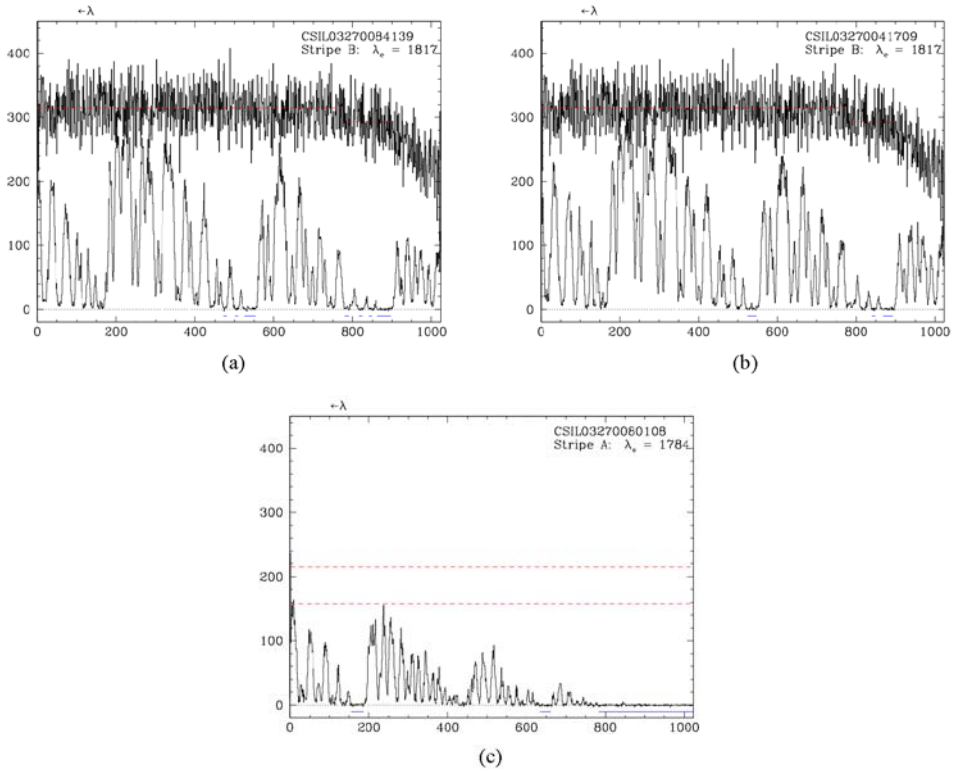

Figure 5.8-2: Data used to calculate the scattered light from the G185M grating. Panels (a) and (b) show stripe B, λ_C=1817Å. The red line denotes the continuum used to calculate the scattered light in the saturated absorption lines, which are noted by the blue lines below the spectra. Panel (c) shows the G185M spectrum in stripe C, which has a central wavelength of 1784Å. The red lines in (c) show the continuum assumed for the scattered light calculation.

5.9 IMAGE STABILITY & DRIFT COMPENSATION

5.9.1 CEI Requirements

Section 4.2.8 of the CEI states that knowledge of the drift shall be provided which allows it to be corrected with a residual uncertainty of not more than 0.25 resolution elements per hour.

5.9.2 Description

During Appendix B (2003) testing a series of tests were conducted where spectra from RASCAL and the internal wavelength calibration lamps (hereafter referred to as "wavecals") were acquired simultaneously. Specifically, data were acquired for G130M, G160M, G140L, and G285M with exposure times of 6500 seconds. In the case of the G285M channel, two 6500 second exposures were acquired, effectively characterizing the drift over a 13,000 second observation. It is also worth noting that 6500 seconds is the maximum observation time for any COS observation, so these observations cover all possible COS exposure times.

The simultaneous wavecal and PSA spectra provide the ability to test different methods for tracking and correcting time dependent drift due to the OSM1 and/or the OSM2 mechanisms. Drift was measured in one of two ways using *only* the wavecal spectra, either by computing the average center of individual emission lines or by cross-correlating a wavecal spectrum acquired at time t against the wavecal spectrum acquired at t=0. Figure 4.9-1 graphically depicts what was done for the G285M data. The drift was measured for wavecal exposure times (twav) ranging from 30 to 180 seconds and times between exposures (tdwell) between 300 and 1200 seconds. In fact, subsequent work demonstrated at an aperiodic sampling could provide more efficient tracking of the drift and was used to generate the FUV resolution curves presented in this document. Aperiodic sampling is also described in more detail in OP-01 (COS-01-0001) and AV-03 (COS-01-0003).

Once the drift was characterized a time dependent correction term, which removes the drift, was added to both the x and y location of individual photon events in the science spectrum. The correction term is simply the measured drift multiplied by –1. The correction terms for those events falling between wavecal exposures were computed by either linearly interpolating between the drift measured at times t1 and t2 or by fitting the data with a 5^{th} order polynomial function and using the derived function to compute the correction term.

The performance of the drift correction was evaluated using two parameters, the FWHM of the time dependent average line center and the FWHM of the line spread function of a drift-corrected emission line in the PSA spectrum. The FWHM of the average line center is a measure of correction algorithm's ability to track and correct drift. The FWHM of the line spread function tracks the performance of the correction algorithm by measuring the pre-and post-correction resolution, the ultimate purpose of the drift correction.

Figure 4.9-2 summarizes the measurement and correction of the drift. The panels at the left show raw and corrected average line centers in the dispersion and cross-dispersion directions for a single emission line in the PSA spectrum. Each figure also shows the FWHM of the corrected line center expressed in resolution elements (for the short wavelength for the exposure), the exposure time for the wavecal (twav), and the time between wavcal exposures (tdwell). The FWHM is computed using the IDL STDDEV function and multiplying the result by 2.354. The diamonds indicate where wavecal exposures were taken. The right hand figures show the measured drift, expressed in pixels, as functions of time. Recall that the drift is measured using the wavecal data only.

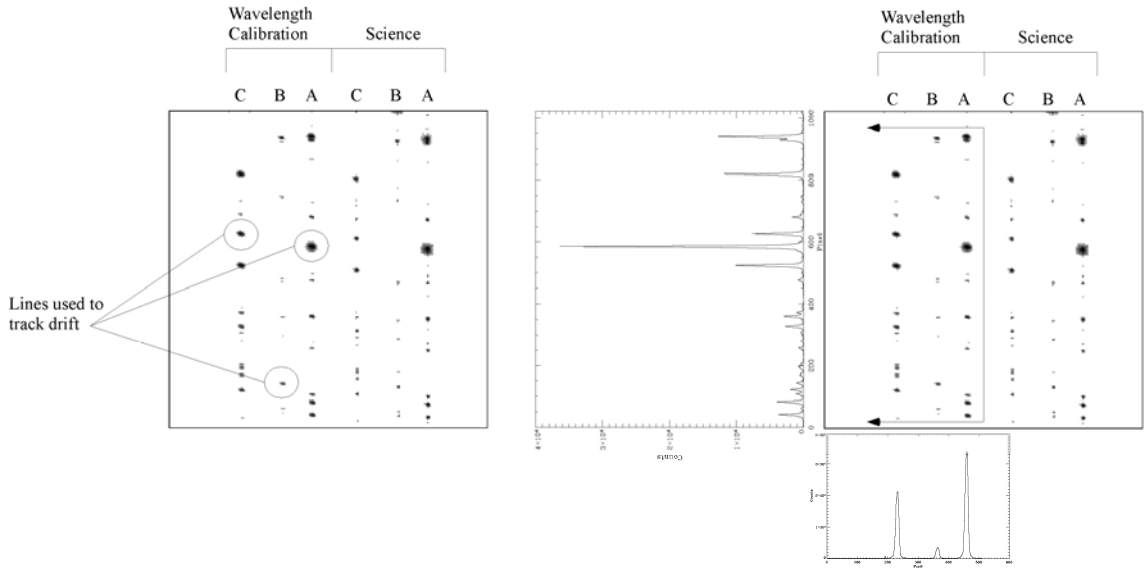

Figure 5.9-1: The left panel shows the G285M image used in this analysis with the 3 emission lines that were used to measure the drift. The right panels show the same data, but with the spectra used in the cross-correlation. For the cross-correlation analysis all three spectra were collapsed together into a single, combined pseudo-spectrum, one for each dimension. This provided more lines for the cross-correlation algorithm and would be simpler in a pipeline processing application.

Figure 4.9-3 shows the line profile of an emission line in the PSA spectrum in the dispersion and cross-dispersion directions before and after correcting for mechanism drift shown in Figure 4.9-2. The FWHM in pixels is computed by first fitting a Gaussian profile to the histogram (shown as a dotted line) and then multiplying the standard deviation by 2.354. Note the significant improvement in spectral width after correcting for drift.

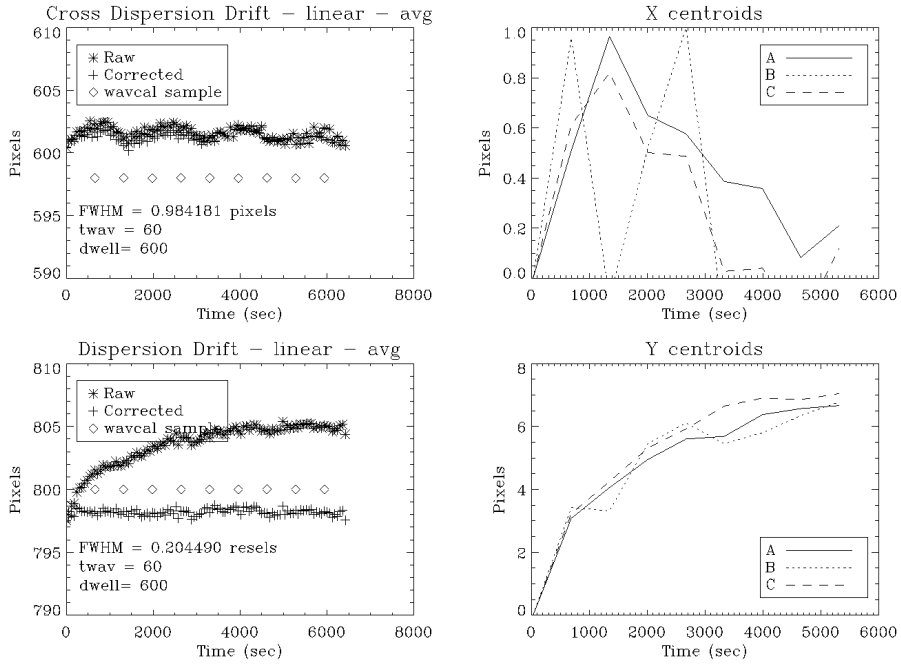

Figure 5.9-2: Drift correction results for the G285M data using line center tracking. Right hand panels show the measured drift for each stripe. Left hand panels show the line center for an emission line in the science spectrum before and after drift correction.

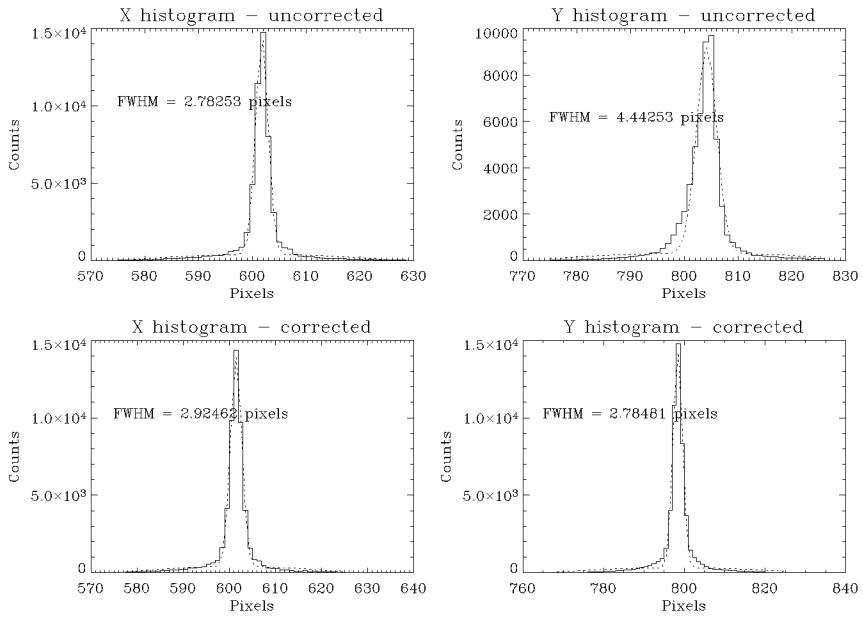

Figure 5.9-3: Line widths for an emission line in the science spectrum before and after correction. Note the improvement in spectral resolution after correction of the drift.

Tests: 2300 FUV Grating Stability

2355 NUV Grating Stability

Relevant Exposures:

Table 5.9-1: Exposure list for 2003 image stability and drift compensation tests.

File	Channel/λ_C	Comments
CSIL03285043406_1_rawtag.fits	G130M / 1309Å	Moderate drift, ~3 pixels
CSIL03285081037_1_rawtag.fits	G160M / 1600Å	Low drift, ~1.5 pixels
CSIL03285101309_1_rawtag.fits	G140L / 1230Å	Large drift, ~8 pixels
CSIL03285123358_1_rawtag.fits	G285M / 2850Å	Large drift, ~8 pixels
CSIL03285144027_1_rawtag.fits	G285M / 2850Å	No drift, ~0 pixels

5.9.3 Results

The first task was to compare the performance of the emission line tracking versus cross-correlation algorithms for measuring the drift of the spectrum. This was conducted using the G285M data, because this data exhibited large spectral drift. The performance of the line tracking versus cross-correlation was evaluated over a range of wavecal exposure times and dwell times. Table 4.9-1 presents the results.

It should also be pointed out that the 5th order polynomial fit, while evaluated, was ultimately dropped for all the analyses presented here. The reason is that the polynomial function required an a priori knowledge of the shape of the drift. A linear interpolation does not require any assumption about the shape of the drift curve and thus can be understood in terms of the data only. When the drift of the mechanisms has been more fully mapped during in orbit operations it may be advantageous to employ a parametric function to model the drift; however, at the time of this writing there is insufficient data to support the use of such a function.

Table 5.9-2: Drift measured with different techniques and time scales.

		Method for Tracking Drift			
		Line Centers		Cross-correlation	
twav (s)	tdwell (s)	FWHM of Centroid (resels)	FWHM of line width (pixels)	FWHM of Centroid (resels)	FWHM of line width (pixels)
10	600	0.44	3.19	0.21	2.91
30	600	0.28	2.88	0.20	2.82
60	**600**	**0.20**	**2.78**	**0.21**	**2.80**
120	600	0.23	2.78	0.21	2.77
60	150	0.23	2.81	0.21	2.81
60	300	0.24	2.86	0.20	2.80
60	**600**	**0.20**	**2.78**	**0.21**	**2.80**
60	900	0.28	2.91	0.23	2.83
60	1200	0.27	2.88	0.27	2.88

Several points regarding these data are worthy of note:

1. Tracking the line centers requires a wavecal exposure time $\geq$ 60 seconds. Presumably, this is because this ensures sufficient photons to accurately compute a average position. This could be alleviated by choosing brighter lines, should they exist.
2. The cross-correlation method does not need as many photons to accurately determine the drift. This is good because it does NOT require detailed understanding of the spectrum for a given wavelength setting.
3. The optimum dwell for this analysis appears to be ~600 seconds. This is because the derivative of the drift is highest in the first 600 seconds. If the tdwell is larger than 600

seconds then the linear interpolation between measured drift points under estimates the drift correction. If a parametric model for the drift is eventually developed then decreasing the frequency of wavecal exposures could be a possibility. Also note that an aperiodic sampling is a more efficient means of accurately tracking the drift while minimizing the total number of wavelength calibration exposures. See OP-01 (COS-01-0001) and AV-03 (COS-01-0003) for additional details on aperiodic sampling of the drift.

In summary, it was determined that a cross-correlation method for measuring the spectral drift was as accurate as tracking the average line center. Cross-correlation also has the advantange that no knowledge of the exact instrument configuration is required, i.e. a list of lines for tracking the drift is not required for each grating configuration. Therefore, all subsequent analyses use cross-correlation to measure the drift and linear interpolation to compute the time dependent drift function.

There remains the question of the validity of these techniques for other gratings, where the drift may be different and could be uncorrectable. To confirm that the technique was robust it was applied to data sets acquired for the G130M, G160M, and G140L channels and also reapplied to the G285M data set over a consistent grid of wavecal exposure time and dwell times. These data are expressed graphically in Figures 4.9-4, 4.9-5, 4.9-6, and 4.9-7. In each case the figure consists of the residual drift, spectral, and spatial widths as functions of tdwell and twav. For the G130M and G160M data the FUV detector segments were each evaluated separately. Table 4.9-2 presents the full data set. Figures 4.9-8, 4.9-9, and 4.9-10 show examples of the drift results for the FUV channels.

The results of the study are encouraging, confirming the validity of the correction algorithm and providing guidance for operating the COS instrument in flight.

Table 5.9-3: Measured drift in spectral and spatial directions.

G130MA Results:		Segment A			Segment B		
tdwell (s)	twav (s)	Drift (resel)	Spectral (p)	Spatial (p)	Drift (resel)	Spectral (p)	Spatial (p)
180	30	0.315	6.411	9.316	0.431	6.788	11.312
180	60	0.227	6.142	9.302	0.436	6.878	11.321
180	90	0.201	6.093	9.294	0.238	6.372	11.324
180	120	0.115	5.964	9.293	0.218	6.333	11.307
180	180	0.122	5.947	9.292	0.197	6.290	11.315

300	30	0.395	6.567	9.307	0.367	6.679	11.315
300	60	0.268	6.267	9.306	0.406	6.849	11.346
300	90	0.153	6.010	9.287	0.331	6.597	11.323
300	120	0.117	5.927	9.288	0.200	6.295	11.312
300	180	0.115	5.942	9.285	0.159	6.208	11.316
600	30	0.255	6.237	9.309	0.572	7.298	11.329
600	60	0.181	6.076	9.300	0.280	6.504	11.336
600	90	0.171	6.013	9.287	0.170	6.259	11.315
600	120	0.109	5.924	9.297	0.184	6.275	11.323
600	180	0.104	5.930	9.281	0.173	6.253	11.319
900	30	0.280	6.252	9.305	0.177	6.249	11.312
900	60	0.240	6.188	9.272	0.429	6.866	11.317
900	90	0.134	5.976	9.290	0.175	6.256	11.304
900	120	0.173	6.052	9.271	0.156	6.249	11.314
900	180	0.116	5.919	9.302	0.191	6.300	11.294

G160MA Results:			Segment A			Segment B	
tdwell (s)	twav (s)	Drift (resel)	Spectral (p)	Spatial (p)	Drift (resel)	Spectral (p)	Spatial (p)
180	30	0.146	6.421	2.989	0.098	5.571	5.152
180	60	0.124	6.383	2.977	0.098	5.541	5.154
180	90	0.121	6.348	2.952	0.104	5.525	5.151
180	120	0.125	6.351	2.949	0.102	5.526	5.152
180	180	0.123	6.335	2.947	0.103	5.522	5.159
300	30	0.138	6.416	2.984	0.094	5.578	5.154
300	60	0.122	6.361	2.973	0.096	5.535	5.154
300	90	0.126	6.359	2.947	0.109	5.536	5.155
300	120	0.137	6.373	2.950	0.096	5.516	5.153
300	180	0.125	6.333	2.933	0.104	5.531	5.159
600	30	0.168	6.442	2.985	0.111	5.578	5.157
600	60	0.126	6.392	2.977	0.103	5.530	5.158
600	90	0.130	6.346	2.953	0.095	5.525	5.154
600	120	0.120	6.323	2.939	0.107	5.529	5.154
600	180	0.123	6.336	2.950	0.112	5.538	5.161
900	30	0.141	6.391	3.015	0.108	5.567	5.161
900	60	0.125	6.346	2.973	0.097	5.556	5.166
900	90	0.126	6.363	2.954	0.099	5.506	5.158
900	120	0.128	6.333	2.967	0.105	5.524	5.157

900	180	0.124	6.331	2.953	0.110	5.548	5.164

G140L Results:			Segment A	
tdwell (s)	twav (s)	Drift (resel)	Spectral (p)	Spatial (p)
180	30	0.107	6.663	3.975
180	60	0.109	6.700	3.959
180	90	0.098	6.694	3.956
180	120	0.101	6.665	3.949
180	180	0.103	6.690	3.957
300	30	0.123	6.687	3.973
300	60	0.123	6.712	3.958
300	90	0.100	6.680	3.956
300	120	0.105	6.670	3.954
300	180	0.112	6.704	3.956
600	30	0.166	6.811	3.974
600	60	0.131	6.731	3.968
600	90	0.138	6.747	3.949
600	120	0.127	6.710	3.954
600	180	0.121	6.722	3.951
900	30	0.184	6.836	3.981
900	60	0.162	6.808	3.957
900	90	0.155	6.764	3.958
900	120	0.163	6.807	3.948
900	180	0.151	6.791	3.948

G285M Results:				
tdwell (s)	twav (s)	Drift (resel)	Spectral (p)	Spatial (p)
180	30	0.211	2.736	2.859
180	60	0.214	2.802	2.801
180	90	0.224	2.716	2.802
180	120	0.220	2.672	2.789
180	180	0.245	2.691	2.871
300	30	0.214	2.728	2.879
300	60	0.205	2.793	2.801
300	90	0.212	2.658	2.795
300	120	0.223	2.663	2.792
300	180	0.238	2.687	2.870

600	30	0.208	2.774	2.826
600	60	0.216	2.774	2.808
600	90	0.212	2.657	2.783
600	120	0.218	2.661	2.771
600	180	0.241	2.676	2.889
900	30	0.255	2.774	2.915
900	60	0.246	2.774	2.832
900	90	0.249	2.774	2.833
900	120	0.251	2.706	2.816
900	180	0.255	2.686	2.917

Notes: Drift is the FWHM of the residual drift of the emission line center measured in resolution elements appropriate for the specific channel. Spectral (p) is the FWHM of the drift-corrected line spread function in the spectral direction measured in pixels. Spatial (p) is FWHM the drift-corrected spatial dimension measured in pixels.

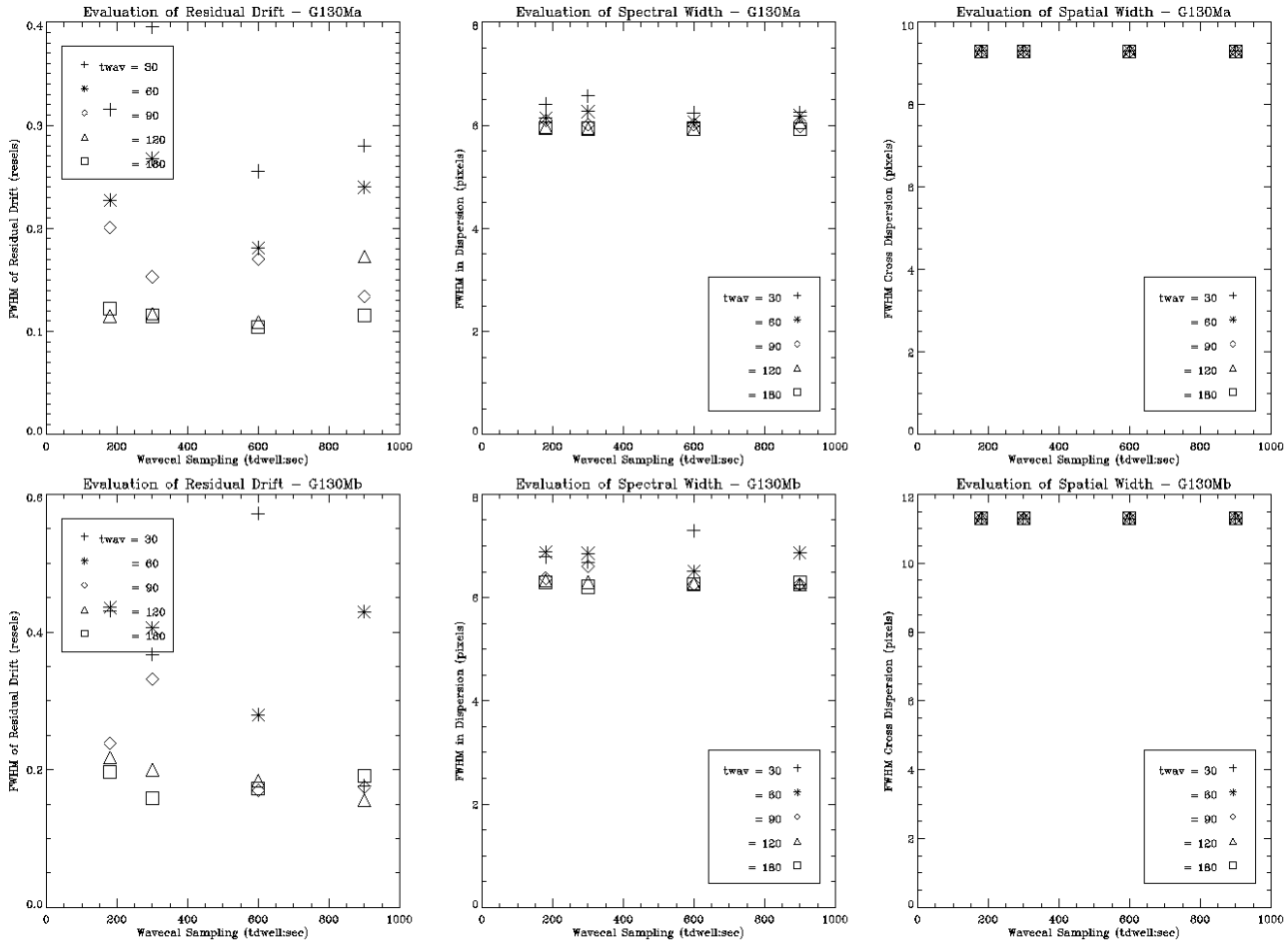

Figure 5.9-4: Drift-correction performance for the G130M channel for segments A and B as a function of wavecal exposure time and dwell time.

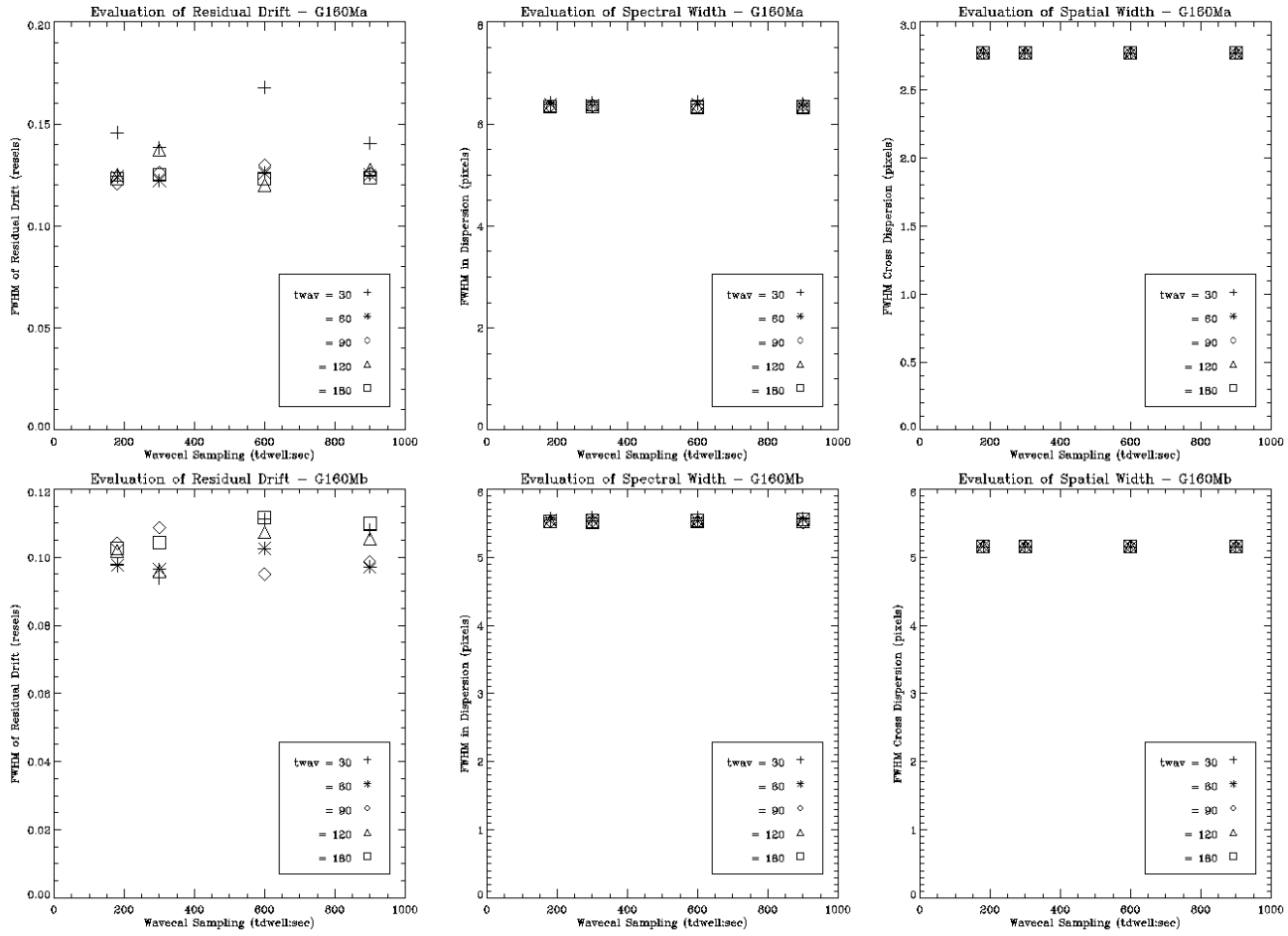

Figure 5.9-5: Drift-correction performance for the G160M channel for segments A and B as a function of wavecal exposure time and dwell time.

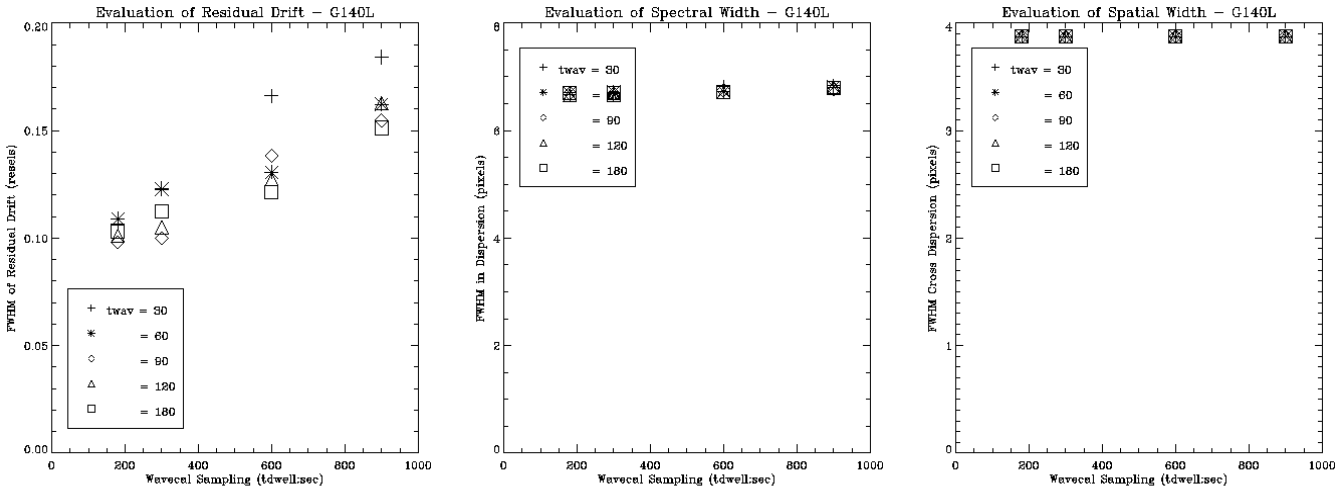

Figure 5.9-6: Drift-correction performance for the G140L channel as a function of wavecal exposure time and dwell time.

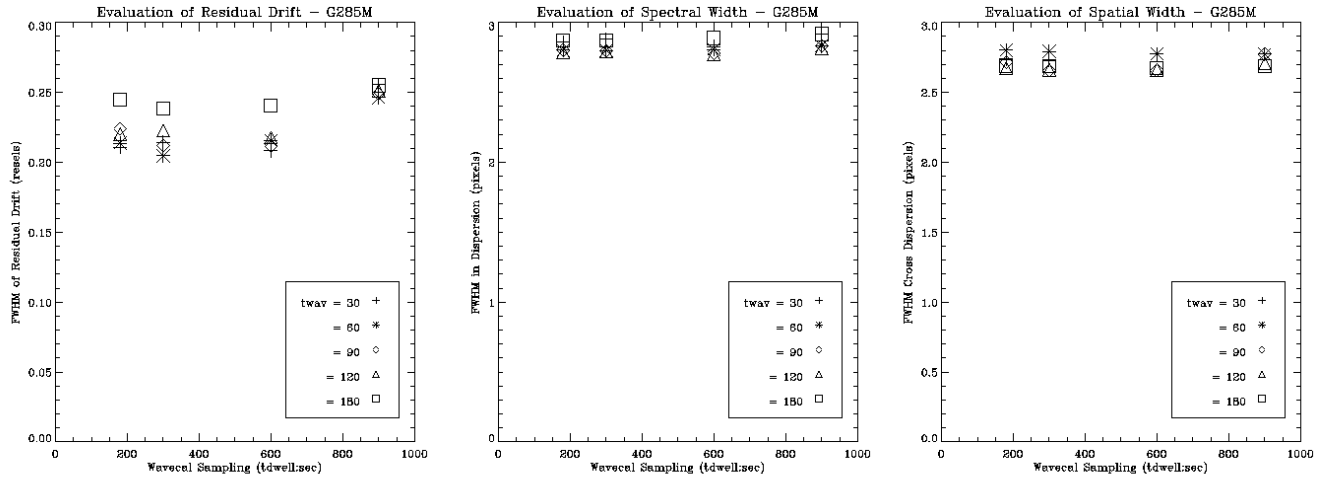

Figure 5.9-7: Drift-correction performance for the G285M channel as a function of wavecal exposure time and dwell time.

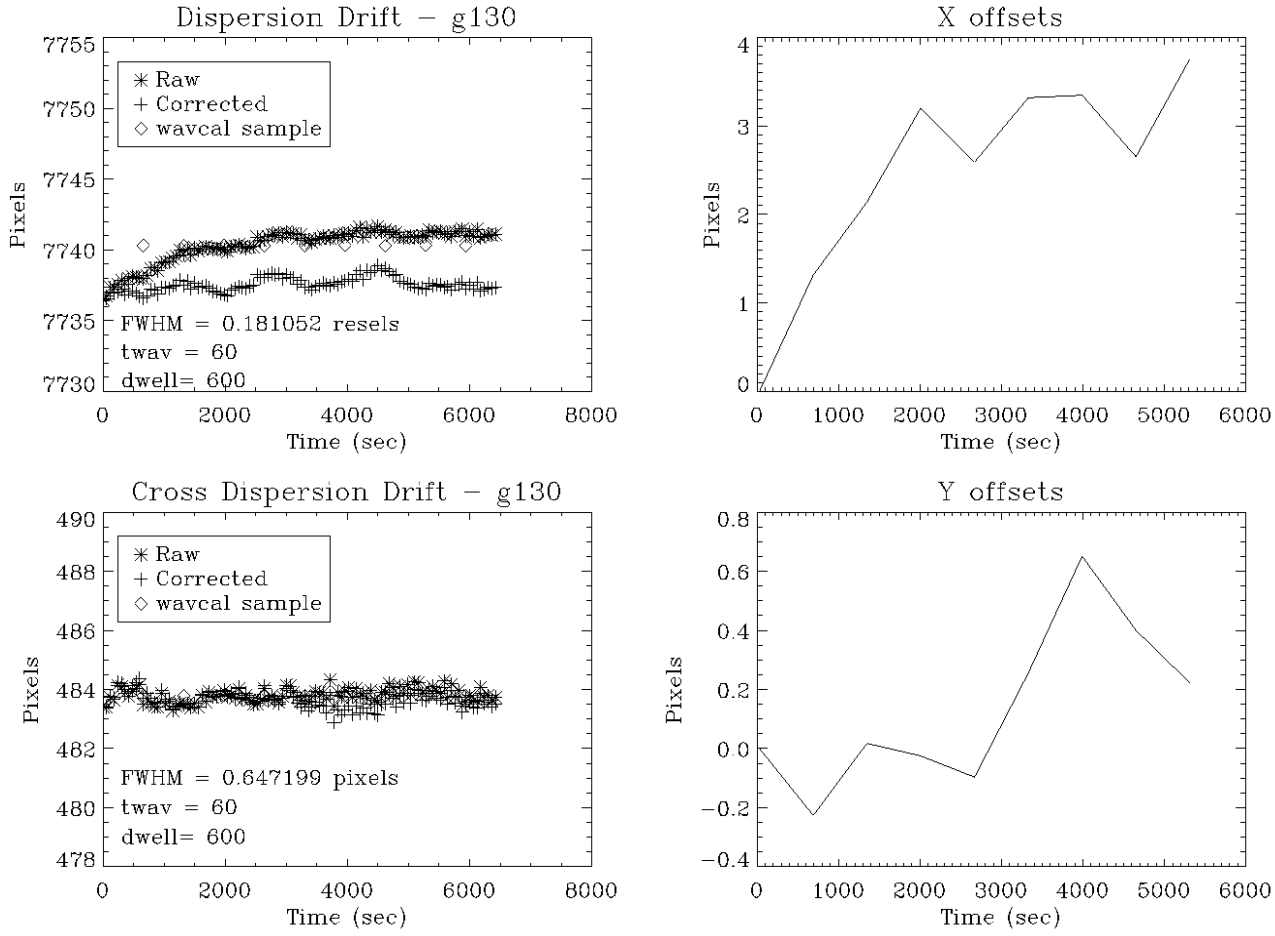

Figure 5.9-8: Drift correction results for G130M data for segment A.

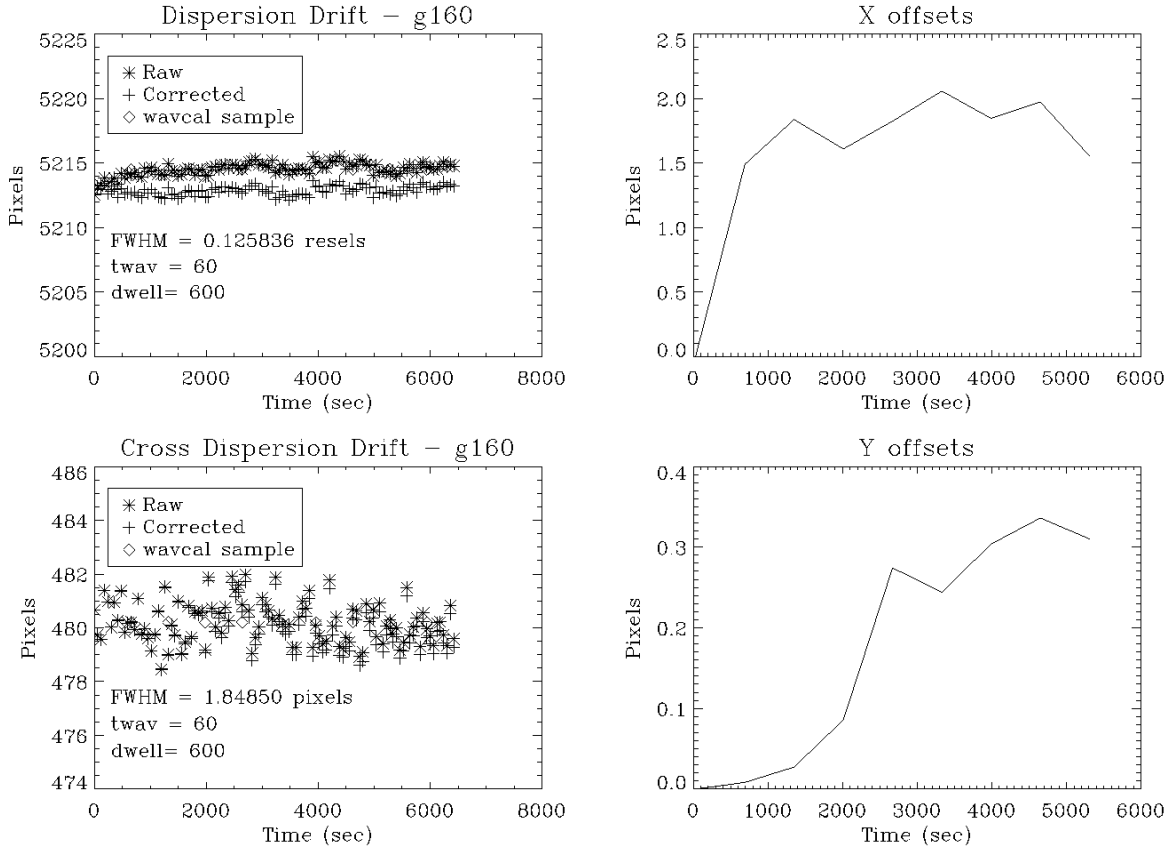

Figure 5.9-9: Drift correction results for G160M data for segment A.

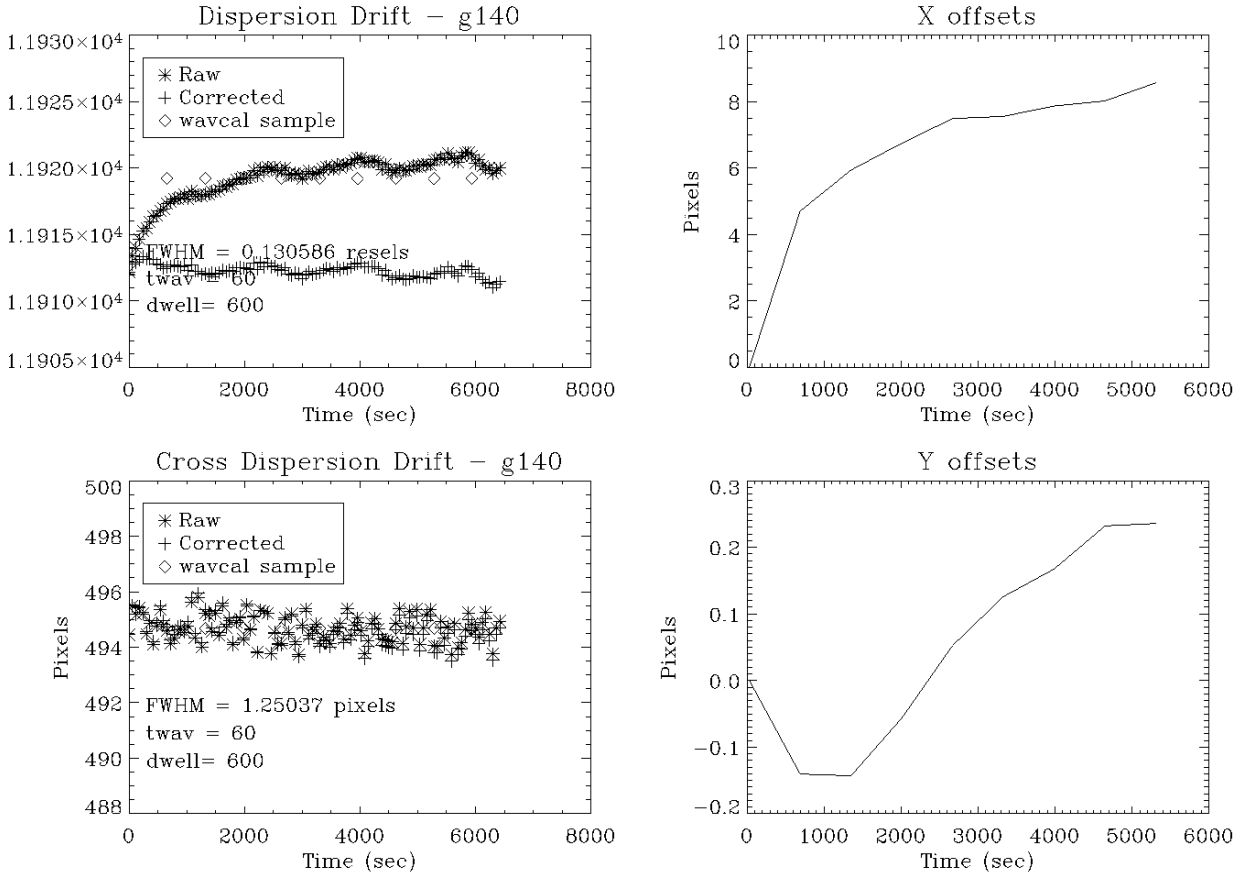

Figure 5.9-10: Drift correction results for G140L data for segment A.

5.9.4 Recommendations

Based on the data presented above the following exposure and dwell times are recommended:

Table 5.9-4: Recommendations for exposure and dwell times for drift correction.

Channel	twav (s)	tdwell (s) (t≤ 1200s)	tdwell (s) (t>1200s)
G130M	90	≤ 600	≤ 3600
G160M	60	≤ 600	≤ 3600

G140L	30	≤ 600	≤ 3600
G285M	60	≤ 600	≤ 3600
Remaining NUV channels	60	≤ 600	≤ 3600

5.9.5 2006 Tag-flash Verification Testing

Tests: 5000 – FUV tag-flash demonstration
5500 – NUV tag-flash demonstration

As a result of the 2003 testing discussed above, it was decided that all COS time-tagged observations would be taken in "tag-flash" observing mode in which the internal wavelength calibration lamp is turned on, or flashed, during science exposures. The lamp will be flashed at the beginning of every exposure and at varying intervals during the exposure, where the timing of the flashes is determined by a number of variables including the length of the exposure and the time since the last major grating wheel move. Implementation of tag-flash in the COS flight software was completed and uploaded prior to 2006 thermal vacuum tests. Appendix C included two lengthy tests to verify the correct execution of tag-flash (as well as subsequent correct treatment of tag-flash wavelength calibration data by calcos, the COS data reduction pipeline). The data were analyzed at Space Telescope Science Institute and the results are published in a STScI instrument report: COS Technical Instrument Report 2007-03 (COS TIR 2007-03), by C. Keyes.

5.10 NUV IMAGING CAPABILITY

5.10.1 CEI Requirements

Section 4.2.9 of the CEI states in part, "The image mode shall be capable of distinguishing two equally bright point sources separated by 1.0 arc second in any direction."

5.10.2 Description

Data for this test was acquired as part of a larger test to characterize the imaging performance of the NUV channel, specifically Test 2250 – NUV spatial Resolution. The test consisted using a row of pinholes as the entrance aperture for RASCAL. Three of these pinholes were evident in the NUV TA1 image. The pinholes were separated such that they formed distinct images separated by 1" at the PSA.

Tests: 2250 – NUV Spatial Resolution

Relevant Exposures:

Table 5.10-1: Exposure list for 2003 NUV spatial resolution test.

File	Channel/λ_C	Comments
CSIL03265193406	TA-1	T_{exp} = 30 sec
CSIL03265195137	TA-1 BRT	T_{exp} = 30 sec

5.10.3 2003 Results

Figure 4.10-1 shows the TA1 image of the 3 pinhole sources. Note how the image widths in Figure 4.10-2 show the TA1-BRT image of the 3 pinhole sources. Immediately apparent is the fact that there is a double image. This was initially discovered during GN2 testing early in the development and is due to the fact that the order sorter has a slight wedge of 30 arc-seconds. The upper three pinhole images are from the front surface reflection off of the order sorter. The lower three images are from light reflecting off of the back surface, thus they are dimmer by a factor of 0.48.

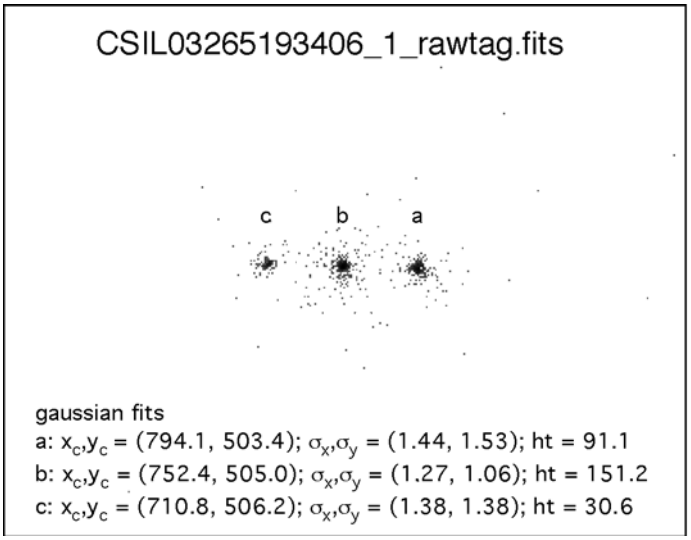

Figure 5.10-1: A TA1 image of the 3 pinhole sources with corresponding 2-D Gaussian profile fits to the data.

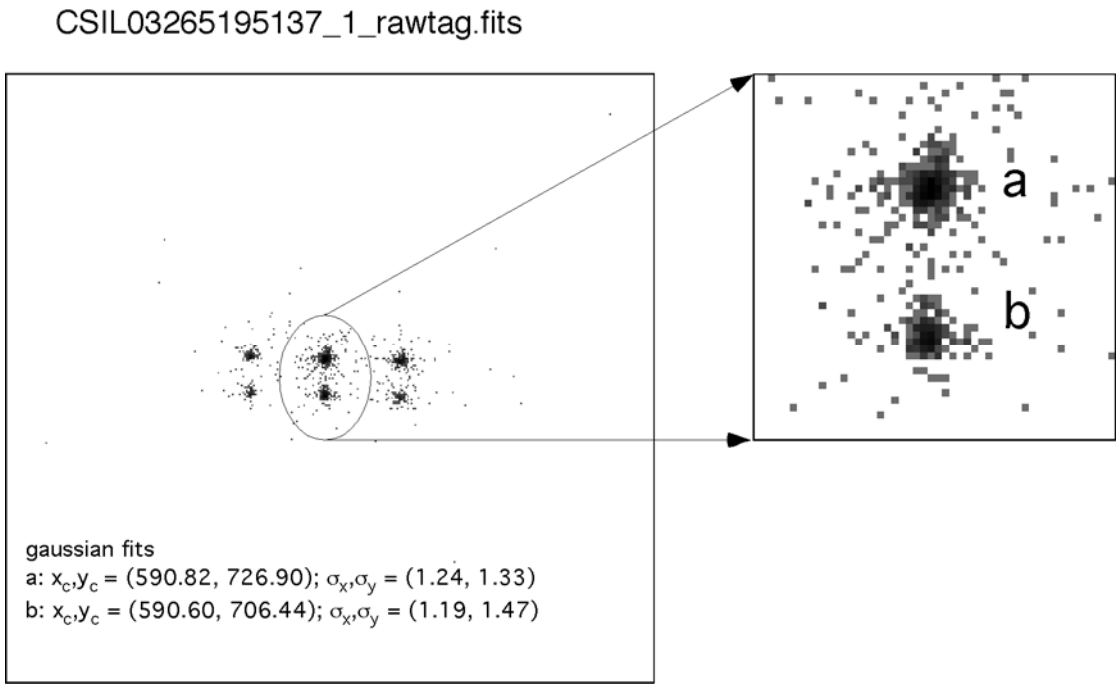

Figure 5.10-2: TA1-BRT image of the 3 pinhole sources including Gaussian fits which indicate that the two images are separated by 20.5 pixels in the dispersion direction.

5.10.4 2006 Results

Test: 2250 – NUV spatial resolution

Observations of the NUV spatial resolution were repeated in 2006 using the same test (#2250) that was performed in 2003. The same pinhole array was also used, creating distinct images separated by 1" at the PSA. Figure 5.10-3 shows the pinhole image from the Appendix C observation. The third pinhole wasn't well illuminated in 2006, so the third pinhole image, though present, is quite faint and is unlabeled in the figure. Because the alignment between RAS/CAL and COS was better in 2006 than in 2003, the image sizes were expected to be smaller in the 2006 data. This is confirmed by the FWHM of the 2-D Gaussian fits to the images, which are of order 2 pixels in 2006 and 3 in 2003. (Note that FWHM is shown here, while σ was given in Figure 5.10-1, so the σ values from 2003 need to be multiplied by 2.355 for comparison with the 2006 results.)

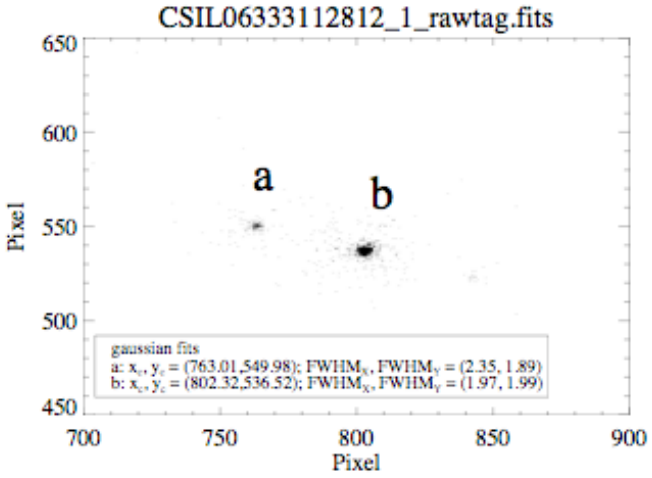

Figure 5.10-3: A TA-1 image of the 3 pinhole sources with corresponding FWHM for 2D Gaussian fits to the data. The third pinhole wasn't strongly illuminated and is not labeled in the figure.

5.11 FUV/NUV BACKGROUND RATES

5.11.1 2003 FUV Background Results

To quantify the FUV detector intrinsic backgrounds, fourteen exposures were taken with no light incident on the detector. Table 4.11-1 below shows the exposure names, exposure times, and counts on each segment ('A' and 'B'). All data were thermally and geometrically corrected prior to co-addition. Figures 4.11-1 and 4.11-2 show the combined highly scaled FUV dark images; circles indicate the location of the stim pulses. For segment 'A', the total number of counts in the dark image was 532539 counts, with a maximum counts/digital element (DE) of 6523. The average count rate over segment 'A' was 9.46 counts/s, or by area, 1.11 counts/s/cm^2. For segment 'B', the total number of counts was 586027 counts, with a maximum counts/DE of 6416. The average count rate over segment 'B' was 10.41 counts/s, or by area, 1.23 counts/s/cm^2.

Table 5.11-1: FUV background files and rates.

Filename	Exposure (sec)	Counts'A'	Counts'B'

CSIL03273035446	6500	103286	107146
CSIL03282011458	1800	13774	17551
CSIL03282031158	1800	37928	15322
CSIL03282050358	1800	12781	17672
CSIL03282065558	1800	14273	17601
CSIL03282084758	1800	14610	18939
CSIL03282112320	6500	49444	56631
CSIL03282200820	6500	102941	58664
CSIL03284021918	6000	4009	5757
CSIL03284031316	1200	7732	11968
CSIL03284053521	6500	41551	61138
CSIL03285021022	6500	41686	56768
CSIL03286141723	6500	39127	75101
CSIL03289225425	6500	49396	65768
Total	56301	532539	586027

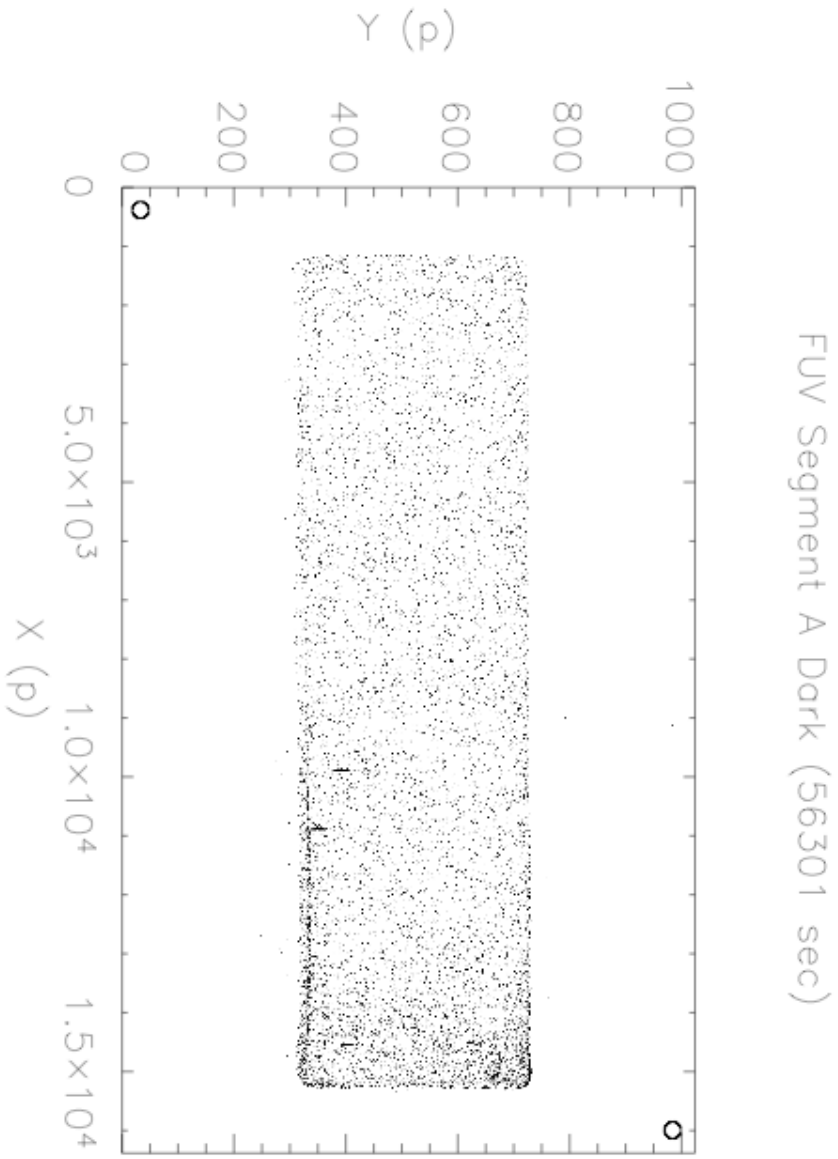

Figure 5.11-1: Background image for segment A of the FUV detector. The total segment background rate is 9.4 cps.

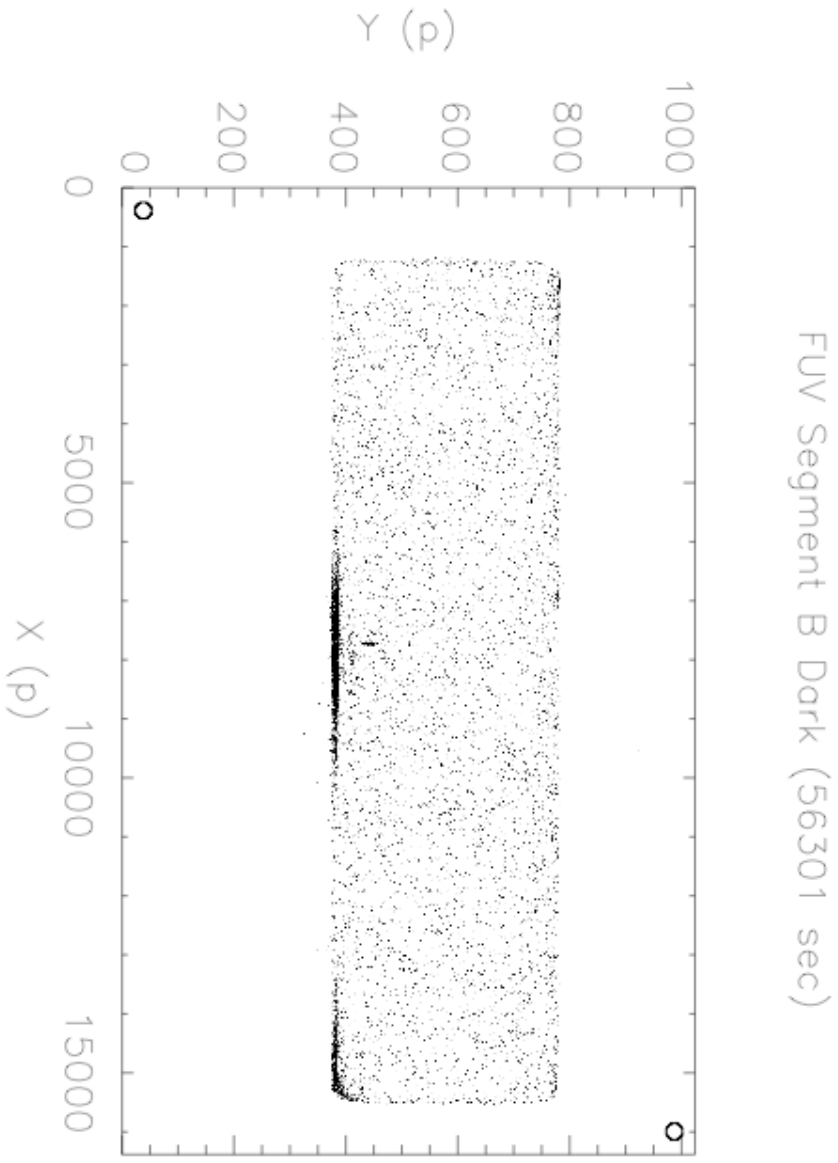

Figure 5.11-2: Background image for segment B of the FUV detector. The total segment background rate is 10.4 cps

5.11.2 2006 FUV Background Results

The CEI specification for the FUV channel is a background rate of < 0.5 counts/sec/cm^2 over the science region of the detector. Each segment of the COS FUV channel has an area of 8.5 cm^2. The initial 2006 FUV dark exposure (CSIL06335132318) showed count rates uniformly elevated with respect to the 2003 FUV dark. It was believed that the FUV ion pump gauge, which had not been on in 2003 but was in 2006 during this exposure, was the source of the higher background. Accordingly, a second 6500 second exposure (CSIL06340002822) with no light incident on the detector and with the ion pump gauge turned off was obtained to verify the dark count rate of the FUV channel. (The ion pump gauge will not be active on orbit once the FUV door has been opened on COS.) After thermal and geometric correction, this exposure showed 23046 counts on the 'A' segment, and 59736 on the 'B' segment over the entire detector. In terms of area, over the entire detector, the 'A' segment had a count rate of 0.417 c/s/cm^2, while for the 'B' segment the count rate was 1.075 cts/s/cm^2. Of note on segment B were 35615 counts along the bottom edge of the detector (a count rate of 5.5 cts/sec) and a hot spot with 308 counts (0.05 counts/sec).

When examined over the spectral region (an extraction stripe 26 'Y' elements high at the nominal PSA location on the detector), the following count rates were observed:

A= 1265 counts/(6500 sec * (26/404)*8.5 cm^2) = 0.356 cts/s/cm^2

B=1328 counts/(6500 sec * (26/387)*8.5 cm^2) = 0.358 cts/s/cm^2

The FUV detector background rate meets the CEI specification.

5.11.3 NUV Background

To quantify the NUV detector intrinsic background, two exposures were taken in Appendix B with no light incident on the detector. The first test (CSIL03271070834) was a 300 sec ACCUM image, while the second test (CSIL03264141459) was a 6500 sec TIME-TAG image. Figure 4.11-3 shows the combined NUV dark image. The total number of counts in the image is 18221. The maximum number of counts in any pixel was 3 (only 1 pixel at [X,Y]=[146,141]). The average count rate over the entire detector was 2.68 counts/s. The count rate per pixel (p) was measured at 2.56E-06 counts/s/p, or by area, 0.409 counts/s/cm^2.

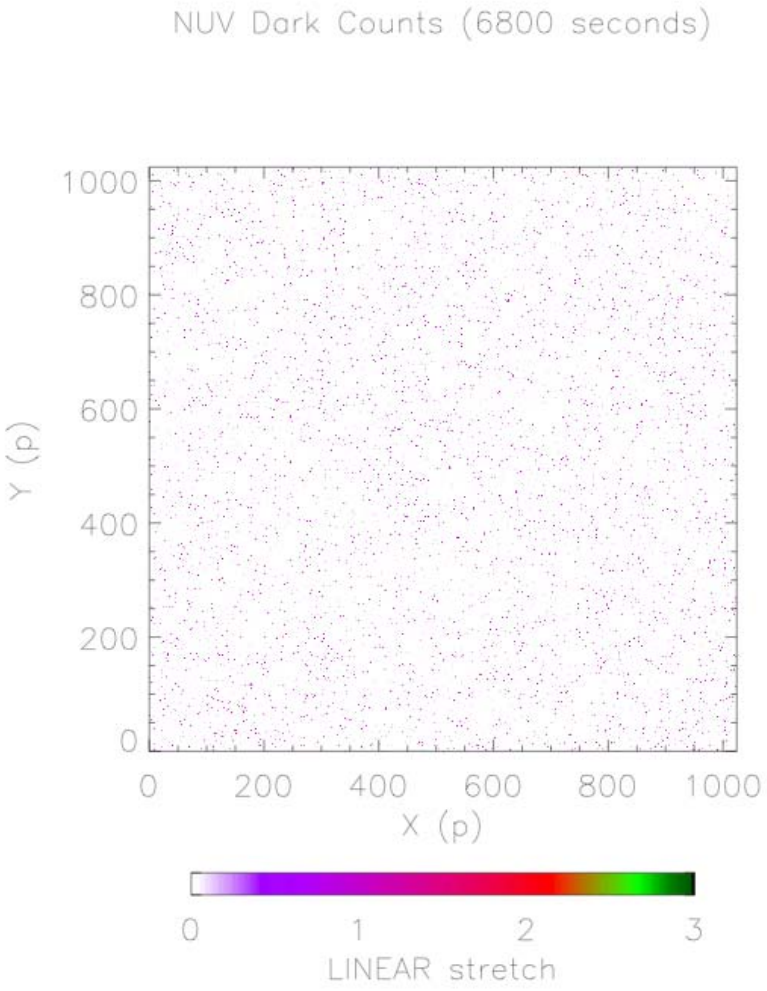

Figure 5.11-3: Background image of the NUV detector. The detector has a background count rate of 2.7 cps.

5.11.3.1 2006 NUV Background Results

The CEI specification for the NUV channel is a background rate of < 4E-6 counts/pixel/sec (0.64 counts/sec/cm^2) over the science region of the detector. The area of the NUV MAMA is 2.56 x 2.56 cm, or 6.5536 cm^2. A 6500 second ACCUM exposure (CSIL06334130410) with no light incident on the detector was obtained to verify the dark count rate of the NUV channel. This exposure showed 22280 counts (3.3E-6 counts/sec/pixel, or 0.523 counts/s/cm^2) uniformly distributed across the detector. A 299 second time-tag dark exposure (CSIL06335154046) contained 994 counts (3.2e-06 counts/sec/pixel, or 0.507 counts/s/cm^2). The NUV detector background rate meets the CEI specification.

5.12 CALIBRATION SUBSYSTEM

5.12.1 CEI Requirements

Section 4.3.2 of the CEI lists the basic requirements of the on-board calibration subsystem. This includes redundant wavelength calibration and flat fielding lamps.

5.12.2 Description

The count rates for the various channel configurations, lamps, and lamp currents were measured from a variety of tests conducted during Appendix A and B in 2003. In all cases the full detector count rate was measured and the data was not background subtracted.

Tests: Appendix A, Tests 200, 300, and 325
Appendix B, Tests 1160, 1170, 1180, 1190, 1110, and 1120

5.12.3 Wavelength Calibration Lamp Count Rates

Table 5.12-1: FUV wavelength lamp count rates.

Grating/λ_c	Measured Count Rate (Segment A/Segment B)					
	LO		MED		HIGH	
	Line 1	Line 2	Line 1	Line 2	Line 1	Line 2
G130M/1291	-	-	250/150	-	-	-
G130M/1300	-	-	250/150	-	-	-
G130M/1309	-	-	240/170	140/90	-	-
G130M/1318	-	-	250/200	-	-	-
G130M/1327	-	-	250/220	-	-	-

G160M/1577	-	-	250/680	-	-	-
G160M/1589	-	-	250/720	-	-	-
G160M/1600	-	-	240/700	200/350	-	-
G160M/1611	-	-	300/700	-	-	-
G160M/1623	-	-	300/700	-	-	-
G140L/1105	-	-	980/ -	-	-	-
G140L/1230	230/ -	55/ -	910/ -	490/ -	-	-

Table 5.12-2: NUV wavelength lamp count rates.

	Measured Count Rate (Line1/Line2)		
Grating/λ_c	LO	MED	HIGH
G185M/1786	-	225	-
G185M/1817	-	325	-
G185M/1835	-	255	-
G185M/1850	-	170/150	-
G185M/1864	-	200	-
G185M/1882	-	240	-
G185M/1890	-	240	-
G185M/1900	-	320	-
G185M/1913	-	300	-
G185M/1921	-	390	-
G185M/1941	-	330	-
G185M/1953	-	260	-
G185M/1971	-	200	-
G185M/1986	-	250	-
G185M/2010	-	300	-
G225M/2186	-	390	-
G225M/2217	-	250	-
G225M/2233	-	350	-
G225M/2250	-	360/310	-
G225M/2268	-	330	-
G225M/2283	-	390	-
G225M/2306	-	340	-
G225M/2325	-	300	-
G225M/2339	-	360	-
G225M/2357	-	460	-

G225M/2373	-	415	-
G225M/2390	-	570	-
G225M/2410	-	340	-
G285M/2617	-	710	-
G285M/2637	-	670	-
G285M/2657	-	870	-
G285M/2676	-	550	-
G285M/2695	-	630	-
G285M/2709	-	670	-
G285M/2719	-	800	-
G285M/2739	-	540	-
G285M/2850	-	630/615	-
G285M/2952	-	610	-
G285M/2979	-	340	-
G285M/2996	-	400	-
G285M/3018	-	430	-
G285M/3035	-	580	-
G285M/3057	-	790	-
G285M/3074	-	380	-
G285M/3094	-	330	-
G230L/2635	450/60	2170	-
G230L/2950		2220	-
G230L/3000	560/105	2250	-
G230L/3360	410/70	1720/1500	5020/3230
TA1	2460/465	-	-
TA1BRT	190/35	-	-

5.12.4 Flat Field Lamp Count Rates

Table 5.12-3: FUV flat field lamp count rates (events/second).

Grating/λ_c	Measured Count Rate (Segment A/Segment B)					
	LO		MED		HIGH	
	Flat 1	Flat 2	Flat 1	Flat 2	Flat 1	Flat 2
G130M/1309	7600/-	6700/-	14100/-	11800/-	-	-

G160M/1600	-/11600	-/10500	-/19200	-/19500	-	-

Table 5.12-4: NUV flat field lamp count rates (events/second).

Grating/λ_c	Measured Count Rate					
	LO		MED		HIGH	
	Flat 1	Flat 2	Flat 1	Flat 2	Flat 1	Flat 2
G185M/1850	-	490				1400
G225M/2250	480	320				
G285M/2850	120	65				

The data above were collected in July 2003 during Appendix A testing (see tests 200 and 250). During Appendix B it was noted that the count rates appeared to be dropping. this was found by evaluating the count rates observed during four Repeatibility Monitors (Test 850). The table below shows the dates, sequence of tests, and observed count rates during interspersed repeatability monitor tests.

Table 5.12-5: Flat field lamp usage in 2003.

		Flat #2/ HI	Flat #1/MED	Flat #1/LOW
Date	Test # & Comments	G185M	G130M-A	G160M-A
9/25,26/2003	1750–NUV internal flats 1&2			
10/2/2003	2515-NUV flat NCM1			
10/9/2003	850-#1	1373	10485	9387
10/11/2003	1700-FUV internal flat (6 hrs)			
10/13/2003	850#2	1359	9913	8984
10/13/2003	3000-FUV internal flat (6 hrs)			
10/15/2003	850-#4	1350	9594	8763
10/15/2003	1720-FUV offset flat field			
10/16/2003	850-#5	1339	9344	8598

This table shows that there is ~0.5% decrease in lamp intensity per hour of use. In total the lamps lost ~10% of their flux during Appendix B testing. Flat #2 has not had as much use as

Flat #1 and therefore has not suffered the same loss in brightness. This should be kept in mind during flat field planning on orbit.

Table 5.12-6 gives the total usage of the COS flight lamps as of June 2008. It does not include the initial lamp evaluation period, which adds roughly five hours to each lamp total.

Table 5.12-6: Total usage of COS flight lamps prior to launch.

	PtNe #1 (hrs)	PtNe#2 (hrs)
LOW	18.0	14.9
MED	112.4	54.0
HIGH	34.8	5.5
	D2 #1 (hrs)	D2 #2 (hrs)
LOW	14.9	4.5
MED	23.4	0.9
HIGH	42.0	17.9

5.13 OPERATIONAL PARAMETERS

5.13.1 FUV

5.13.1.1 Nominal Stim Locations

Table 5.13-1 gives the nominal stim locations for detector segment A. The final values for the stim locations for both detector segments is given in COS-03-0090, "Generating the COS Reference Files."

Table 5.13-1: Stim locations for FUV detector segment A.

Stim Locations, Segment A		
Left hand stim location, DISP direction	S_{x1}	383
Left hand stim location, X-DISP direction	S_{y1}	33
Right hand stim location, DISP direction	S_{x2}	15994
Right hand stim location, X-DISP direction	S_{y2}	984

5.13.1.2 Geometric Distortion Map

The geometric distortion of the FUV02 detector was measured during Appendix B Test 2730. A full description of the derivation of the geometric distortion map is presented in COS-03-0090, "Generating the COS Reference Files."

5.13.1.3 Location of Spectra

These tables present the locations of the spectra in units of pixels from 2003 data. In all cases the location of spectrum is described using a linear function of the form, y = mx + b.

Table 5.13-2: Locations of FUV spectra in 2003 thermal vacuum testing.

PSA Spectral Constants							
		G130M		G160M		G140L	
Detector Segment		A	B	A	B	A	B
Slope ($x10^{-5}$)	**m**	0.379	5.08	-5.92	-0.885	10.0	-
y-intercepts							
Spectrum	**b**	483.8	543.4	478.3	537.1	489.2	-
Background region 1	$\mathbf{b_{bk1}}$	547.8	607.4	542.3	601.1	553.2	-
Background region 2	$\mathbf{b_{bk2}}$	419.8	479.4	414.3	473.1	425.2	-
Spectrum extraction half height	**Δn**	64	64	64	64	64	64
Background extraction half height	**Δn2**	64	64	64	64	64	64
Background extraction width	**Δw**	TBD	TBD	TBD	TBD	TBD	TBD

WCA Spectral Constants							
		G130M		G160M		G140L	
Detector Segment		A	B	A	B	A	B
Slope ($x10^{-5}$)	**m**	5.05	7.54	-0.312	-0.283	19.2	-
y-intercept	**b**	587.9	647.0	582.2	640.4	595.8	-

5.13.2 NUV

5.13.2.1 Location of Spectra

These tables present the location of the relevant spectra in pixels from 2003 data. In all the cases the locations of the spectral stripes are described using a linear function of the form, x = my + b.

Table 5.13-3: Location of NUV spectra in 2003 thermal vacuum testing.

PSA Spectral Constants					
		G185M	G225M	G285M	G230L
Slope					
Spectrum A	$\mathbf{m_a}$	-0.00420	-0.000925	-0.00386	-0.00143
Spectrum B	$\mathbf{m_b}$	-0.00479	-0.00137	-0.00374	-0.00224
Spectrum C	$\mathbf{m_c}$	-0.00559	-0.00304	-0.00542	-0.00591
y-intercepts					
Spectrum A	$\mathbf{b_a}$	845	859	833	857
Spectrum B	$\mathbf{b_b}$	749	754	737	754
Spectrum C	$\mathbf{b_c}$	617	613	604	614
Background region 1	$\mathbf{b_{bk1}}$	950	950	950	950
Background region 2	$\mathbf{b_{bk2}}$	150	150	150	150
Spectrum extraction half height	$\mathbf{\Delta n}$	32	32	32	32
Background extraction half height	$\mathbf{\Delta n2}$	32	32	32	32
Background extraction width	$\mathbf{\Delta w}$	TBD	TBD	TBD	TBD

WCA Spectral Constants					
		G185M	G225M	G285M	G230L
Slope					
Spectrum A	$\mathbf{m_a}$	-0.00612	0.000544	-0.00294	-0.00137
Spectrum B	$\mathbf{m_b}$	-0.00445	-0.00197	-0.00284	-0.00261
Spectrum C	$\mathbf{m_c}$	-0.00507	-0.00254	-0.00331	-0.00191
y-intercepts					
Spectrum A	$\mathbf{b_a}$	467	487	459	486
Spectrum B	$\mathbf{b_b}$	373	384	363	384
Spectrum C	$\mathbf{b_c}$	242	244	233	246

5.13.3 Target Acquisition

See Appendix 5.4 for detailed calibration results regarding target acquisition.

6. APPENDIX

6.1 2003 CALIBRATION PLANNING

test **test** **day** **date**

number	name	completed	
	RASCAL tip/tilt adjustment for COS	Sat/Sun	9/20/2003
	RASCAL tip/tilt for PMT	Sun	9/21/2003
	Tom's flaming doughnut	Sun	9/21/2003
50	TA1 aperture scan	Sat/Sun	9/20/2003
50	TA1 Focus Sweeps	Mon	10/20/2003
50	TA1 Focus Sweeps	Tues	10/21/2003
60	NUV focus sweeps, TA1	Sat/Sun	9/21/2003
65	NUV focus sweeps, grating	Sun	9/21/2003
66	G185M, G225M, G230L focus sweeps	Tue	9/23/2003
70	FUV focus sweeps	Thur	10/9/2003
850	Repeatability monitor #1	Thur	10/09/03
850	Repeatability Monitor #2	Mon	10/13/2003
850	Repeatability monitor #3	Wed	10/15/2003
850	Repeatability monitor 4	Thur	10/16/2003
1110	FUV CDS Pt-Ne Group 1	Mon	10/13/03
1120	FUV CDS Pt-Ne Group 2	Mon	10/13/03
1155	NUV G185M CDS Pt-Ne Spectra in N2	Tues	10/21/2003
1156	NUV G225M CDS Pt-Ne Spectra in N2	Wed	10/22/2003
1160	NUV CDS Pt-Ne G185M	Mon	9/22/2003
1170	NUV CDS Pt-Ne G225M	Tue	9/23/2003
1180	NUV CDS Pt-Ne G285M	Tue	9/23/2003
1190	NUV CDS Pt-Ne G230L	Tue	9/23/2003
1210	FUV G130M sensitivity	Sat	10/11/03
1220	FUV G160M sensitivity	Sat	10/11/03
1230	FUV G140L sensitivity	Sat	10/11/03
1240	FUV sensitivity with QE grid off	Sat	10/11/03
1250	NUV G185M sensitivity	Mon	9/22/2003
1255	G185M/G225M sensitivity	Wed	9/24/2003
1260	NUV G225M sensitivity	Sun	9/21/2003
1265	G225M 2nd order sensitivity	Sun	10/12/03
1270	NUV G285M sensitivity	Sun	9/21/2003
1280	NUV G230L sensitivity	Mon	9/22/2003
1290	NUV TA1 sensitivity	Mon	9/22/2003
1295	NUV TA1-BRT sensitivity	Mon	9/22/2003
1350	NUV CDS D2 lamp brightness	Thur	9/25/2003
1360	RASCAL tip/tilt adjustments	Thur	9/25/2003
1370	PSA offsets	Thur	9/25/2003
1385	Dry run of NUV flat-field test	Thur	9/25/2003
1390	Refine FCA position	Wed	9/24/2003
1410	TA1 FOV mapping	Fri	9/26/2003
1420	Spiral search	Fri	9/26/2003
1430	Image mode TA centroids	Fri	9/26/2003

1433	NUV TA IMCALs with Mech. Offsets	Sun	9/28/2003
1435	Flooded PSA with Pt-Ne lamp	Sun	9/28/2003
1437	NUV TA flooded aperture with Kr	Thur	10/16/2003
1440	TA image mode target centering	Fri	9/26/2003
1450	TA dispersed mode centroids	Tues	10/14/2003
1455	NUV Dispersed mode TA centroids	Sat	9/27/2003
1460	TA dispersed light phase 4	Tues	10/14/2003
1465	NUV TA dispersed light phase 4	Sat	9/27/2003
1470	TA dispersed light phase 5	Tues	10/14/2003
1475	NUVTA dispersed light phase 5	Sat	9/27/2003
1700	FUV cal ss flats S/N=30	Sat	10/11/03
1720	FUV flats aperture offset 2	Wed	10/15/2003
1730	FUV flats aperture offset 3	Fri	10/17/2003
1750	NUV cal SS flat-field, S/N = 30 #1	Thur	9/25/2003
1750	NUV cal SS flat-field, S/N = 30 #2	Fri	9/26/2003
2100	FUV CO initial spectra	Wed	10/15/2003
2110	FUV scattered light	Thur	10/16/2003
2120	FUV high quality spectra	Thur	10/16/2003
2150	NUV O2 initial spectra	Fri/Sat	9/27/2003
2160	NUV scattered light	Sat	9/27/2003
2170	NUV high quality spectra	Sat	9/27/2003
2170	High S/N O2 spectra	Thur	10/2/2003
2250	NUV spatial resolution	Mon	9/22/2003
2300	FUV grating stability	Sun	10/12/03
2305	FUV grating stability	Sun	10/12/03
2306	G130M Grating Stability #1	Mon	10/13/2003
2306	G130M Grating Stability #2	Wed	10/15/2003
2307	FUV stability	Fri	10/17/2003
2307	NUV stability	Mon	10/20/2003
2350	NUV grating stability	Wed	9/24/2003
2355	G285M Stability	Sun	9/28/2003
2355	NUV grating stability	Sun	10/12/03
2355	NUV grating stability	Sun	10/12/03
2505	NUV CDS flat-field, S/N = 30	Thur/Fri	9/26/2003
2506	NUV flats with CDS D2 lamp	Thur	10/16/2003
2515	NUV Flat-field NCM1 position refinement	Thur	10/2/2003
2700	FUV HV variability	Thur	10/09/03
2705	FUV HV variability	Thur	10/09/03
2706	FUV HV variability	Thur	10/09/03
2710	FUV timing threshold settings	Fri	10/10/03
2715	FUV timing threshold settings	Fri	10/10/03
2725	FUV walk settings	Fri	10/10/03

2726	FUV walk settings	Fri	10/10/03
2730	FUV geometric corrections PSA	Wed	10/15/2003
2731	Geom Corrections PSA 7x7 pinhole	Wed	10/15/2003
2735	Geometrical Correction WCA part	Sun	10/12/03
2735	Geom Corrections WCA	Tues	10/14/2003
2740	FUV dark count rate #1	Thur	10/09/03
2740	FUV dark count rate #2	Fri	10/10/03
2740	FUV dark count rate #3	Sat	10/11/03
2740	FUV dark count rate 3	Thur	10/16/2003
2741	FUV dark count rate, QE grid off	Mon	10/13/03
2745	NUV dark count rate	Sun	9/21/2003
2750	FUV resolution, QE grid off	Mon	10/13/2003
2800	FUV high local count rate	Sun	10/12/03
2805	FUV high local count rates G160M	Mon	10/13/2003
2950	NUV resolution, FUV offsets	Wed	9/24/2003
3000	FUV Cal SS flats, S/N = 100	Mon	10/13/2003
3300	FUV BOA throughput & resolution	Sun	10/12/03
3310	NUV BOA transmission & resolution	Wed	9/24/2003
3310	NUV BOA with D2 lamp	Tue	9/30/2003
3400	Side 2 Mechanism Verification	Sat	10/18/2003
3500	FUV OSM1 position checks	Sat	10/11/03
3550	NUV OSM2 Position Checks	Sat	9/20/2003
3600	FUV Accum Check	Fri	10/10/03
3650	NUV Accum Check	Sat	9/20/2003
3700	NUV Efficiency Supplement	Sat	10/18/2003

End of FUV Appendix B calibration tests raising shroud temperature for post-test contamination certification

6.2 2006 CALIBRATION PLANNING

Test #	Test Name	Date Executed
850	Repeatability monitor	12/07/06
1111	FUV external wavecals group 1 settings	12/02/06
1121	FUV group 2 settings	12/05/06
1161	G185M external wavecals	11/28/06

1171	G225M wavecals	11/28/06
1181	G285M wavecals	11/28/06
1191	G230L wavecals	11/28/06
1210	G130M sensitivity	12/01/06
1220	G160M sensitivity	11/30/06
1230	G140L sensitivity	12/01/06
1250	G185M sensitivity	11/29/06
1255	G185M/G225M crossover	11/29/06
1260	G225M sensitivity	11/29/06
1260	G185M sensitivity #2	12/07/06
1270	G285M sensitivity	11/30/06
1270	G225M sensitivity #2	12/07/06
1280	G230L sensitivity	12/01/06
1290	TA1 sensitivity	11/30/06
1290	TA1 sensitivity #2	12/07/06
1295	TA1-BRT sensitivity	12/02/06
1300	FUV external flat-field S/N=30	12/06/06
1301	FUV CDS lamp brightness	12/05/06
1399	FUV faint source	12/06/06
2250	NUV spatial resolution	11/29/06
2740	FUV Dark	12/01/06
2740	FUV Dark #2	12/05/06
2745	NUV Dark	11/30/06
3300	FUV BOA transmission & resolution	12/02/06
3310	NUV BOA transmission & resolution	12/03/06
3500	FUV OSM1 position checks	11/29/06
3550	NUV OSM2 position checks	11/28/06
3600	FUV ACCUM check	12/02/06
3650	NUV ACCUM test	11/29/06
5000	FUV tag-flash demonstration	12/04/06
5500	NUV tag-flash demonstration	12/04/06
6000	Grating efficiency test	11/29/06
7000	NUV Internal Wavecals	12/07/06
8000	NCM1 flat verification	12/06/06

9000	Side Two operations	12/06/06

6.3 TARGET ACQUISITION DATA

The following parameters and test data were generated by Robert Gillet to support the TA testing during Appendix B. It is included as part of this document for posterity and because it is not documented anywhere else.

This document describes what target acq flight software parameters (patchable constants) need to be updated as a result of thermal vac testing, and suggests ways for deriving the new values.

Patchable constant	**New Value**	**Method**
Pcta_XDispIntercept Coeff--for linear map of X-disp coordinates from B seg to A seg.	-3376990 (i.e. -33.76990) but may change ----->>>	Steve Penton looked at the following G130M and G160M images: CSIL03286021646.SDI (G130M PtNe #1 internal) CSIL03286022659.SDI (G130M external) CSIL03268033938.SDI ACTUALLY WE SHOULD USE DATA DAY 284 AND LATER, AFTER THE CSIL03268034546.SDI FUV WALK/TIMING/NOMAB patches and did a least-squares fit of the 4 points (B seg Xdisp center, A seg Xdisp center) to come up with this linear model (where "center" is a Gauss fit).
Pcta_XDispSlope Coeff	97912 (i.e. 0.97912) but may change	
pcta_XImCalTarget Offset--distance from cal image to sci image in NUV TA1 mode.		In between Appendix A and Appendix B (July/August...his 8/20/03 email), Steve discovered the 4-pixel dispersion difference between the cal-to-sci offset for TA1 and that for RVMM. Tom wasn't surprised by this (talked to him 8/22/03) and I think we do need to have a different offset for RVMM than we do for TA1 (i.e. make these two constants into arrays and change the software to be smart enough to know which one to use). I may be thinking about this wrong, but an error of 4 pixels on the NUV is about 0.1 arcseconds, since the plate scale is about 25 milli-arcseconds/pixel. I believe the tightest target acq CEI spec is 0.1 arcseconds, which would mean this difference eats up all the error budget--not good. And isn't the dispersion direction the one that really matters for target acq? I think our plan was to look at the cal-to-sci offsets from the 1430 test and determine the offsets for each mode that way. We ran an LTAIMCAL followed by an LTAIMAGE in each of the 4 modes (TA1, RVMM, TA1BOA, RVMMBOA) and the IMCALs tell where it found the internal lamp and the IMAGEs tell where the science was. (Maybe the BOA ones are unnecessary, if there is no chance of a BOA target acq on orbit.) The "flood" images (1435) come into play for these offsets too, but I

		think their only usefulness will be to verify the accuracy of Tom's centering by determining the center of the PSA from a flood image for that mode and then comparing it to where LTAIMAGE found the external light...not sure what to do with any difference though...it may be the error in determining the center with the flood images will be greater than the difference. Then there was test 1437, which interleaved images of the internal cal lamp with flooded apertures, for the express purpose of measuring the offset. Hmm...is that the data to use? Ok, I'm officially confused. One final thought on these constants: since, in RVMM, there are double images of both the internal lamp and the external science, and we use a median to find the lamp but a moving-box-flux-weighted-centroid to find the science, there is an inherent problem: the cal lamp measured location will be pulled down (a pixel or two?) by the double image, but the science measured location will not be affected by the double image, hence the distance between them will be wrong. However, maybe this is ok, if we use the target acq testing from thermal vac to determine the distance--because that testing would have had that bias built into it. OK, one more final thought: Tom said, at some point during thermal vac, that determining the vector from the cal image to the sci image could be done theoretically by doing a ray-trace model or something, since all we're really doing is imaging the back of the aperture plate, and we know the parameters of the optics and we know the physical distance between the apertures. I don't know if doing this and comparing it to the offsets derived by the above methods makes sense or not. Maybe we would go with the empirical data anyway.
pcta_YImCalTarget Offset		
pcta_CalTarget Offset[ ][ ]--the distance from the cal stripe to the science stripe, in 10ths of pixels, for each grating, and for PSA vs. BOA.		Steve and I started this...he identified some NUV data that would give the X-disp cal-to-sci distance: G230L: BOA: 267 21 26 08 (CSIL03.....SDI) PSA: 267 21 38 04 WCA: (there were wavecals with both the above images) G225M: PSA: 266 08 52 44 WCA: ditto above G185M: 271 01 54 30 & 271 02 01 01 (was this second one a BOA?) were there wavecals with these? G285M: PSA I assume: 266 16 56 03, with wavecal FUV gratings: there are tons of these. Suggest using data after day 284 (FUV patches). Of course Steve already did this with Appendix A data so maybe doing

		it again is redundant. However it hasn't been done on a grating-by-grating basis or PSA/BOA, and maybe it needs to be. Note that we were requesting slews in the 1450 test when we should have been perfectly centered, and if we were perfectly centered, the only other thing I can think of that would cause a slew request is an incorrect offset.
pcta_*MilliArcsecsPerPixel*--plate scales		I know we have to measure these on orbit but could we do an empirical estimation of the NUV plate scales by taking our flood images (1435 or maybe 1437) and saying that the diameter of the circle is 2.5 arcseconds on the sky, and dividing to get the answer? Probably wouldn't be at all accurate.

This report describes my verifications of the results of the target acq tests that were run in COS thermal vac / calibration (September & October 2003).

The table shows the dump file and what I verified in the header to ensure that the test was successful. (I did not go into details about why the data values prove success, but it'll be clear to anyone knowlegdable of target acq who thinks about it.) Obviously the CCL proc and the test procedures (Appendix A and Appendix B) will be necessary to make complete sense of the testing.

Test	**CCL**	**Dump file** CSIL03...SDI	**Verification**
1420	TL1420TA12X2FWC	269145449	1st point saw light. LQTAXPOS = -881, i.e. about half of stepsize 1767. LQTADPOS = -880; ditto. LQTADSLW = 3, LQTAXSLW = -1765 LQTAFX01 = 5328; FX02-FX04 < 10.
"	"	269151020	2nd point saw light. LQTAXPOS = -881 LQTADPOS = 882 LQTAXSLW = -1765, LQTADSLW = 1766 LQTAFX02 = 5185; others < 10
"	"	269152449	3rd point saw light. LQTAXPOS = 882 LQTADPOS = 882 LQTAXSLW = -1 LQTADSLW = 1765 LQTAFX03 = 5255; others < 10
"	"	269153449	4th point saw light. LQTAXPOS = 883 LQTADPOS = -881 LQTAXSLW = -1 LQTADSLW = 2 LQTAFX04 = 5312; others < 10

"	TL1420TA1RTB	269154819	1st point saw light. LQTAXPOS = -884 LQTADPOS = -884 LQTAXSLW = -1767 LQTADSLW = 0 LQTAFX01 = 5465; others < 25
"	TL1420TA13X3	269160250	2nd point saw light. LQTAXPOS = 0 LQTADPOS = 1767 LQTAXSLW = 1767 LQTADSLW = 0 LQTAFX02 = 5474; others < 32
"	"	269161919	4th point saw light. LQTAXPOS = 1767 LQTADPOS = 0 LQTAXSLW = 3534 LQTADSLW = -1767 LQTAFX04 = 5465; others <25
"	"	269163449	5th and 7th points saw light. LQTAXPOS = -221 LQTADPOS = -1767 LQTAXSLW = 1546 (+221 = 1767) LQTADSLW = -3534 LQTAFX05 = 4386; LQTAFX07 = 5639; others < 25 (1767*4386 + -1767*5639)/(4386 + 5639) = -220.85 (rounds to -221 and confirms LQTAXPOS)
"	"	269164819	9th point saw light. LQTAXPOS = -1767 LQTADPOS = 1767 LQTAXSLW = 0 LQTADSLW = 0 LQTAFX09 = 5814; others < 28 LQTALOCL = 581
1430	TL1430IMCAL	269185520	LQTAXCOR = 380 LQTAYCOR = 466 No previous images to compare to, but reasonable in that (380, 466) + SW offset (376, 42) = (756, 508) is near Tom's (754, 517) "TA1 center" value. (There is data later that confirms it. Gauss fits on 286153832.SDI, a TA1/LINE1 image, show the cal spot at (377, 463), which is very close to what this phase found.) LQTATOTL = 5402
"	TL1430IMAGE	269190619	LQTAMXCR = 752.2 LQTAMYCR = 506 Looking at the image downlinked from this phase, this measured location is right on the center of the image. LQTADXCR = 756

			LQTADYCR = 508, matching calculation in row above this one LQTAXSLW = -90 (= x plate scale of -23.5 * 3.8) LQTADSLW = -47 (= y plate scale of -23.55 * 2)
"	TL1430IMCALRVMM	269191719	LQTAXCOR = 217 LQTAYCOR = 687 A picture of LINE1 in RVMM later, 286154520.SDI, shows (Gauss fit) the cal spot at (215, 691), which is very close to what this phase found. LQTATOTL = 1404
"	TL1430IMAGERVMM	269193549	LQTAMXCR = 589.8 LQTAMYCR = 726.9 Looking at the image downlinked from this phase, this measured location is right on the top (main) image (RVMM produces a double image). LQTADXCR = 593 LQTADYCR = 729 Reasonably close; will probably need to tweak cal-to-sci offsets a little bit. LQTAXSLW = -76 (= x plate scale of –23.5 * 3.2) LQTADSLW = -50 (= y plate scale of –23.55 * 2.1)
"	TL1430IMCAL run before TL1430IMAGEBOA	269200949	LQTAXCOR = 380 LQTAYCOR = 461 (reasonably close to previous IMCAL 269185520)
"	TL1430IMAGEBOA	269201848	LQTAMXCR = 743 LQTAMYCR = 502 Looking at the image downlinked from this phase, this measured location is right on the bright part of the image (which is a distorted shape due to the BOA). LQTADXCR = 756 LQTADYCR = 503 Reasonably close; may need new cal-to-sci offset for BOA. LQTAXSLW = -305 (= x plate scale of –23.5 * 13) LQTADSLW = -23 (= y plate scale of –23.55 * 1)
"	TL1430IMCALRVMM run before TL1430IMAGEBOARVMM	269202749	LQTAXCOR = 216 LQTAYCOR = 686 (reasonably close to the previous IMCALRVMM 269191719)
"	TL1430IMAGEBOARVMM	269203750	LQTAMXCR = 581 LQTAMYCR = 727.2 Looking at the image downlinked from this phase, this measured location is right on the brightest point of the top image (BOA + RVMM produces a distorted shape plus a double image of that distorted shape) LQTADXCR = 592 LQTADYCR = 728 Reasonably close; will probably have to tweak cal-to-sci

			offset, if there is any chance of target acq done with the BOA (may need a new, separate offset for this config). LQTAXSLW = -259 (= x plate scale of –23.5 * 11) LQTADSLW = -18 (= y plate scale of –23.55 * 0.8)
1433			The purpose of 1433 was to find out if mechanism motion was behind the 20 pixel difference I detected in later runs of 1430—therefore 1433 doesn't need looking at.
1435			The purpose of 1435 was to locate the center of the aperture, so that we could confirm that our external source was centered. It was not a target acq test so it doesn't need looking at here (but may be used for cal-to-offset calculations—although 1437 is probably much better).
1437			The purpose of 1437 was to get the cal-to-sci offsets, and does not need verifying here.
1440	TL1440IMCAL	270100220	This was run to show where the cal spot was before moving the aperture. It found: LQTAXCOR = 380 LQTAYCOR = 485 Then we moved the ap mech (+5, +5). The result is in the next row.
"	"	270101719	LQTAXCOR = 389 5 steps in X * 0.0478 arc-sec-per-step = 0.239 arc-sec 0.239 arc-sec / 0.0235 arc-secs-per-pixel = 10.17 pixels (measured 9 pixels—good) LQTAYCOR = 475 5 steps in Y * 0.0449 arc-sec-per-step = 0.2245 arc-sec 0.2245 arc-sec / 0.02355 arc-secs-per-pixel = 9.53 arc-sec (measured 10 pixels—good) LQTATOTL = 5627
"	TL1440IMAGE	270102650	LQTAMXCR = 743.8 LQTAMYCR = 544.7 The sci spot is where it is; it's not relevant to the success of this test. LQTADXCR = 765 (389 + offset of 376) LQTADYCR = 517 (485 + offset of 42) LQTAXSLW = -499 (= x plate scale of –23.5 * 21.2) LQTADSLW = 651 (= y plate scale of –23.55 * -27.7)
"	TL1440IMCAL	270110020	For this test, the ap mech was (-5, -5) from nominal. LQTAXCOR = 367 (vs. 380 nominal) Same as above: 5 ap X steps is 10.17 pixels (measured 13—reasonable) LQTAYCOR = 494 (vs. 485 nominal) Same as above: 5 ap Y steps is 9.53 pixels (measured 9—good) LQTATOTL = 5616
"	TL1440IMAGE	270110749	LQTAMXCR = 743.2 LQTAMYCR = 544.2

			Right where it was in the previous. LQTADXCR = 743 (367 + offset of 376) LQTADYCR = 536 (494 + offset of 42) LQTAXSLW = 4 (= x plate scale of –23.5 * -0.2) LQTADSLW = 192 (= y plate scale of –23.55 * -8.2)
"	TL1440IMCAL	270111720	For this test, the ap mech was (+15, 0) from nominal. LQTAXCOR = 409 (vs. 380 nominal) 15 steps is 3 times the 5 step amount, i.e. 30.51 pixels (measured 29—good) LQTAYCOR = 484 (vs. 485 nominal—good) LQTATOTL = 5506
"	TL1440IMAGE	270112220	LQTAMXCR = 743.8 LQTAMYCR = 544.1 Right where it was in the previous. LQTADXCR = 785 (409 + offset of 376) LQTADYCR = 526 (484 + offset of 42) LQTAXSLW = -969 (= x plate scale of –23.5 * 41.2) LQTADSLW = 427 (= y plate scale of –23.55 * -18.1)
"	TL1440IMCAL	270112819	For this test, the ap mech was (0, -15) from nominal. LQTAXCOR = 377 (vs. 380 nominal--good) LQTAYCOR = 512 (vs. 485 nominal) 15 steps is 3 times the 5 step amount, i.e. 28.59 pixels (measured 27—good) LQTATOTL = 5426
"	TL1440IMAGE	270113321	LQTAMXCR = 743.1 LQTAMYCR = 543.9 Still in the same place! LQTADXCR = 753 (377 + offset of 376) LQTADYCR = 554 (512 + offset of 42) LQTAXSLW = -232 (= x plate scale of –23.5 * 9.9) LQTADSLW = -238 (= y plate scale of –23.55 * 10.1)
"	TL1440IMCAL	270113849	For this test, the ap mech was (-10, +20) from nominal. LQTAXCOR = 358 (vs. 380 nominal) 10 steps is 2 times the 5 step amount, i.e. 20.34 pixels (measured 22—good) LQTAYCOR = 446 (vs. 485 nominal) 20 steps is 4 times the 5 step amount, i.e. 38.12 pixels (measured 39—good) LQTATOTL = 5443
"	TL1440IMAGE	270114350	LQTAMXCR = 744.6 LQTAMYCR = 545.5 Science still nearly in the same place. LQTADXCR = 734 (358 + offset of 376) LQTADYCR = 488 (446 + offset of 42) LQTAXSLW = 250 (= x plate scale of –23.5 * -10.6) LQTADSLW = 1355 (= y plate scale of –23.55 * -57.5)
"	TL1440IMCAL	270114849	For this test, the ap mech was (+15, -26) from nominal.

			LQTAXCOR = 409 (vs. 380 nominal) 15 steps is 3 times the 5 step amount, i.e. 28.59 pixels (measured 29—good) LQTAYCOR = 533 (vs. 485 nominal) 26 steps in Y * 0.0449 arc-sec-per-step = 1.1674 arc-sec 1.1674 arc-sec / 0.02355 arc-secs-per-pixel = 49.57 arc-sec (measured 48—good) LQTATOTL = 5413
"	TL1440IMAGE	270115319	LQTAMXCR = 743.2 LQTAMYCR = 543.3 Still in the same place. LQTADXCR = 785 (409 + offset of 376) LQTADYCR = 575 (533 + offset of 42) LQTAXSLW = -983 (= x plate scale of –23.5 * 41.8) LQTADSLW = -746 (= y plate scale of –23.55 * 31.7)
1450	TL1450G140LCALMEAN	287142901	LQTAXCOR = 568.1 (right about where Tom said it would be) LQTATOTL = 17014
“	TL1450G140LPKXDMEAN	287143731	LQTAMXCR = 479.5 (right about where Tom said it would be) LQTADXCR = 484.8 (= 568.l + offset of –83.3) Apparently our cal-to-sci offset is off a bit (or we’re not all that well centered…but we assume Tom got us perfectly centered)—likely a new set of offsets will come out of this data. LQTAXSLW = 550 (= x plate scale of 104.82 * 5.3…remember that the MXCR and DXCR values above are reported in tenths, but the software keeps all significant digits when it does calculations, so while 104.82 * 5.3 = 555, this is within acceptable error. . . .05 error in each of the subtraction terms makes 0.1 error; multiplied by 104.82 makes for a max error 10.482)
“	TL1450G140LCALMED	287145002	LQTAXCOR = 567 (near where we found it with the mean, above) LQTATOTL = 16759
“	TL1450G140LPKXDMED	287145731	LQTAMXCR = 479 (near where we found it with the mean, above) LQTADXCR = 483.7 LQTAXSLW = 493 (= x plate scale of 104.82 * 4.7)
“	TL1450G130MCALMEAN	287150702	LQTAXCOR = 563.5 (right about where Tom said it would be) LQTATOTL = 11023
“	TL1450G130MPKXDMEAN	287151902	LQTAMXCR = 480.4 (near where Tom said it would be) LQTADXCR = 480.2 (= 563.5 + offset of –83.3) Very nice—right on! LQTAXSLW = -21 (= x plate scale of 104.82 * -0.2)
“	TL1450G130MCALMED	287152400	LQTAXCOR = 564 (near where we found it with the

			mean, above) LQTATOTL = 10785
"	TL1450G130MPKXDMED	287153102	LQTAMXCR = 482 (near where we found it with the mean, above) LQTADXCR = 480.7 LQTAXSLW = -136 (= x plate scale of 104.82 * -1.3)
1455	TL1455G285MCALMEAN	270122551	LQTAXCOR = 360.3 (near where Tom said it would be) LQTATOTL = 799
"	TL1455G285MPKXDMEAN	270123351	LQTAMXCR = 728 (within 9 pixels of where Tom said it would be) LQTADXCR = 731.5 (= 360.3 + offset of 371.2) LQTAXSLW = -84 (= x plate scale of –23.84 * 3.5)
"	TL1455G285MCALMED	270124451	LQTAXCOR = 360 (near where we found it with the mean, above) LQTATOTL = 811
"	TL1455G285MPKXDMED	270125251	LQTAMXCR = 727 (near where we found it with the mean, above) LQTADXCR = 731.2 (= 360 + offset of 371.2) LQTAXSLW = -100 (= x plate scale of –23.84 * 4.2)
1460	TL1460G140LCAL	287160203	Ap mech was offset (+5, 0) steps for this test. Previous to this test, 287142901 found the cal stripe at 568.1. LQTAXCOR = 564.8 5 steps in X * 0.0478 arc-sec-per-step = 0.239 arc-sec 0.239 arc-sec / 0.10482 arc-secs-per-pixel = 2.28 pixels (measured 3.3 pixels—good) LQTATOTL = 15912
"	TL1460G140LPKXD	287161002	LQTAMXCR = 479.2 (right about where it was in test 1450, above) LQTADXCR = 481.5 (= 564.8 + offset of –83.3) LQTAXSLW = 238 (= x plate scale of –104.82 * 2.3, within 3 pixels—again, the error bars are larger than that)
"	TL1460G140LCAL	287162433	Ap mech was offset (+9, 0) steps for this test. LQTAXCOR = 562.8 9 steps is 9/5 * 2.28 = 4.10 pixels (measured 5.3--okay) LQTATOTL = 15573
"	TL1460G140LPKXD	287163332	LQTAMXCR = 479.3 (still in the same place) LQTADXCR = 479.5 (= 562.8 + offset of –83.3) Yes, we're almost perfectly at the desired locations, even though we're offset by 9…but as in 1450 (G140L) above, we are either not centered or the offset is wrong. LQTAXSLW = 14 (= x plate scale of –104.82 * 0.2, within 7 pixels—within error bar)
"	TL1460G140LCAL	287164433	Ap mech was offset (-7, 0) for this test. LQTAXCOR = 571.5 7 steps is 7/5 * 2.28 = 3.19 pixels (measured 3.4—good) LQTATOTL = 17411
"	TL1460G140LPKXD	287165202	LQTAMXCR = 479.4 (still in the same place)

			LQTADXCR = 488.2 (= 562.8 + offset of –83.3) LQTAXSLW = 927 (= x plate scale of –104.82 * 8.8 within error bar)
"	TL1460G130MCAL	287170301	Ap mech was offset (+5, 0) for this test. Previous to this test, 287150702 found cal at 563.5. LQTAXCOR = 560.9 As above, 5 steps in X is 2.28 pixels (measured 2.6—good) LQTATOTL = 11217
"	TL1460G130MPKXD	287170801	LQTAMXCR = 480.6 (right about where it was in test 1450, above) LQTADXCR = 477.6 (= 560.9 + offset of –83.3) LQTAXSLW = -321 (= x plate scale of –104.82 * 3, within error bar)
"	TL1460G130MCAL	287171432	Ap mech was offset (+9, 0) for this test. LQTAXCOR = 558.8 As above, 9 steps is 4.10 pixels (measured 4.7—good) LQTATOTL = 11473
"	TL1460G130MPKXD	287172132	LQTAMXCR = 480.4 (still in the same place) LQTADXCR = 475.5 LQTAXSLW = -515 (= x plate scale of –104.82 * 4.9, within error bar)
"	TL1460G130MCAL	287172932	Ap mech was offset (-7, 0) for this test. LQTAXCOR = 566.5 As above, 7 steps is 3.19 pixels (measured 3—good) LQTATOTL = 11188
"	TL1460G130MPKXD	287173502	LQTAMXCR = 480.7 (still in the same place) LQTADXCR = 483.2 LQTAXSLW = 267 (= x plate scale of –104.82 * 2.5, within error bar)
1465	TL1465G285MCAL	270133020	Ap mech was offset (+5, 0) for this test. Previous to this test, 270122551 found cal at 360. LQTAXCOR = 370 5 steps in X * 0.0478 arc-sec-per-step = 0.239 arc-sec 0.239 arc-sec / 0.02384 arc-secs-per-pixel = 10.03 pixels (measured 10—good) LQTATOTL = 833
"	TL1465G285MPKXD	270140951	LQTAMXCR = 728 (same place it was found in test 1455 above) LQTADXCR = 741.2 (= 370 + offset of 371.2) LQTAXSLW = -315 (= x plate scale of –23.84 * 13.2)
"	TL1465G285MCAL	270141820	Ap mech was offset (+9, 0) for this test. LQTAXCOR = 380 9 steps is 9/5 * 10.03 = 18.05 pixels (measured 20—good) LQTATOTL = 847
"	TL1465G285MPKXD	270142550	LQTAMXCR = 728 (still in the same place) LQTADXCR = 751.2 LQTAXSLW = -553 (= x plate scale –23.84 * 23.2)

“	TL1465G285MCAL	270143620	Ap mech was offset (-7, 0) for this test. LQTAXCOR = 349 7 steps is 7/5 * 10.03 = 14.04 pixels (measured 11—ok) LQTATOTL = 741
“	TL1465G285MPKXD	270144250	LQTAMXCR = 728 (still in the same place) LQTADXCR = 720.2 LQTAXSLW = 186 (= x plate scale –23.84 * -7.8)
1470	TL1470G140LFWC3	287180303	3rd dwell point saw light. LQTADPOS = 600 LQTADSLW = 0 LQTAFX03 = 11100; others = 0.
“	TL1470G140LFWC4	287181132	1st dwell point saw light. LQTADPOS = 0 LQTADSLW = -1200 LQTAFX01 = 11738; others < 3.
“	TL1470G140LFWC5	287182032	3rd dwell point saw light. LQTADPOS = -599 (pulled a little by the noise at the other points) LQTADSLW = -1799 LQTAFX03 = 11918; others < 9
“	TL1470G140LFWC7	287183132	5th and 6th dwell points saw light. LQTADPOS = 900 LQTADSLW = -900 LQTAFX05 = 12070; LQTAFX06 = 12091; others < 23. (12070* 600 + 12091*1200) / (12070 + 12091) = 900.26 rounds to 900. LQTALOCL = 1209
“	TL1470G130MFWC3	287184202	3rd dwell point saw light. LQTADPOS = 600 LQTADSLW = 0 LQTAFX03 = 13751; others < 3
“	TL1470G130MFWC4	287185002	1st dwell point saw light. LQTADPOS = 0 LQTADSLW = -1200 LQTAFX01 = 13820; others > 6
“	TL1470G130MFWC5	287190303	3rd dwell point saw light. LQTADPOS = -599 (pulled a little by the noise at the other points) LQTADSLW = -1799 LQTAFX03 = 13587; others < 11
“	TL1470G130MFWC7	287191402	5th and 6th dwell points saw light. LQTADPOS = 899 LQTADSLW = -901 LQTAFX05 = 13389; LQTAFX06 = 13311; others < 47. (13389*600 + 13311*1200) / (13389 + 13311) = 899.12 LQTALOCL = 1338
“	TL1470G130MRTB	287192602	3rd dwell point saw light.

			LQTADPOS = 600 LQTADSLW = 0 LQTAFX03 = 14410; others < 52.
"	TL1470G130MRTB	287193302	2nd dwell point saw light. LQTADPOS = -600 LQTADSLW = -1200 LQTAFX02 = 13711; others < 44.
1475	TL1475G285MFWC3	270145551	3rd dwell point saw light. LQTADPOS = 600 LQTADSLW = 0 LQTAFX03 = 2836; others = 0.
"	TL1475G285MFWC4	270150650	1st dwell point saw light. LQTADPOS = 0 LQTADSLW = -1200 LQTAFX01 = 2643; others < 12.
"	TL1475G285MFWC5	270152119	3rd dwell point saw light. LQTADPOS = -622 (based on the flux log, the shutter must have been open at dwell point #2 as well) LQTADSLW = -1822 LQTAFX02 = 110; LQTAFX03 = 2610; others < 5. (110*-1200 + 2610*-600) / (110 + 2610) = -624.26 (not exactly –622 because of noise at other dwell points)
"	TL1475G285MFWC7	270153950	5th and 6th dwell points saw light. LQTADPOS = 893 LQTADSLW = -907 LQTAFX05 = 2561; LQTAFX06 = 2439; others < 28. (2561*600 + 2439*1200) / (2561 + 2439) = 892.68 rounds to 893. LQTALOCL = 256
"	TL1475G285MRTB	270154751	3rd dwell point saw light. LQTADPOS = 600 LQTADSLW = 0 LQTAFX03 = 2447; others < 28
"	TL1475G285MRTB	270155520	2nd dwell point saw light. LQTADPOS = -600 LQTADSLW = -1200 LQTAFX02 = 2401; others < 29